DESIGN AND DEVELOPMENT OF HIGHLY FLEXIBLE TRIAZINE BASED COVALENT ORGANIC FRAMEWORKS FOR SEPARATION AND REMOVAL OF ORGANIC DYES FROM WATER

Vaibhav Pal

MS15051

A dissertation submitted for the partial fulfillment of BS-MS Dual Degree in Science

Indian Institute of Science Education and Research Mohali

June 2020

DEDICATED to

ALL INDIAN FARMERS

and

INDIAN ARMY

Certificate of Examination

This is to certify that the dissertation titled "Design and Development of Highly Flexible Triazine Based Covalent Organic Frameworks for Separation and Removal of Organic Dyes from Water" submitted by Mr. Vaibhav Pal (Reg. No. MS15051) for the partial fulfillment of BS-MS dual degree programme of the Institute has been examined by the thesis committee members duly appointed by the Institute. The committee finds the work done by the candidate satisfactory and recommends that the thesis be accepted.

Dr. Ananth Venkatesan	Dr. Ramesh Ramachandran	Prof. Sanjay Mandal
(Member)	(Member)	(Supervisor)

Dated: June 15, 2020

Declaration

The work presented in this dissertation has been carried out by me under the guidance of Prof. Sanjay Mandal at the Indian Institute of Science Education and Research Mohali.

This work has not been submitted in part or in full for a degree, a diploma, or a fellowship to any other university or institute. Whenever contributions of others are involved, every effort is made to indicate this clearly, with due acknowledgement of collaborative research and discussions. This thesis is a bonafide record of original work done by me and all sources listed within have been detailed in the bibliography.

Vaibhav Pal

Dated: June 15, 2020

In my capacity as the supervisor of the candidate's project work, I certify that the above statements by the candidate are true to the best of my knowledge.

Prof. Sanjay Mandal

Dated: June 15, 2020

Acknowledgements

First and foremost, I would like to thank my supervisor, Prof. Sanjay Mandal, for providing me with this opportunity to work with him and for the knowledge imparted to me. His advice, consistence guidance and overall direction to the research will help for growing me as a good researcher. The discussions I had with him have enhanced my capabilities. He is truly a great mentor. I could not have imagined having a better advisor and mentor for my Master's. Special thanks go to Dr. Prasenjit Das for his valuable comments and advice throughout the project. The completion of this thesis would have never been possible without his support.

Besides my advisor, I thank other thesis committee members, Dr. Ramesh Ramachandran and Dr. Ananth Venkatesan. Their brilliant comments and suggestions have encouraged me to carry forward this research with in-depth investigation and analysis.

I would like to thank Alisha and Sheeba for all the help and inputs provided during the project work. I also would like to thank Himanshi for helping and motivating me during the project. Further, I also thank my current and previous lab member Shradha Gandhi, Alokananda Chanda, Hari, Dr. Biswajit Laha, Dr. Vijay Gupta, Dr. Sandeep Kashyap, Dr. Gauri Chakroborty, Dr. Datta Markad, and Dr. Smriti Thakur for all support and love.

A special thanks to Amit, Yash, Vaibhav who were always with me in my good and bad times. They have a lot of contribution to shaping my academic carrier and taught me a multitude of things which would be very difficult to mention in this short communication. I would also thank my Dr. Monika Gupta, who was my first mentor. She taught me various lab techniques and encouraged me for research. I would also like to express my heartfelt thanks to Rina Ma'am for her love, care and support.

Words are inadequate to express my hearty thanks to my friends Ankita, Amisha, Dharam, Himanshu, Saurabh, Raj for their love, care and support throughout this time. I also want to thank my juniors Gaurav, Rahul, Yuvraj, Deepraj, Suraj, Vishal, Monu, Nitin and Mahima for their good wishes and support in the hour of need. I take this opportunity to

thank Somoshree for shaping my initial academic career and all the moments we had together. I also thank Shweta for her love that have always given me the strength to overcome the difficult times during this phase. Thanks for cheering me up throughout this period. I also would like to acknowledge Bob's café, where I spent some time and learnt the lesson of life. Special thanks to my mother and father, who is working day and night for me and must be happy to see his son accomplish his dream.

I expand my thanks to my lovely brother Sunny and Raju Pal who have been a constant source of motivation for me. They were always beside me during the happy moments. I want to thank IISER Mohali to have blessed me with this opportunity to work and learn in such an exciting research environment and I duly acknowledge the financial support from DST-INSPIRE Scholarship to pursue BS-MS at IISER Mohali.

Above all, I owe it all to Almighty for granting me wisdom, strength and mercifulness in accomplishing this work.

List of Figures

Chapter I (Introduction)

Chapter III (Results and Discussion)

List of Schemes

Chapter III (Results and Discussion)

List of Tables

Chapter III (Results and Discussion)

Contents

Abstract

The covalent organic framework is an emerging field of porous materials, and the development of this is still in progress. In this direction, researchers have put their efforts, but the development of highly flexible COF is always a challenging and important task. In order to contribute, three highly flexible COFs have been synthesized using the solvothermal method and characterized by numerous analytical methods. Since the formation of highly flexible COF is callous, we have studied the growth mechanism of all three COFs using FESEM and HRTEM. Among all three COFs, O-COF owns beautiful microtubular morphology with AA stacking and high thermal stability. The morphology of O-COF converters spherical to tubular morphology. Recent achievements in the field of COF towards covering most of the real-life applications and water purification is one of them, so all synthesized COFs have been used to remove organic pollutants from water solution for water treatment application. During dye removal application, it has been found that O-COF is predominant in terms of morphology and serves good adsorbent for RhB dye from the water waste. Along with this, dye separation was also shown based on electrostatic interaction and hydrogen bonding interactions. It was observed that O-COF is selectively adsorbed cationic dyes. A prototype was also done, in which O-COF was successfully employed as solid phase in liquid chromatography for the separation of cationic and anionic dyes. We observed that oxygen is playing crucial role for the adsorption process due to more electron negative nature compared to carbon. To understand dye adsorption process, pseudo first order, pseudo second order, and interparticle diffusion model have been used. The adsorption isotherm was fitted into Langmuir model. Moreover, all the synthesized COFs were characterized using Fourier transform infrared spectroscopy, solid-state ultraviolet–visible spectroscopy, thermogravimetric analysis, and X-ray diffraction, scanning electron microscopy. Furthermore, the stability of O-COF in the presence of dyes was investigated by powder X-ray diffraction and field emission scanning electron microscopy with good retention of crystallinity and morphology.

CHAPTER I

INTRODUCTION

The main driving force for the development of various materials was fully depends on the requirement of the society which has significant impact on the scientific community. The evolution of porous materials is one of them (Figure 1.1). Zeolite is the most common example of porous material, which is low cost and has been widely considered.[1] A wide range of applications made zeolites desirable materials.[2] However, zeolites tend to reduce their performance in various conditions such as moisture and are very difficult to functionalize that restrict their extensive applications.[3] Thus, enthusiasm for the development of different kinds of porous materials has started in the previous decades because of their potential applications in various fields of science.[4,5]

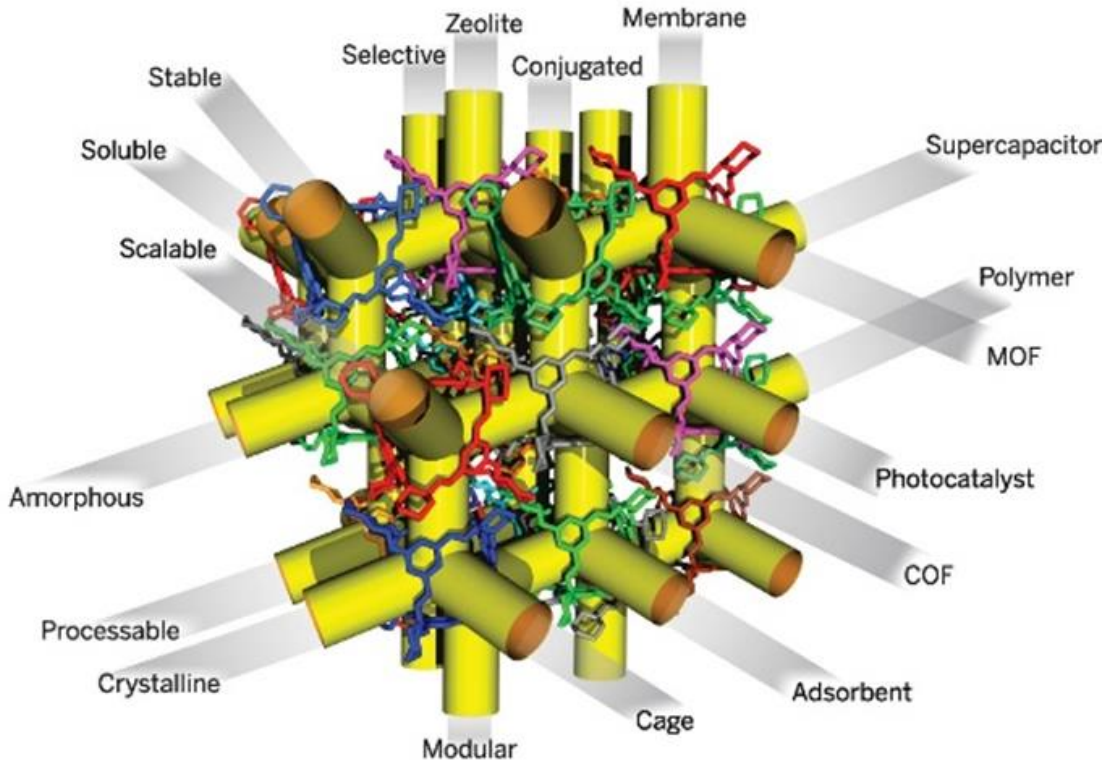

Figure 1.1. Porous Materials ((Adapted from reference 6).

Over the past few years, various porous materials have been developed. Researches have classified the porous materials into mainly two ways. The first category is based on pore size and the second is based on building units.[6] There are three types of porous solids based on pores size: microporous materials (pore size < 2 nm), mesoporous materials (2 < pore

size < 50 nm), and microporous materials (pore size > 50 nm).[7] Further, there are three types of porous materials depending on the building units: Purely organic, Organic-inorganic, purely organic based porous materials. Silica, Metal-organic frameworks (MOFs), and covalent organic frameworks (COFs) are the examples of these materials, respectively.

In order to overcome the restrictions of zeolites, researchers have discovered covalent organic frameworks (COFs) and metal-organic frameworks (MOFs) which are the comparatively new class of porous solids and have enormous features mainly depending upon various sizes, shapes, functionality and composition of the building units.[8] These materials are exceptionally stable towards heat and are nearly inert. These covers a lot of applications such as catalysis, energy storage, sensing, drug delivery, optoelectronics, gas storage and separation applications.[9-14] In the thesis work, the design and construction COFs and their applications are described.

1.1 Covalent Organic Frameworks

Covalent Organic Frameworks (COFs) are a whole new class of crystalline porous polymers. Bottom-up approach are used for the formation of COFs.[15] The first COFs COF-1 and COF-5 were synthesized by the self-condensation reaction of boronic acids and co-condensation reaction of catechol and boronic acids, respectively (Figure 1.2).[16] After the first report, various reactions and conditions have been reported for the formation of COFs to date including boroxine[17], imine[18], azine-linked[19], boronatedester[20], phenazine, hydrazone[21], b-ketoenamine[22], imide condensation reactions[23] (Figure 1.3). Organic Synthesis is a very diverse field and it offers room for unlimited possible COFs design with the combination numerous possible functionalities. The notable growth in COF research because of its self-healing nature and thermodynamic controlled covalent strategy gives a long-range order and crystallinity to the COF structure. Along with this, COFs possess various exciting properties that are not found in other materials, discussed below:

(i) Low Density. All of the COFs are mainly composed of light elements for example; hydrogen, boron, carbon, nitrogen, and oxygen, that helps to give an excellent gravimetric performance for various applications.

(ii) Stability. COFs shows high thermal and chemical stability as compared to most of the MOFs because COFs are connected with strong covalent bonds. They show excellent

stability in organic solvents and other condition such as oxidative reductive, acidic as well as basic conditions. Additionally, π-π stacking and hydrogen bonding give strength to the structure and protect it from solvation and hydrolysis.

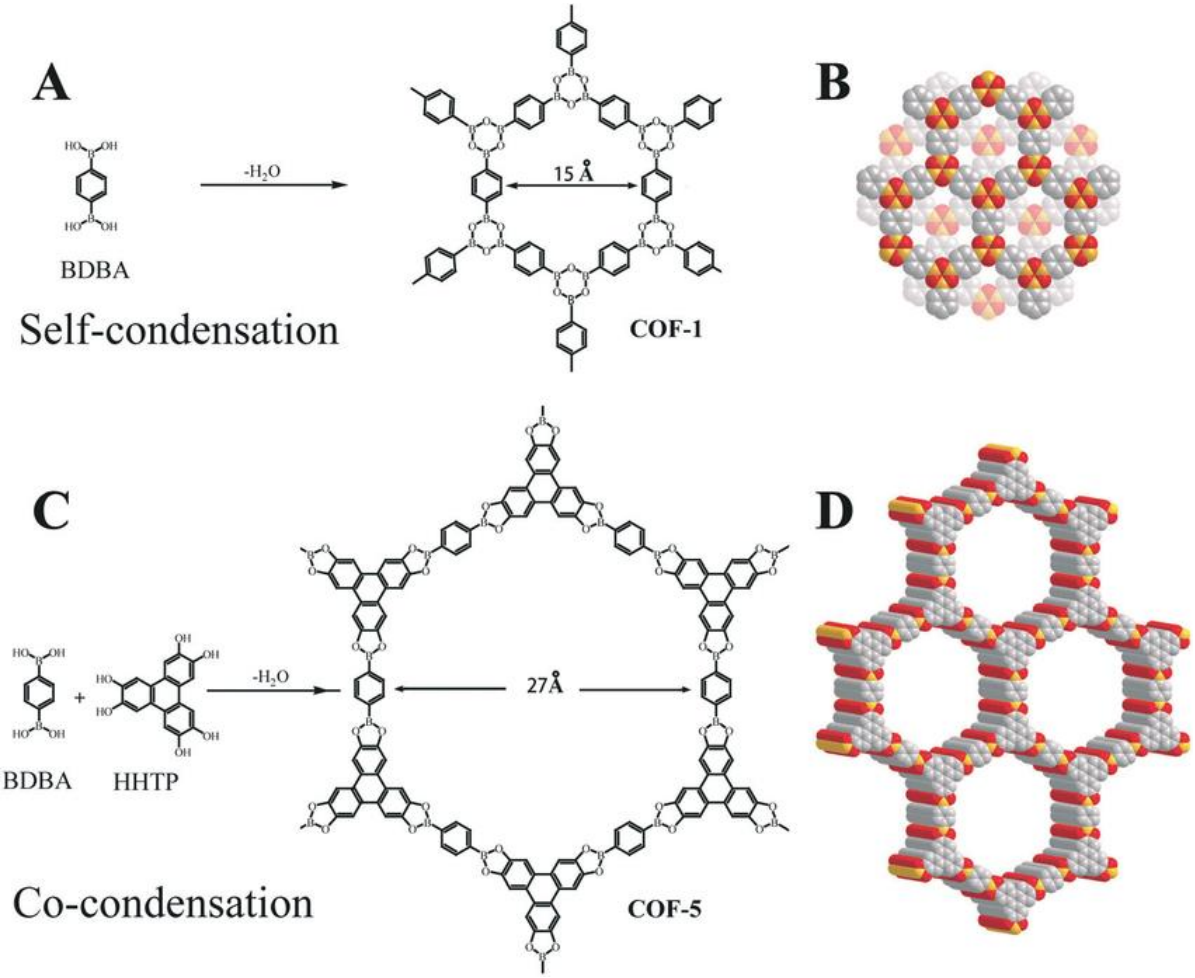

Figure 1.2. The synthetic strategy for the construction of first COFs (a) COF-1, (b) picture of the proposed structure of COF-1, (c) COF-5 and (d) picture of the proposed structure of COF-5. (Adapted from reference 16)

(iii) Crystallinity. COFs are highly crystalline porous polymer; they offer control over structure and functional group position. Due to this control, it is easy to predict the structure-property relationship so that they can be used in potential applications.

(iv) Porosity. COFs have higher and uniform porosity which allows these to be utilized for excellent gas adsorption, separation, and catalysis application. A high surface area is required in these applications. The highest surface area of any COF reported till date is 5083 m^2/g.[24]

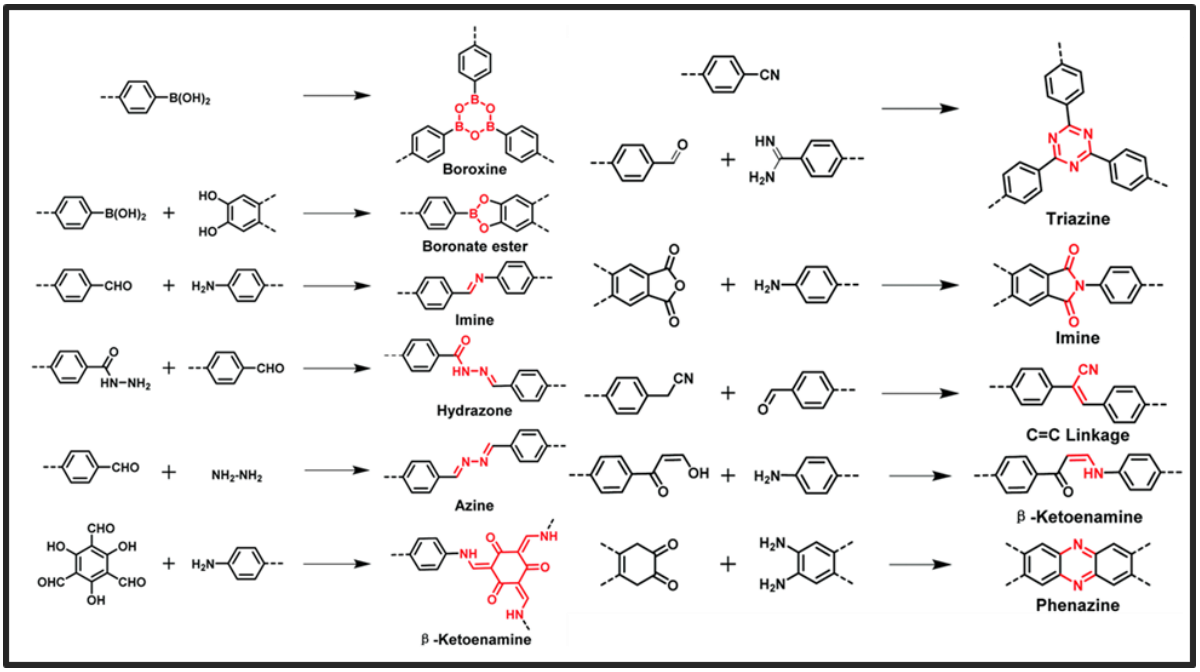

Figure 1.3. The list of reactions used for COF synthesis. (Adapted from reference 25)

1.2 Geometry and Design

In the COF structures, the geometry of the linkers decides the geometry of the COF. The main factor behind the topological design is the direction of covalent bond formation, which guides the growth of the framework. It requires a clear path and symmetrically distributed covalent bonds present in the monomers. For example, C_3 symmetric linkers

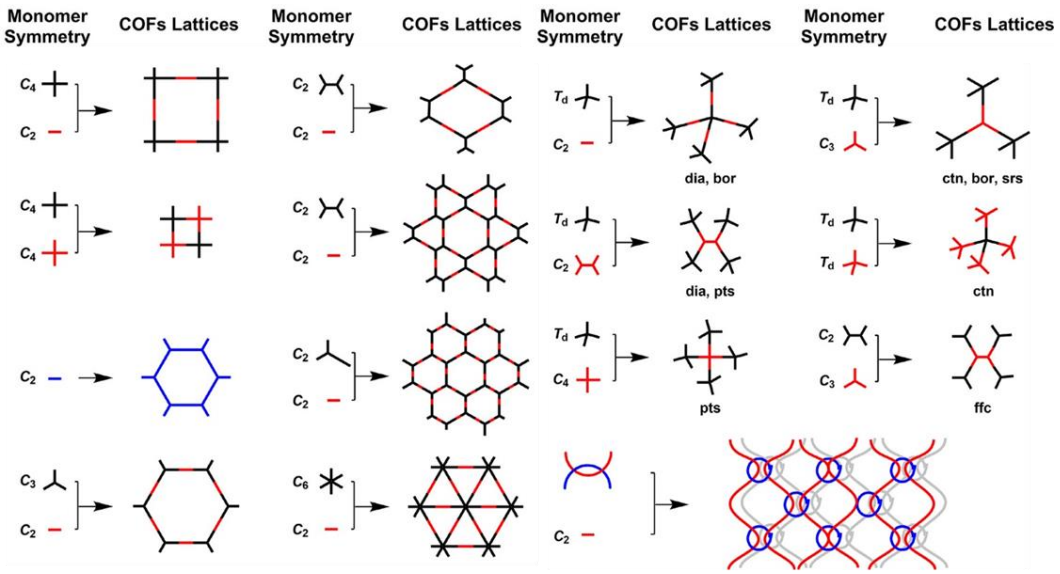

Figure 1.4. Basic topology for designing various dimensional COFs. (Adapted from reference 26)

lead to the formation of hexagonal pores, whereas C_3 + C_2 symmetric linkers yield hexagonal pores. COFs that are constructed from 2D building units are called 2D COFs, while COFs build from 3D building blocks are called 3D COFs. An overviw of the geometries is given in the Figure 1.4.

1.3 Synthetic routes

It is crucial to have control over the crystallinity in the COFs synthesis. It is the leading property that differentiates covalent organic frameworks from organic polymers. Therefore, significant efforts have been made to understand which synthetic routes can be used to provide a long-range ordering in the structure. Generally, COFs were synthesized by using reversible chemical reactions. In summary, the covalent bond which does not match will break for error correction and it will reorganize to form stable thermodynamic product.[27] Keeping this in mind, as shown in Figure 1.5 various synthetic methods and strategies have been developed like solvothermal synthesis, mechanochemical synthesis, microwave synthesis, room temperature synthesis, etc.

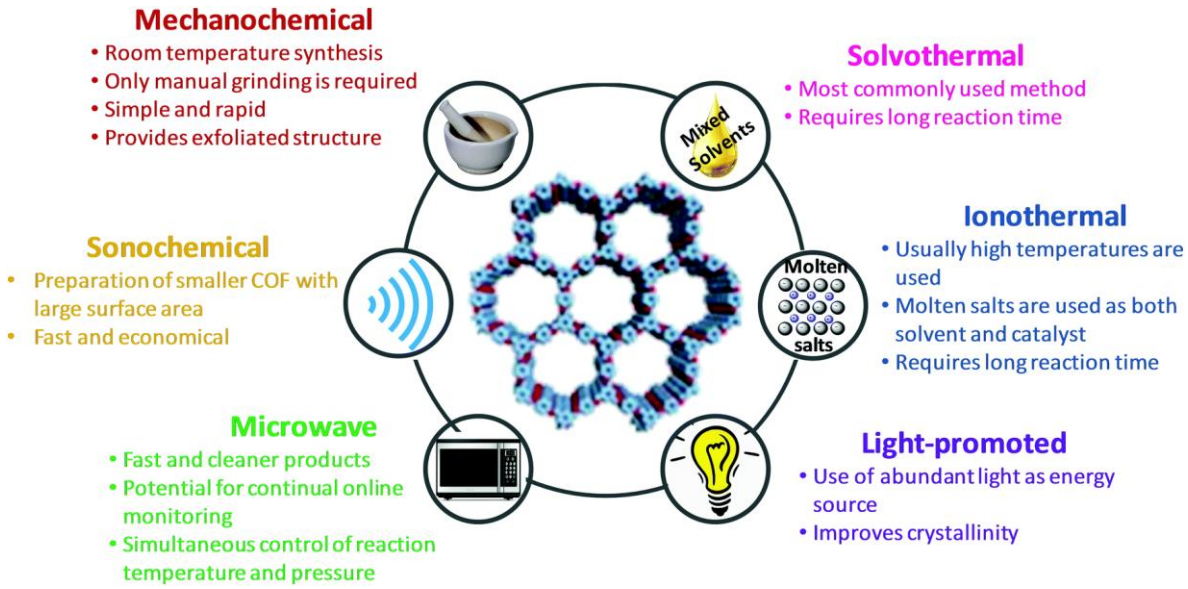

Figure 1.5. Advantages and properties for several COF synthetic methods. (Adapted from reference 28)

(i) Solvothermal/Hydrothermal synthesis

Solvothermal synthesis is the most popular and frequently used method to synthesize COFs. The first COF was also synthesized using the solvothermal method.[16] In the general procedure, the reaction mixture with suitable monomer, catalyst, and solvent combination

is taken in a closed container like Pyrex or Schlenk tube. This reaction mixture is sonicated, followed by degassing using freeze and thaw method. Then, it is kept at a high temperature for a specific time period. After the reaction, the tube is cooled, and the product is filtered and washed with suitable solvents to remove high boiling solvents and unreacted starting materials. Afterward, the product is dried under vacuum. In this method, solubility, reactivity of the reactants, reaction time, temperature, catalyst's concentration, solvent ratio, and reversibility of the reaction are important factors which majorly influence the crystallinity of the COFs. Gram scale COF can be prepared by using this method. For example, TPT-COF-1 can be made on a gram scale by using solvothermal synthesis which shows high BET surface area and high crystallinity.[25]

Figure 1.6. Stainless steel teflon reactor for solvothermal/hydrothermal reactions and its schematic diagram.

(ii) Microwave Synthesis

Since solvothermal synthesis takes a longer time for the formation of COFs, people have used microwave irradiation for the synthesis of COFs to overcome the time restriction. First microwave synthesis of COF reported by Campbell and his co-workers in 2009.[29] They showed that the formation of COF-5 took only 20 min by using microwave synthesis. Compared to the solvothermal method, BET surface area is more for COF if synthesized by microwave method. As a general procedure, a reaction mixture with suitable reactants and solvents is taken in a sealed microwave reactor under vacuum or nitrogen, and it is heated at suitable temperature for a specific time period. After the reaction, the product is collected, washed, and dried under vacuum. There are various advantages of this process over the solvothermal method that includes time to time monitoring, control on temperature

and pressure, and reaction time. So far, the synthesis of COF-5,[29]TpPa-COF,[30] COF-102[31] have been successfully demonstrated using this mode.

(iii) Mechanochemical Synthesis

Both the above synthetic methods require complex conditions such as inert atmosphere, a specific reaction set up, temperature, etc. that are the main limitations in taking these methods to an industrial level. For this, a simple synthetic procedure is required. Mechanochemical synthesis is a simple, rapid, green, and economical method in which covalent bonds are reversibly formed by simple grinding in the mortar-pestle at room temperature. Generally, COFs which were synthesized by mechanochemical methods showed less crystallinity compared to the solvothermal method. To explore further this synthesis, researchers developed liquid-assisted grinding technique where a slight catalyst solution is added while grinding. Banerjee et al. recently reported the synthesis of TpBD, TpPa-1, and TpPa-2 COFs by using this method (Figure 1.7).[32] Along with this, various other COFs like TpPa-NO_2, TpBD-$(NO2)_2$, TpPa-F4, TpBD-$(OMe)_2$, TpBD, and TpBD-Me_2 are synthesized by the mechanochemical method.[33]

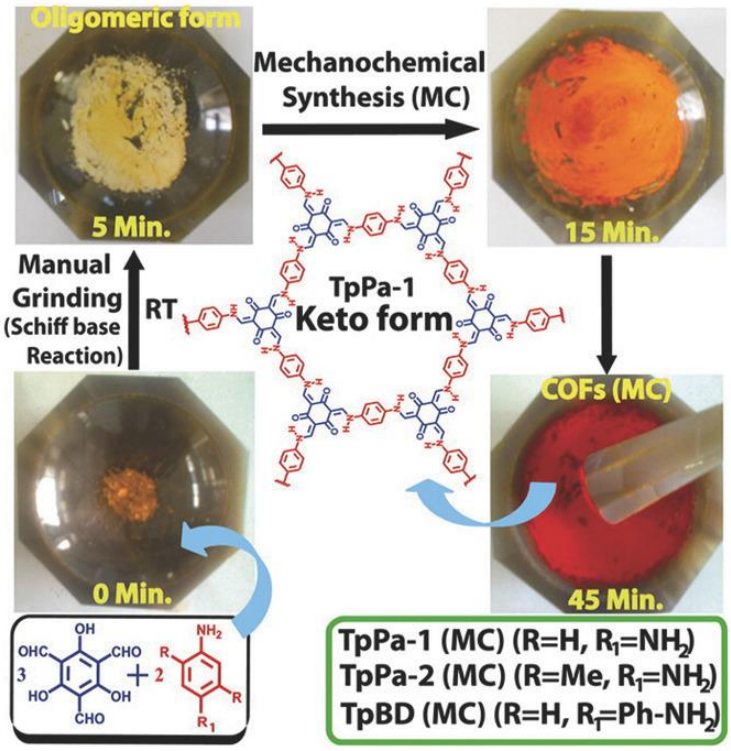

Figure 1.7. Diagram of mechanochemical synthesis of TpBD, TpPa-1, and TpPa-2 COFs. (Adapted from reference 32).

1.4 Applications of COFs

Covalent organic frameworks have all the essential properties, like high surface area, low density, high stability, porosity, well-defined structure and pores, tunable pore size and multiple functionalities that make them useful for various application such as gas storage, adsorption-based gas, and molecular separation, sensing, catalysis, molecule adsorption, optoelectronics, and drug delivery.

1.4.1 Storage of Gases

Inspired from MOFs and other porous materials, COF was first evaluated for gas storage application. COFs are made up of lightweight elements, thus low density that shows good gravimetric capacity which makes COFs potential candidate to storge any analyte or gases. Since there is a high requirement of clean energy in the coming years and H_2 is an excellent candidate for future fuel, researchers have made great efforts in designing COFs for this purpose.

Hydrogen storage was the first application which was tested for COFs. In 2009, Furukawa and Yaghi reported the highest volumetric capacity of COF-102 in terms of H_2 storage.[34] They claim COF-102 demonstrates maximum hydrogen uptake of 40.4 g/L at 100 bar. Later, a lot of 2D and 3D COFs have been investigated for H_2 storage. However, it was found that 3D COFs with medium pore size show excellent H_2 storage among all the reported COFs.

In addition to that, COFs are also used for removal or storage of harmful gases such as ammonia. Capable adsorbents for capturing NH_3 is highly required for various places like industrial NH_3 transportation, separation of ammonia from hydrogen and nitrogen gas as well as in shielding equipments. Boronic ester or Boroxine based COFs can be used for high NH_3 capture since ammonia is basic in nature and boron is Lewis acidic center which provides room for trapping ammonia by forming boron-ammonia classical coordinate complex. COF-10 shows exceptionally high ammonia uptake that is 15 mol/kg.[35] It is noteworthy to say that adsorbed ammonia by COF-10 can be completely removed by using specific temperature and pressure.

CO_2 has a major role to the target against global warming. CO_2 is mainly emitted from the burning of carbon-based fuels. Hence, it is essential to capture and convert it into value-added products. For this purpose, people have used various covalent organic

frameworks.[36,37] Carbon dioxide uptake can be improved by incorporating more and more Lewis basic sites because CO_2 is considered as a Lewis acid so the formation of acid–base pairs occurs during the CO_2 adsorption process.[38]

1.4.2 Catalysis

COFs possess well-defined pores, functional diversity, high thermal stability, and high surface area that offer an advantage over conventional catalysts because active sites are readily accessible. Due to the control on geometry and structure, we can easily manipulate and rearrange catalytic centers accordingly. COFs also provide a unique benefit in terms of heterogeneous catalysis: they provide sites for active nano-partials that minimize the agglomeration of NPs, and a large number of catalytic sites are accessible within the same COF.[39] Due to all these properties, COFs have been utilized as catalysts in several C-C coupling reactions,[40,41] and various other reactions such as cycloaddition,[42] oxidation, reduction,[43,44] asymmetric synthesis,[45] condensation,[46] CO_2 fixation[47,48] etc. COFs made up of photoactive building units can be used as photocatalyst. Several reactions like H_2 evolution reaction,[49] carbon dioxide reduction,[50] and water splitting[51] are reported where COFs are used as electrocatalysts.

1.4.3 Sensing

COF materials shows good photophysical properties and therefore, can be used as effective chemical sensors. Due to the functional diversity, COFs have been successfully employed in various sensing applications such as electrochemical colorimetric, and other colorimetric sensing. Donglin Jiang and his co-workers reported azine-based COF which was synthesised by using hydrazine and 1,3,6,8- tetrakis(4- formylphenyl) pyrene. It shows highly luminescent property and is tested for nitroaromatics sensing.[52] It was shown that synthesized COFs is highly sensitive and selective towards TNP. This was the report on chemosensory application where COFs have been utilized. In addition, people have put their efforts to use the COFs in the selective detection of Hg^{2+} and Cu^{2+}.[53,54]

1.4.4 Separation application

Separation is one of the most crucial process in the daily life and in industries. So, it is necessary to develop new porous materials for selective and efficient separation. For this purpose, COF have been used in various separation applications (Figure 1.8). For example, the separation of chiral molecules,[55] methane gas,[56] CO_2/N_2 separation,[57] water treatment,[58]

toxic ions,[59] hydrogen isotope,[60] and organic molecules[61]. Separation performance mainly depends on the pore size and functional groups present inside the pore. COF provides facile tailoring of the functional groups through post-synthetic modification that gives great control over its interaction with the guest molecules. This also helps to improve selectivity. COFs hold one more advantage over zeolites and MOFs in the sense that fabrication of its membranes is more facile compared to other crystalline materials.

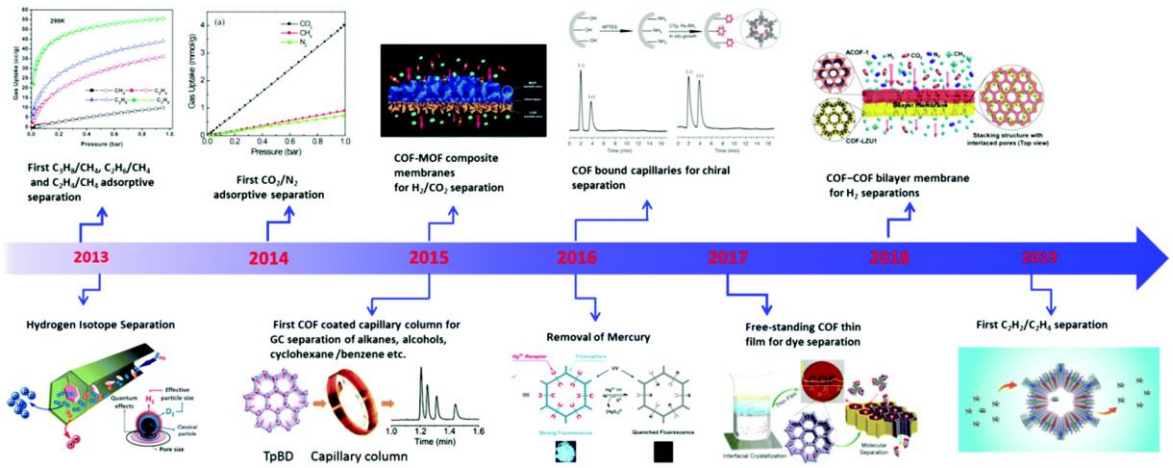

Figure 1.8. Timeline for application of COFs as separation or adsorbent medium. (Adapted from reference 62).

Adsorbents and membrane made up of COFs have been used in diverse applications. Generally, separation applications based on flow medium are classified into two types. The first is gas-phase separation which includes CO_2 capture/separation, H_2 purification, and other petrochemical separation such as methane purification, separation of acetylene from ethylene.[62] Separation of gases largely depends on the interaction and affinity of gas molecules with the pore walls. Second one is liquid phase separation and is further it divided into two types: Water treatment and Chromatographic separation.[62] In this work, the focus is mainly on liquid phase separation that is discussed below:

(a) Water treatment. Seventy percent of the whole world is covered by water but there is only 2.5% freshwater. Among available water, only 1% of water is accessible for our needs and that is also decreasing day by day due to water pollution by different industries which are producing enormous wastewater and has a huge impact on society. In order to solve this problem, people have developed several methods to get available clean water by removing contamination from water source and purifying seawater.[63,64] Due to having all the necessary properties, COFs have been employed for water treatment in many ways like seawater distillation, heavy metal, dyes, and other organic contamination removal. In 2017,

Loh and his co-workers reported salicylideneanilines-based COFs which shows reversible tautomerism. Consequently, it shows a reversible change in ionic properties. Therefore, it is the foundation for size, charge, and chemo selective separation of dye molecules from water (rhodamine B, chrome azurol S, anthraflavic acid, and methylene blue).[65]

Further, Ma group fabricated a cationic COF membrane by using bottom-up approach via Schiff-base chemistry.[66] This membrane is highly selective towards anionic dyes and molecules. For example: it shows 99.2% removal of fluorescein sodium salt, 99.6% removal of methyl orange, and 98.1% removal of potassium permanganate. These results clearly demonstrate the separation performance highly depends on the charge on the COF material.

Covalent organic frameworks also have been used for the removal of various toxic ions from water. For this purpose, to achieve fast uptake and high capacity of toxic ions, there should be abundant chelating sites for binding the ions. Wang and his co-workers reported the first example where detection and removal of Hg^{2+} was shown by using thioether functionalized COF.[67] The reason for high uptake attributed to soft nucleophilic and π-donor character of sulphur which is present inside the pore and work as ionophoric receptor for Hg^{2+}. Recently, Yan's group synthesized a cationic covalent organic nanosheet for the efficient removal of ReO_4^-.[68]

(b) Chromatographic separation. Chromatography is one of the most essential technique in every field of science and technology like pharmaceutical industry, organic chemistry, chemical engineering, and environmental science.[69-71] The separation efficiency and capabilities of the chromatography depend on the stationary phase.[72] There are various factors which influence the separation performance which includes non-covalent interactions between analytes and stationary phase (hydrophobic, hydrophilic, chiral-specific and size-specific interactions). So, it is necessary to develop more efficient materials for stationary phase. Due to the high surface area, excellent stability in various conditions, and tuneable pore size, COF material is most desirable for the stationary phase.

The first time, Yan's group used TpBD COF stationary phase in a capillary column for the application of gas chromatography.[73] By using this COF, they have shown the separation of linear alkanes due to their relative van der walls interactions with the framework, separation of cyclohexane and benzene. The reason for the separation was attributed to π-π interaction within the column and the separation of the alcohols based on their difference

in the hydrogen bonding interactions with carbonyl and amino groups of TpBD COF. Recently, researchers have shown that chiral COF materials have good potential to use it in chiral separation.[74,75] In 2016, Yan and co-workers have done pioneer work in chiral separation for COFs.[55] Since then, a lot of chiral COFs have been reported for stationary material in GC and HPLC. As compared to stationary phase based on COFs for GC, stationary phase for liquid chromatography are rarely reported.

1.5 Motivation and significance

This thesis deals with the development of new COF based stationary phase material for Liquid Chromatography (LC) to showcase the dye adsorption and separation from water. Out of all the water pollution, 10-15% water is polluted by organic dyes. Mainly dyes are used in colouring, printing, rubber, plastic, and food industry from which these dyes are mixed into water and make the water toxic. Along with that organic dyes are hazardous, carcinogenic which can affect very severely on humans. If we can remove these dyes from wastewater that are coming from industries and recycle it, then we could able to use the accessible water for a significant period. This practice will be very beneficial because water crises are prevalent in many cities in the world.

There are several methods reported in the literature to remove dyes from wastewater which is classified into three categories.[76] The first category is by chemical methods, such as Fenton reagent technique, ozonisation, and photocatalysis. The second category is via physical methods which include adsorption, filtration, ion exchange, and coagulation, and the third category is as biological methods. In this category aerobic and anaerobic degradation come into role. In all these methods, adsorption is one of the efficient techniques because it is an easy, low cost and also very less amount of material that is needed in this process. In this direction, researchers have reported various fancy materials, including zeolites, MOFs, COFs, activated carbon and agriculture waste. Among these, fewer reports are there in which COFs have been used to remove organic dyes from wastewater. Since the first COF was reported, this field is growing very fast due to the wide range of applications. The scope of the use of the COFs has been increased to cover most of the real-life applications. The different properties of COFs usually depend on chemical motifs that are present in the building blocks. Still, it does not only depend on these motifs and chemical structure but also their nanoscale morphologies.

In literature, most of the COFs are reported with rigid linkers. There are very fewer reports available where tensile linkers are used in COF synthesis (Figure 1.9).[77-84] Mainly people have used either both rigid moieties or one rigid and one flexible moiety to get crystalline COF. Still, it is a challenging task to get highly flexible crystalline COF. There is only one report available where both flexible linkers are used to synthesize crystalline COF because it is very challenging to get a highly ordered crystalline framework from flexible linkers.[84] The reason is attributed to the high degree rotation of flexible linkers. So, we took the challenge to synthesize the flexible COF.

COFs synthesized from flexible monomers could have broad lattices that make COFs a suitable candidate for the dye removal and separation applications. The target of the thesis is to design and synthesise highly flexible COFs and utilize them for water purification.

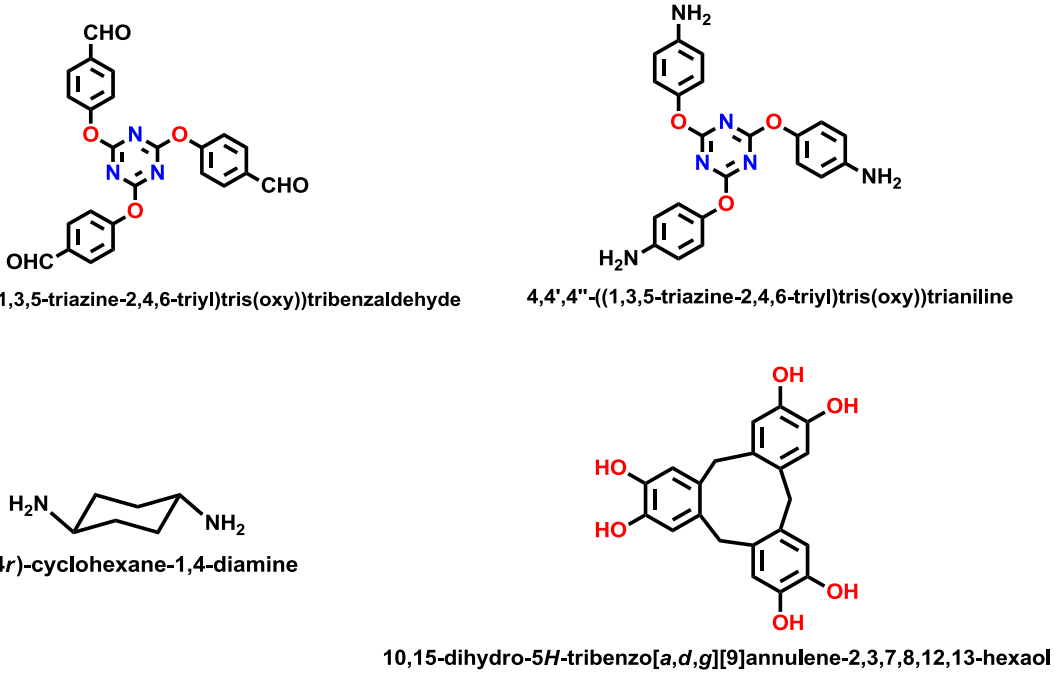

Figure 1.9. Flexible likers reported in the literature for COFs synthesis.

1.6 Present Work

2,4,6-Tris(p-formyl phenoxy)-1,3,5-triazine (TFPC), C_3 symmetric, tri-aldehyde monomer has attracted the attention for the synthesis of 2D COFs because of its unique properties such as flexibility, highly basic (nitrogen-rich) and electron-deficient nature that make it a suitable candidate as a monomer for the synthesis of flexible COFs.[82,84,86-89]

In this work, first TFPC was synthesized by using a simple S_N2 reaction. TFPC was further used with three others flexible (4,4'-diaminobiphenyl ether, 4,4'-diaminobiphenylmethane

and 2,2-bis(4-aminophenyl) hexafluoro propane to synthesize a new highly flexible COFs by using bottom-up approach through the solvothermal synthetic method (Figure 1.10). We devoted our efforts to design, synthesize, and characterize three different highly flexible COFs, using the monomers shown in Figure 1.11, with minor changes in chemical motifs to specific positions to showcase its application in dye removal from water waste and dye separation. We have shown efficient separation of Rhodamine B and fluorescence dye.

We have also demonstrated a prototype where synthesized material was used as a stationary phase in the liquid chromatography for dye separation. ^{1}H NMR was used to confirm the purity of the linkers. The synthesized COFs were extensively characterized by various characterization techniques: FTIR, solid-state UV, thermogravimetric analysis, solid state NMR, Small-angle X-ray scattering (SAXS), scanning electron microscope (SEM) and transmission electron microscope (TEM). In dye adsorption and separation experiments, concentration of dyes was tracked by using UV-Vis spectroscopy. Adsorption kinetics study was also done to understand the adsorption process.

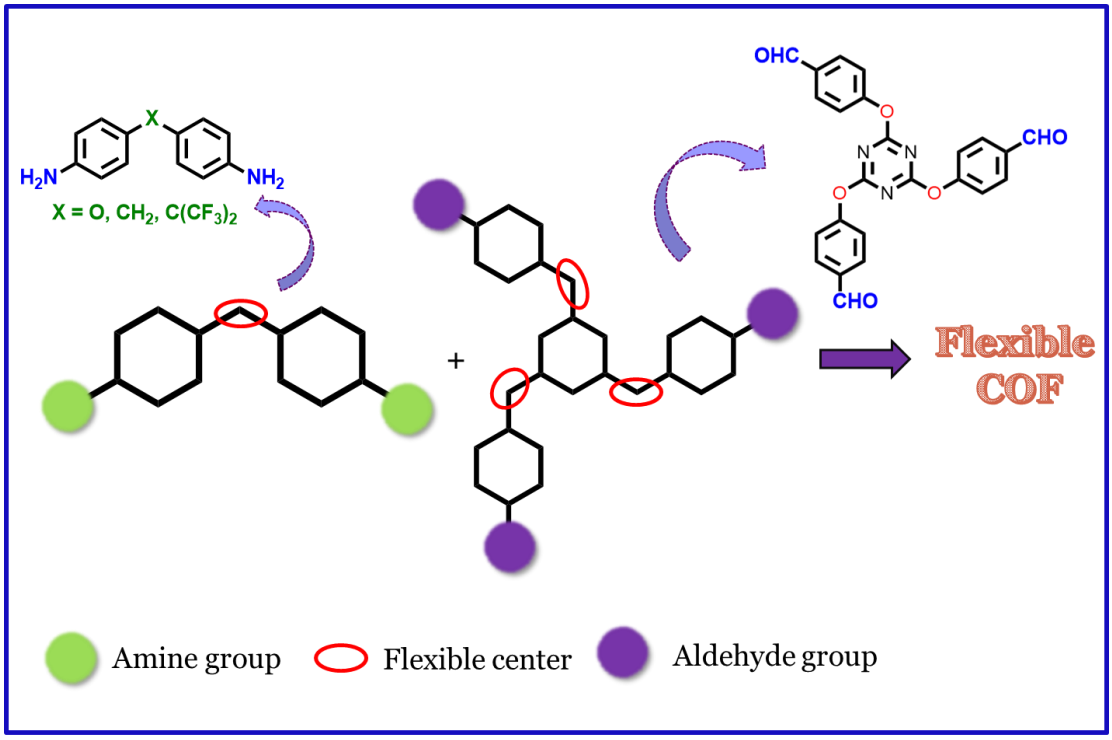

Figure 1.10. Strategy for the present work.

The properties of COFs usually depend on chemical motifs which are present in the building blocks. However, along with the motifs and chemical structure, their nanoscale morphologies also play an important role. So, we have also done the time-dependent

morphology study to understand the growth of the crystalline porous polymers by using SEM and TEM techniques.

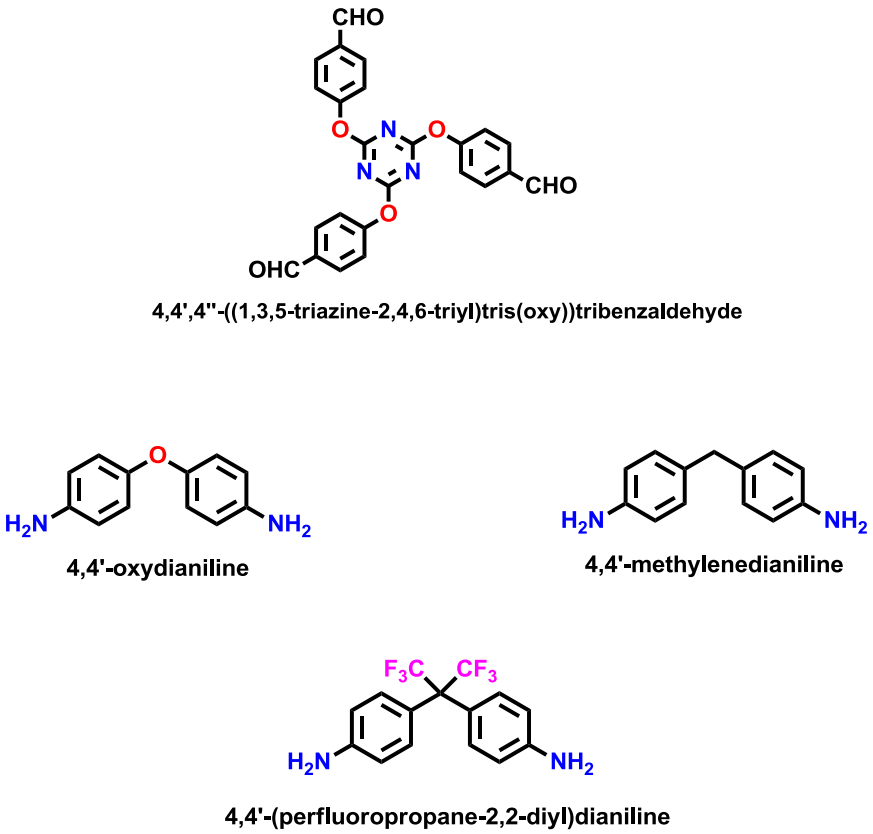

Figure 1.11. Monomers used in present work.

CHAPTER II

EXPERIMENTAL SECTION

1.1 Materials

Cyanuric chloride and 4-hydroxybenzaldehyde were obtained from Sigma Aldrich. 4,4'-Diaminobiphenyl ether and 2,2-Bis(4-aminophenyl) hexafluoropropane was obtained from TCI. 4,4'-Diaminobiphenylmethane was obtained from Alfa Aesar. All these chemicals are used as received without further purification. All the solvents were of reagent grade and without purified for the synthesis of ligand and both COFs.

1.2 Physical Measurements

Nuclear Magnetic Resonance (NMR)

Nuclear magnetic resonance (NMR) spectroscopy is a physical technique which has become essential for the chemical characterization and obtaining chemical structure. NMR is an adsorption spectroscopy in which transition of electron occurs between two energy states when radio waves are adsorbed by the nuclei having non zero nuclear spin under magnetic field. Each nucleus has different electronic environment that leads to give different signals and provide information about chemical environment. In liquid NMR, we get sharp peaks due to Brownian motion which leads to averaging the anisotropic effect whereas we get broad signals in solid state NMR due to anisotropy and non-zero internuclear dipole-dipole interaction. In order to minimize the broadening in solid state NMR, the sample is rotated about an axis which is oriented at 54.74^{o} with respect to external magnetic field. ^{1}H NMR spectra of the linkers were recorded with 400 MHz using Bruker ARX 400 spectrometer, with TMS as an internal standard. ^{13}C cross polarization magic angle spinning solid state NMR was recorded at 400 MHz using JEOL ECX 400 spectrophotometer. Mnova software was used to analyse the data obtained from solution NMR as well as solid state NMR.

Fourier Transform Infrared (FTIR) Spectroscopy

FTIR is an adsorption spectroscopy. It is very powerful technique which give the information about the functional group present in the organic and inorganic material since

distinct functional groups absorb at known characteristic frequencies. There should be dipole moment change for a molecule to be IR active. When light is irradiated upon the molecules, the frequency of IR light matches with natural frequency of bonds present in the molecule gets adsorbed and provide IR spectrum. The range of FTIR spectroscopy is between 4000 to 400cm^{-1}. FTIR spectrum was recorded with 16 scans on a Perkin Elmer Spectrum RX I FT-IR spectrometer using KBr pellets.

Thermogravimetric Analyses (TGA)

TGA is a thermal analysis technique which measures loss in the mass of the sample as a function of controlled temperature and under a controlled atmosphere (For example: N_2, O_2). It is allowing us to give structural characteristics like decomposition, transition, oxidation, condensation, removal of crystal water and thermal stability. Data collection were carried out in a Shimadzu DTG-60H analyser with a controlled heating rate (10°C/min) under a continuous flow of nitrogen atmosphere from 25–500 ˚C by using alumina pan.

Small-angle X-ray scattering (SAXS)

SAXS is a small-angle scattering, non-destructive analytical technique which is mainly used to characterize crystalline materials. This works on the Bragg's law and helps to identify the arrangement of atoms and determines crystallinity of the sample, lattice parameters, phase identification, size and strain broadening. The measurements were carried out using Xeuss Model C HP100 fm from Xenocs in the 2θ = 1-30° range with a Pilatus 200 hybrid pixel detector from Dectris.

UV-vis Spectrophotometer

UV-Vis spectroscopy is considered an important and powerful technique in analytical chemistry. It is mainly used for quantitative analysis of organic and inorganic compounds in solution. It works based on Beer-Lambert's law. In this, an absorption measures the electronic transition from ground state (HOMO) to excited state (LUMO). By using solid state-reflectance UV spectra, we can calculate band gap of the given material. The application of UV-Vis spectroscopy in research can be divided into two groups: One is the quantitative analysis and the second is the characterization of electronic and optical properties. The UV-vis absorption spectra were recorded on Cary 5000 UV-Vis-NIR

spectrophotometer from200-800 nm. Solid state-reflectance spectra were also obtained using Cary 5000 by Agilent Technology from 200-800 nm.

Scanning Electron Microscopy (SEM)

The scanning electron microscope (SEM) is a of electron microscope which scans the surface of the material via focused beam of electrons that provide a topographic image exhibit a better resolution as compare to the simple microscope. The electrons collide and interact with the atoms at the solid surface of the sample and give a different kind of signals. The signals include secondary electrons, backscattered electrons, diffracted backscattered electrons, X-rays, etc. Backscattered electrons that are scattered elastically after interaction contain information composition. Additionally, secondary electron which are produced after inelastic collision produces image and analyse atomic composition. The SEM was done on JEOL JSM-7600F. Samples were prepared by dispersion in MeOH and drop casted on a silicon wafer, dried and sputtered with gold for a time period of 20 minutes for increasing the conductivity of the sample. The working distance of 4.5 to 15 mm was used with a voltage of 10 to 15 kV.

Transmission Electron Microscopy (TEM)

Transmission Electron Microscopy (TEM) is also a type of electron microscope which gives information about the topography and internal structure of the specimen. In TEM and SEM, the illumination system is almost the same. The image is formed from the interaction with the sample as the beam is transmitted through the specimen. Generally, the sample is prepared on a copper grid. The thickness of the sample should not be more than 100 nm because it creates a problem in the transmission. TEM was performed on JEOL JEM-F200 equipped with ZrO/W thermal electron field-emission gun operated at 200 Kv. Sample (less than 1 mg) was dispersed in MeOH (2 mL) using a sonicator for 20 minutes and then put it on the copper grid, which was allowed to dry in vacuum for 30-40 minutes.

2.3 Synthesis of TFPC Monomer

To a solution of sodium hydroxide (781 mg, 19.54 mmol) in 15 mL distilled water 4-hydroxy benzaldehyde (213 mg, 17.35mmol) was added in a 50 mL two necked round-bottomed flask and stirred for 30 minutes. The reaction mixture was then kept in ice to reduce the temperature below 5°C using ice bath. A dropping funnel was arranged and a cyanuric

chloride (1.2 g, 6.5 mmol) solution prepared in 15 mL acetone, was added dropwise into the reaction mixture over about one hour under vigorous stirring at low temperature. The reaction was left for constant stirring for about 24 hours. The reaction was monitored with thin layer chromatography with EtOAc and hexane mixture. After the reaction, the reaction mixture was poured onto the crust ice slowly, the white solid was separated by using filtration and washed the powder several times by using cold distilled water. Then the resulting white solid was purified by column chromatography over silica gel using hexane and ethyl acetate as the eluent. Yield: 2.15 g (84%) Melting point: 169–171°C (literature 174 °C). ^{1}H NMR ($CDCl_3$, 400 MHz): δ 7.93 (*d*, 6H), 7.34 (*d*, 6H) 10.01 (*s*, 3H) ppm. FTIR peaks (using KBr pellet, cm^{-1}): 3432 (w), 2925(w), 2853 (w), 1701 (s), 1602 (m), 1575 (vs), 1501 (w), 1374 (vs), 1294 (m), 1210 (s), 1162 (m), 1015 (w), 842 (m), 806 (m), 618 (w).

2.4 Synthesis of COFs

2.4.1 Synthesis of O-COF

For O-COF synthesis, a mixture of 100 mg (0.228 mmol) of TFPC and 68.06mg (0.338 mmol) of 4,4'-diaminobiphenyl ether in 4 mL mesitylene/1 ml dioxane (4:1) and 0.3 ml acetic acid was taken in a 15 mL Schlenk tube. The reaction mixture was heated at 120 °C for 72 h. A yellow-brown powder was collected by filtering. The powder was washed by using acetone and kept in dimethylacetamide (DMA) mixture for 12 h, washed several times using acetone to remove any starting material and solvent. Further, the washed COF was dried in a vacuum oven for 4 h at 120 °C. Yield: 130.1 mg (83.7 %). ^{13}C Solid State NMR (CPMAS, 400 MHz): 174.4, 155.2, 154.6, 146.0, 133.6, 121.7, 121.5, 117.3 ppm. Band gap from Solid-state reflectance: 2.76 eV. Selected FTIR peaks (KBr pellet, cm^{-1}): 2920 (w), 2851 (w), 1630(w), 1569(m), 1492 (w), 1369 (w), 1197 (w), 815 (m).

2.4.2. Synthesis of C-COF

For C-COF synthesis, a mixture of 100 mg (0.228 mmol) of TFPC and 67 mg (0.340 mmol) of 4,4'-diaminobiphenylmethane in 4 mL mesitylene/1 ml dioxane (4:1) and 0.3 ml acetic acid was taken in a 15 mL Schlenk tube. The reaction mixture was heated at 120 °C for 72 h. A yellow powder was collected by filtration. The powder was washed by using acetone and kept in Dimethylacetamide (DMA) mixture for 12 h, washed several times using acetone to remove any

starting material and solvent present, and after that dried in a vacuum oven for 4 h at 120 °C. Yield: 110 mg (71.07 %). ^{13}C Solid State NMR (CPMAS, 400 MHz): 173.7, 156.8, 153.63, 150.30, 139.71, 134.08, 129.3, 129.0, 121.9, 121.1, 40.08 ppm. Band gap from Solid-state reflectance: 2.93eV. Selected FTIR peaks (KBr pellet, cm^{-1}): 2923 (w), 2853 (w), 1628 (w), 1567(m), 1368 (m), 1414 (w), 1198 (w), 814 (w).

2.4.3 Synthesis of CF_3-COF

For CF_3-COF synthesis, a mixture of 100 mg (0.228 mmol) of TFPC and 113.66 mg (0.340 mmol) of 2,2-Bis(4-aminophenyl) hexafluoro propane in 4 mL mesitylene/1 ml dioxane (4:1) and 0.3 ml acetic acid was taken in a 15 mL Schlenk tube. The reaction mixture was heated at 120 °C for 72 h. A light-yellow powder was collected by filtration. The powder was washed by using acetone several times to remove any starting material and solvent present, and after that dried in a vacuum oven for 4 h at 120 °C. Yield: 160 mg (75.11 %). ^{13}C Solid State NMR (CPMAS, 400 MHz): 173.85, 154.31, 146.76, 133.14, 130, 121.2, 113.31, 64.24 ppm. Band gap from Solid-state reflectance: 2.80eV. Selected FTIR peaks (KBr pellet, cm^{-1}): 2930 (w), 2860 (w), 1628 (w), 1572(m), 1363 (m), 1254 (m), 1208 (m), 838 (w).

2.5 Dye Adsorption experiment

Rhodamine B (RhB), Congo red (CR), Methyl orange (MO), sodium fluorescein (FL), Methylene blue (MB) and Methylene green (MG) dyes were chosen to study adsorption and separation abilities of as-synthesized O-COF, C-COF and CF_3-COF. First, 3 mg of COF material was taken with 2mL solution of dye at room temperature with initial concentration of 5 $mg \cdot L^{-1}$. The solution of COFs and dye was stirred for 10, 20, 30, 40, 50, 60, 70, 80, 90, 100, 110, and 120 min. The solution of RhB was separated using microfiltration membrane and concentration of the supernatant solution was determined at different times by using UV-Vis spectrophotometer.

2.6 Time dependent Morphology study

Generally, flexible COFs show good morphology. To study this, we have also done time-dependent morphology study of the synthesized COFs. For time-dependent morphology studies, COF reaction mixture was taken into different Schlenk tubes and the reactions were carried out by solvothermal process. The reactions were quenched at different time scales. The products

were filtered, washed that dried in a vacuum oven for 4 h at 120 °C. After that, SEM and TEM images were taken to understand the growth of the COFs.

2.7 Adsorption kinetics study

First, a calibration curve was made to calculate the absorbance for higher concentration. For that, standard solutions of RhB with concentration 1, 3, 5, 7, 9, 11 mg/L were analysed using single-wavelength method at highest absorbance wavelength. The absorbance was measured and plotted linearly with respect to the concentration using least square fit method.

After plotting calibration curve, adsorption capacity of O-COF, were determined by using the equation:

$$\boldsymbol{Q_t = \frac{V\,(C_O - C_t)}{M}}$$

Where, Q_t = adsorption capacity,

C_0 = initial concentration of dyes

C_t = equilibrium concentration at time t

V = total volume of the solution

M = mass of the COF

Further, several models such as intra-particle diffusion models, pseudo-first order and, pseudo-second order were used to understand the kinetics of RhB adsorption.

2.8 Adsorption Isotherm

For this, 3 mg of O-COF material was taken in 2 mL of RhB dye in different vials which contains different concentration of dyes (1-100 mg L^{-1}). After reaching the adsorption equilibrium, solution was filtered and concentration of dye was measured.

If adsorption process is monolayer, then no further adsorption will take place at the specific sight. Therefore, here adsorption process is mainly associated with surface area and van der Walls forces are involved in it. Langmuir model talks about monolayer adsorption and the equation is described as follows:

$$\boldsymbol{\frac{C_e}{Q_e} = \frac{1}{q_{max}K_L} + \frac{C_e}{q_{max}}}$$

Where, C_e = the equilibrium concentration of the dye

q_e = adsorption capacity at equilibrium

K_L = Langmuir adsorption constant

q_{max} = maximum adsorption capacity at equilibrium

The Freundlich model that is related to related to multilayer adsorption process. The equation for this model is expressed as:

$$\ln q_e = \ln K_F + \frac{1}{n} \ln C_e$$

Where, q_e = adsorption capacity at equilibrium

C_e = the equilibrium concertation of the dye

K_F = Freundlich adsorption constant

n = Freundlich constant

K_F is related to adsorption capacity and n represents adsorption intensity. The term 1/n measures the heterogeneity of the adsorbate and adsorption density. If n > 1, then adsorption process is favourable.

2.9 COFs Structure Solution

Structure simulation and solution was carried out using BIOVIA Material Studio 2017R2. The structure of the molecule was optimized using the DFT-D calculation (CASTEP method). Then, the powder data was refined by the combination of Pawley and Rietveld refinements. The experimental and simulated PXRD patterns were well fitted using X-cell program. $P_{6/m}$ space group was approved for further confirming the unit cell parameter.

2.10 Brunauer–Emmett–Teller (BET) Surface Area Analysis

For the BET surface area analysis, the BET equation is used:

$$v = \frac{cv_m x}{(1-x)[1+(c-1)x]}$$

where, $x = (p/p_0)$ v volume of nitrogen adsorbed per gram of COF at STP

v_m = the monolayer capacity, and c corresponds to the heat of adsorption.

It is noted that the line is fitted to the low-pressure isotherm data with range 0.05 < x < 0.3.

After that surface area was calculated by using the formula:

$$\boldsymbol{A = v_m \sigma_0 N_{av}}$$

where, σ_0 = cross-sectional area of nitrogen at liquid density (16.2 Å)

N_{av} = Avogadro's number

All the calculations were done using the "BET analysis" and "Langmuir analysis" function that is embedded in the Belsorp Adsorption/Desorption Data Analysis software version 6.3.1.0.

2.11 Recyclability Experiment

Recyclability is essential for industrial applications. For that, we have evaluated the recyclability of O-COF. In detail, an experiment of RhB adsorption-desorption was carried out where the concentration of RhB solution was tracked by using UV-Vis spectroscopy. O-COF material was taken in 5 mg/L RhB dye solution. From the solution, RhB was adsorbed for 24 h and the concentration of RhB was determined. After adsorption, RhB@COF was washed by using methanol. The colour change from colourless to red indicates that adsorbed RhB dye is getting desorbed. Finally, washed COF material was separated and dried it properly. Again, the experiment was repeated up to five cycles.

CHAPTER III

Results and Discussion

3.1 Ligand

3.1.1 Synthesis of TFPC ligand

TFPC ligand was synthesized using previously reported method in a single step from commercially available 4-hydroxy benzaldehyde and cyanuric chloride in yield of 84%. The synthesis of TFPC linker was shown in the scheme 3.1. In this reaction, first deprotonation of 4-hydroxy benzaldehyde occurs. Then generated anion attack on the carbon center of cyanuric chloride via S_N2 mechanism that resulted in the formation of flexible TFPC linker. The product was obtained as white colour solid with good yield.

Scheme 3.1. Synthesis of TFPC linker.

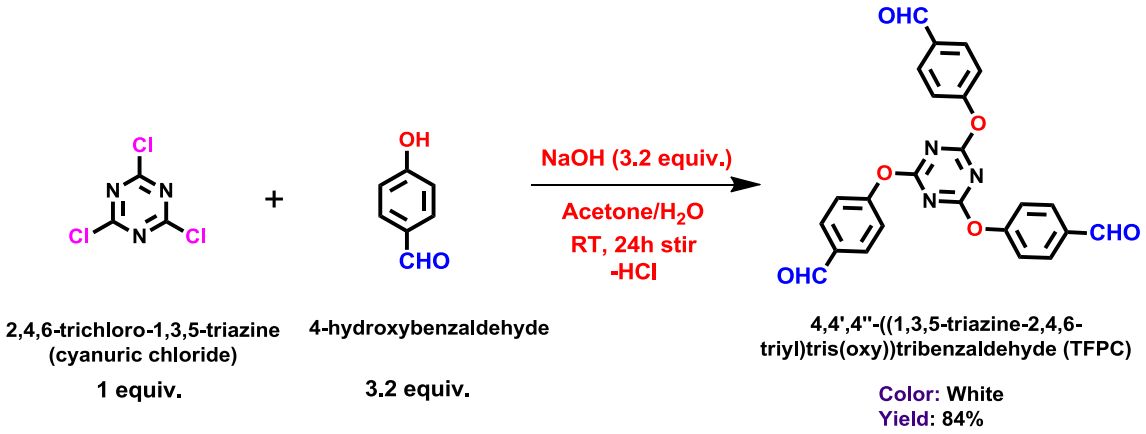

3.1.2 Characterization of TFPC ligand

The formation of synthesized TFPC ligand was confirmed using characterization techniques such as FTIR and ^{1}H NMR spectroscopy.

3.1.2.1 *^{1}H NMR Spectra.* The ^{1}H NMR spectrum confirmed the formation of TFPC. The proton NMR spectra of TFPC are shown in the Figure 3.1. Since TFPC is a highly symmetric molecule, the ^{1}H NMR shows only three different types of signals: A singlet at 10.01 ppm which corresponds to three protons of aldehyde and aromatic region have two doublets at 7.93 ppm (6H) and 7.34 (6H).

3.1.2.2 *FTIR spectra.* TFPC linker was also characterize using FTIR spectroscopy. The spectrum was shown in the Figure 3.2. The FTIR spectrum of TFPC was also compared

with the literature. A peak at 1701 cm^{-1} corresponds to carbonyl stretching frequency and a peak at 1575 cm^{-1} corresponds to C=N stretching in triazine ring.

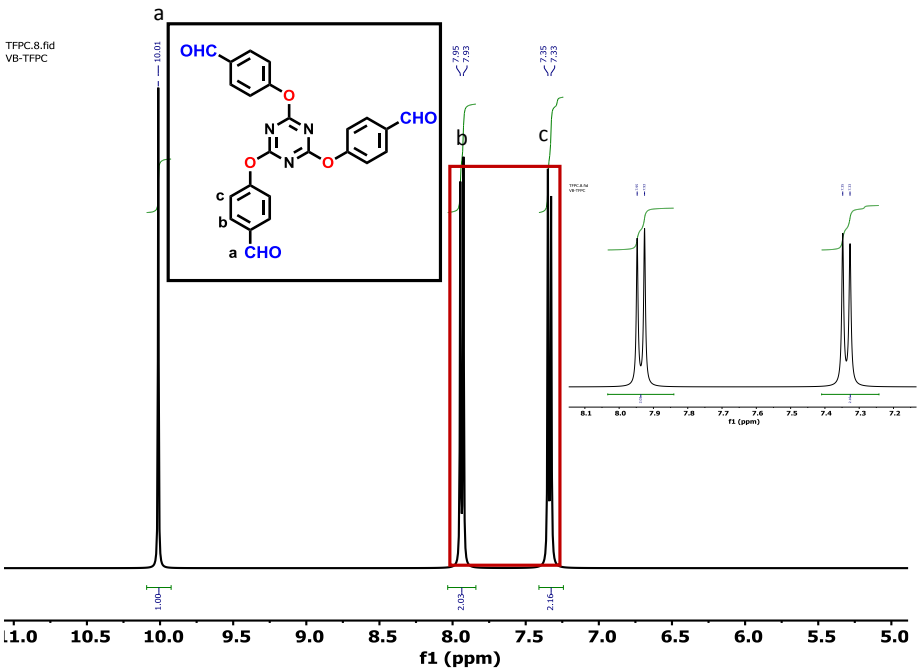

Figure 3.1. ^{1}H NMR spectrum of synthesized TFPC linker.

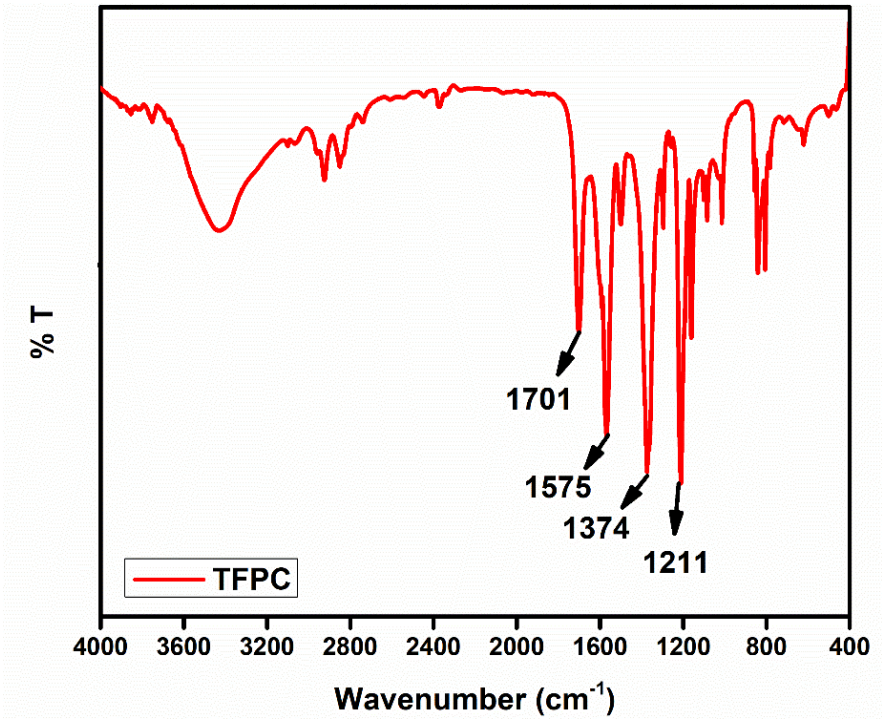

Figure 3.2. FTIR spectrum of synthesized TFPC linker.

3.2 Covalent organic frameworks

3.2.1 Synthesis of COFs

The rotations around the flexible bonds of TFPC and C2 symmetric linkers makes it challenging to achieve high degree crystallinity in such COFs. For this, various solvent combinations were tried to get crystalline COF. Finally, dioxane and mesitylene solvent ratio was chosen as desirable solvent mixture for synthesis and highly flexible COFs were synthesized by reacting TFPC and corresponding amines in a 1:1.5 ratio in Dioxane/Mesitylene by solvothermal method at 120 ^{o}C for 72 h (Scheme 3.2, 3.3, 3.4). Schiff- base chemistry was used to form the product. Among all synthesized COFs, O-COF was obtained in maximum yield. O-COF is brown, C-COF is yellow powder, and CF_3-COF is light yellow in colour. The Chem draw structures of the all three synthesized COFs are shown in Figures 3.3, 3.4 and 3.5.

Scheme 3.2. Synthesis of **O-COF**.

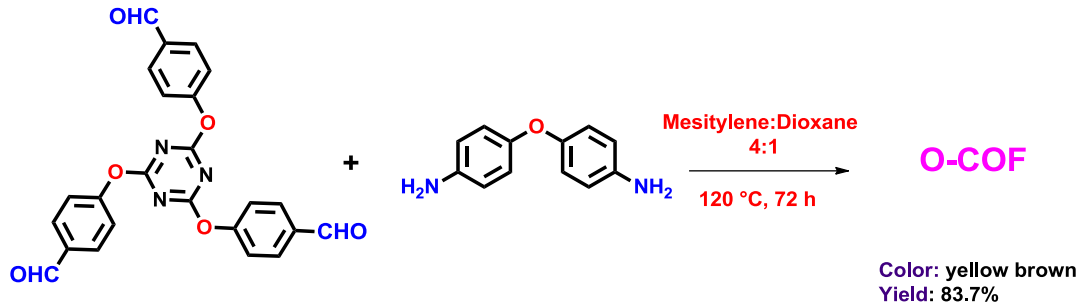

Scheme 3.3. Synthesis of **C-COF**.

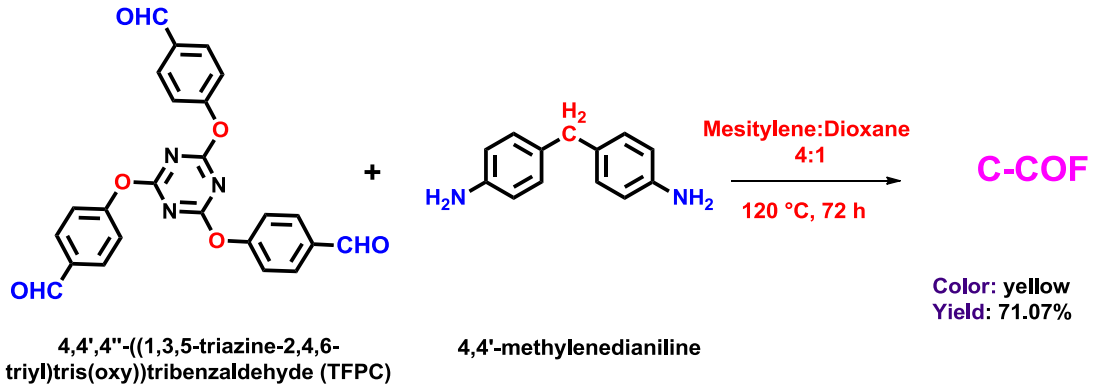

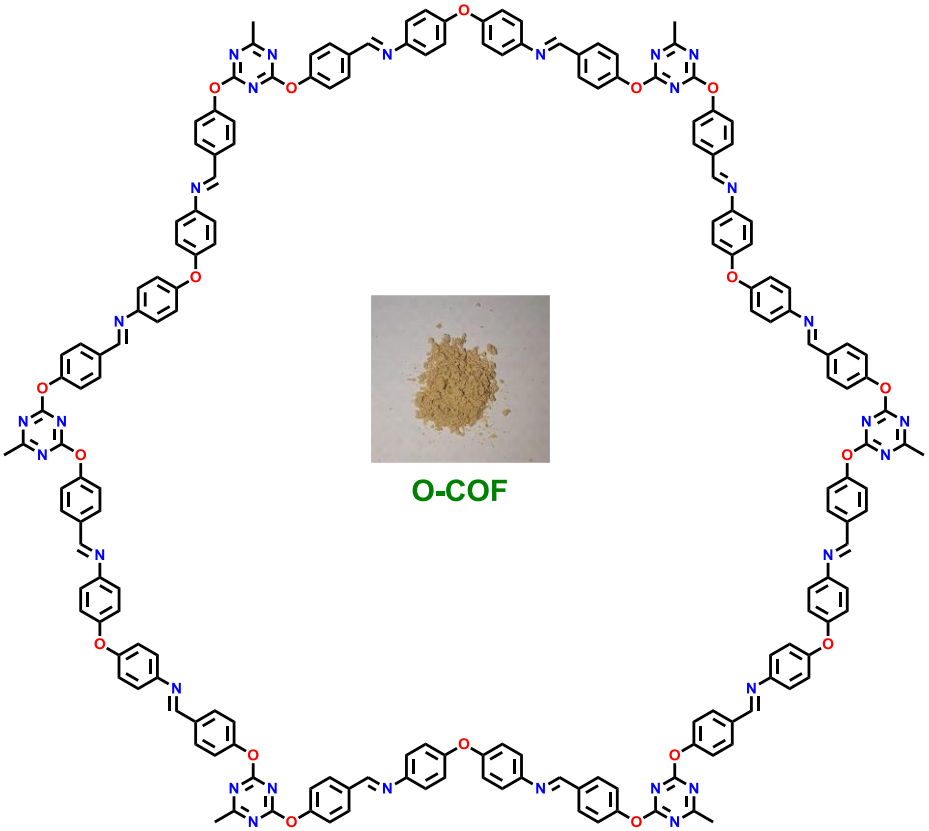

Figure 3.3. Chem Draw structure of **O-COF**.

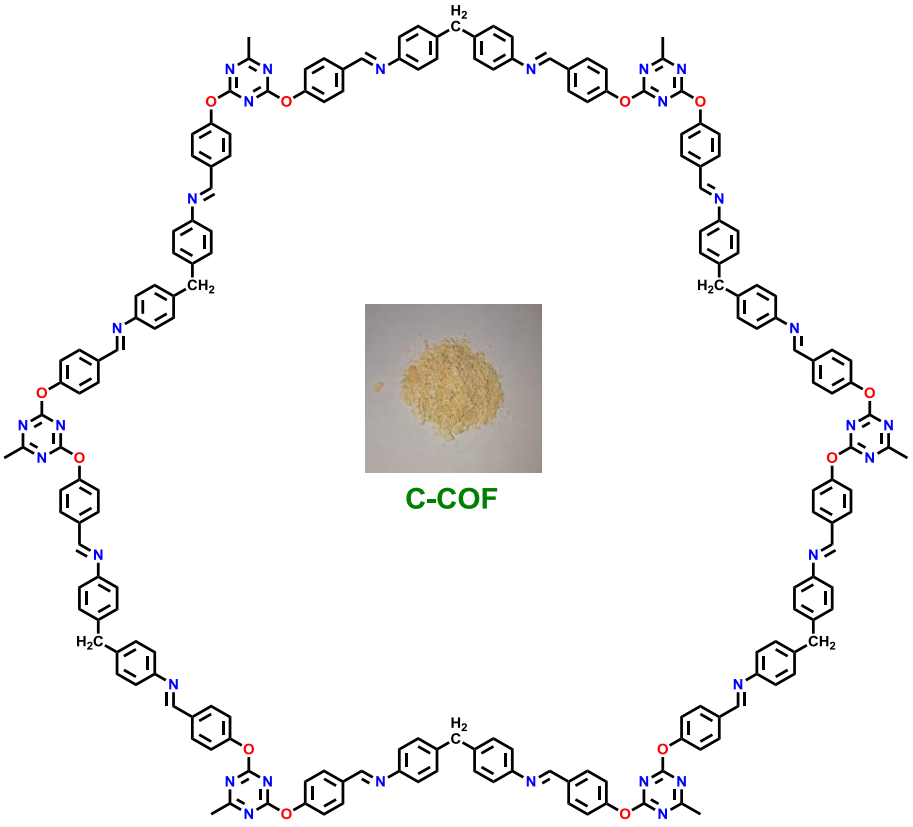

Figure 3.4. Chem Draw structure of **C-COF**.

Scheme 3.4. Synthesis of **CF_3-COF**.

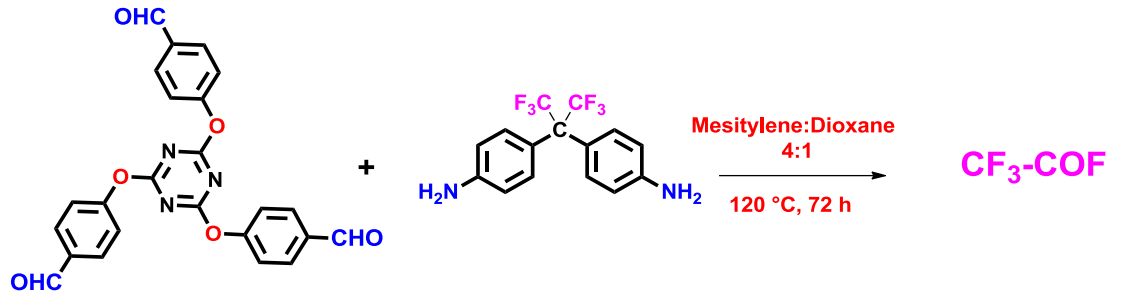

4,4',4''-((1,3,5-triazine-2,4,6-triyl)tris(oxy))tribenzaldehyde (TFPC)

4,4'-(perfluoropropane-2,2-diyl)dianiline

Color: light yellow
Yield: 71.07%

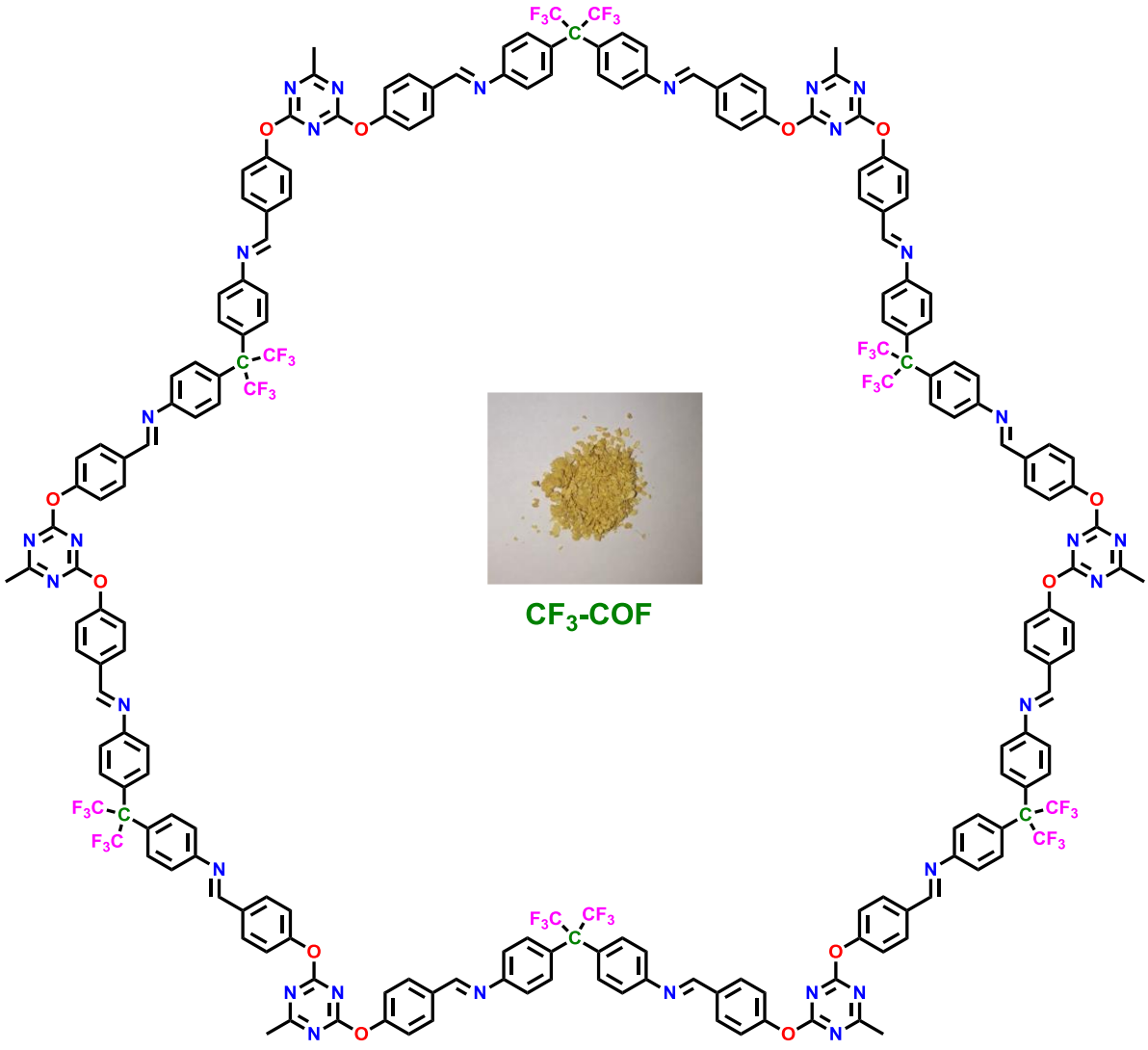

Figure 3.5. Chem Draw structure of **CF_3-COF**.

3.2.2 Characterization of COFs

All three synthesized COFs were characterized using FTIR, SAXS, TGA, UV-Vis, Solid-state NMR, SEM and TEM.

3.2.2.1 FTIR spectra

The successful formation of O-COF, C-COF, and CF_3-COF has been confirmed by FT-IR. A strong band at 1701 cm^{-1} in the spectrum of TFPC which corresponds to carbonyl stretching frequency is absent in the FTIR spectrum of all three COFs. This indicates the consumption of TFPC linker. The FT-IR spectra of synthesized COFs are also compared with the FTIR of TFPC linkers that are shown in Figures 3.6, 3.7 and 3.8. The appearance of characteristic band of C=N stretching at 1630 cm^{-1}, 1628 cm^{-1}, and 1628 cm^{-1} reveals the formation of O-COF, C-COF and CF_3-COF respectively.

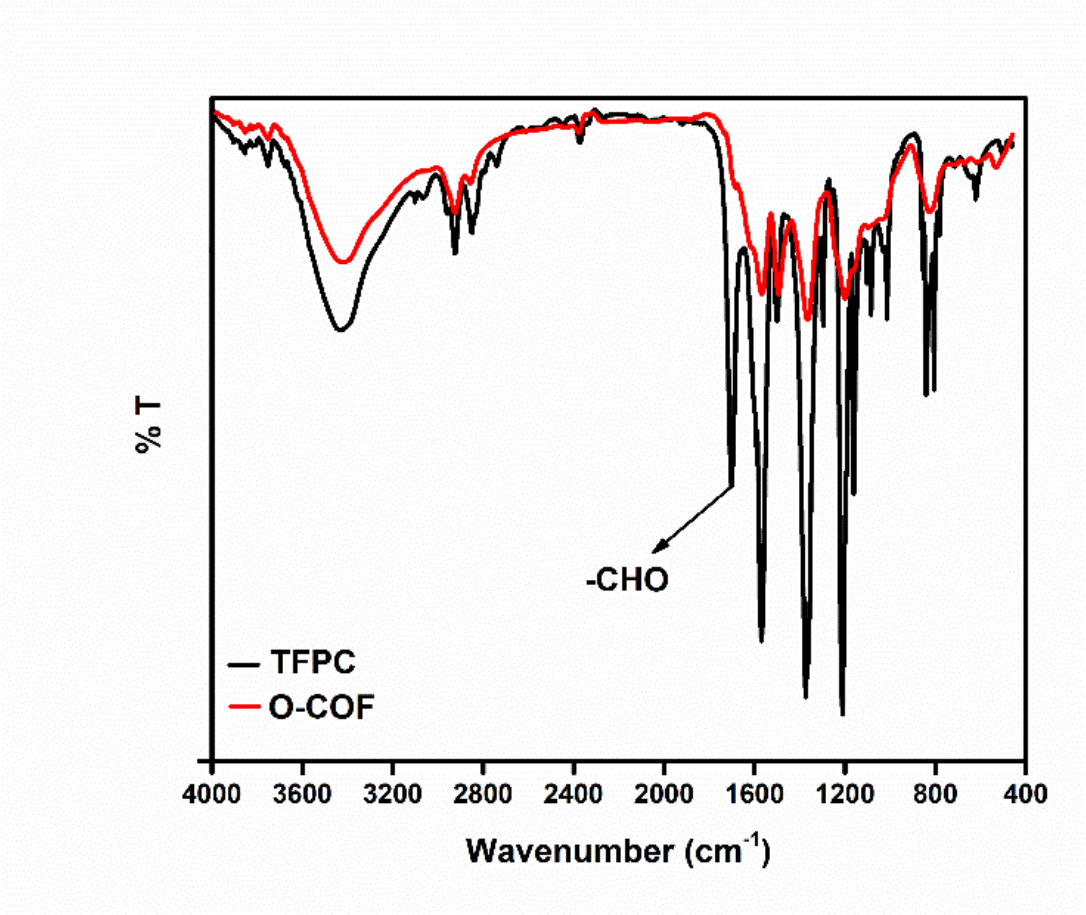

Figure 3.6. FTIR spectrum of **O-COF**.

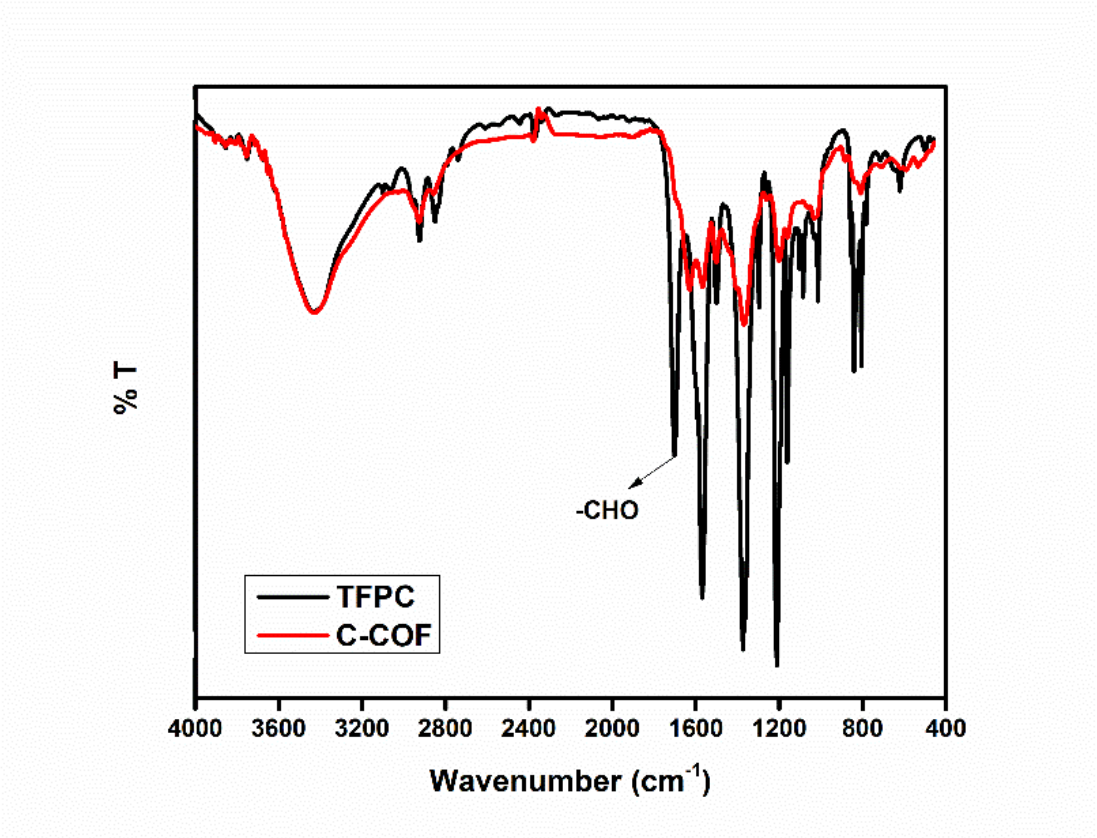

Figure 3.7. FTIR spectrum of **C-COF**.

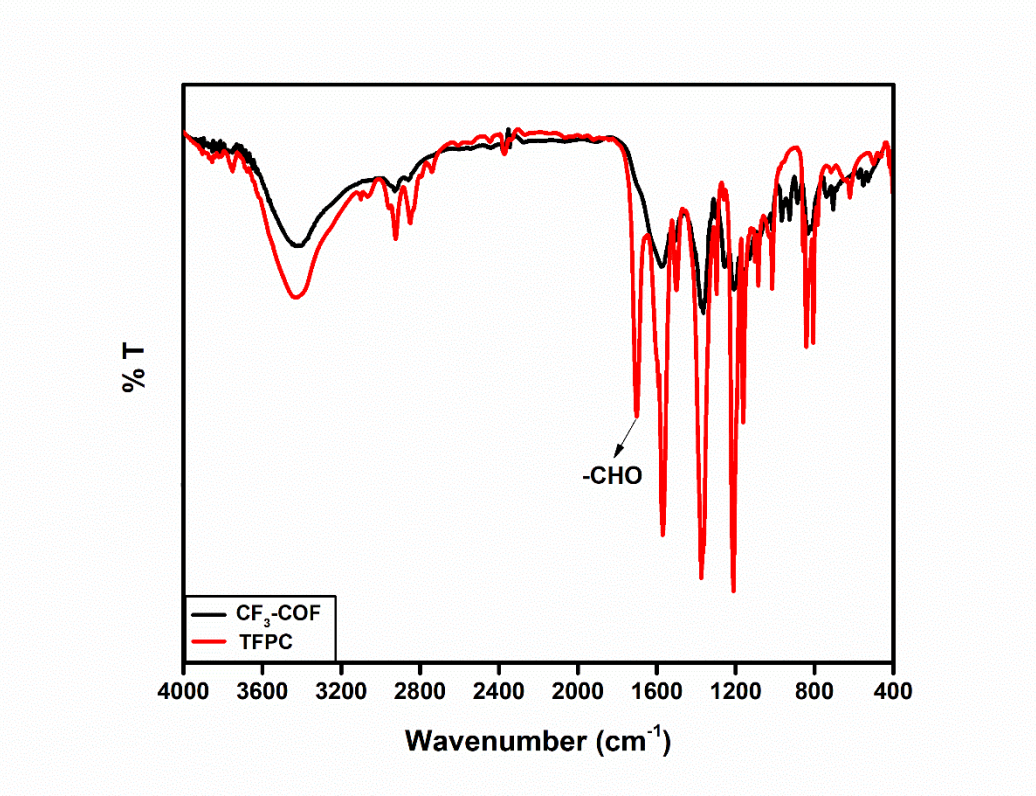

Figure 3.8. FTIR spectrum of **CF_3-COF**.

3.2.2.2 Structure Solution of COFs.

COFs were synthesized from flexible linkers; therefore, structure solution was a challenging task for us. First of all, WAXS spectra were recorded of as-synthesized O-COF, C-COF, and CF_3-COF. The powder diffraction pattern of O-COF and C-COF confirms the crystallinity of the synthesized frameworks. However, CF_3-COF does not show good crystallinity. Therefore, the structure solution was performed using O-COF (Figures 3.9 and 3.10) and C-COF (Figures 3.11 and 3.12). Bragg's equation ($2d\sin\theta = n\lambda$ where $n = 1$ and $\lambda = 0.154$ nm) was used to calculate the planes. In O-COF, diffraction peak appears at $2\Theta = 1.7°$, 8.4°, and 21.1°, which corresponds to the (100), (320), (001) facets, respectively. Similarly, in C-COF, diffraction peak appears at $2\Theta = 1.8°$, 4.9°, 8.5° and 21.1° that corresponds to (100), (210), (320) and (001) facets, respectively.

Generally, COFs synthesized from C_3 symmetric ligand and C_2 symmetric ditopic ligand shows a hexagonal structure. So, in order to check the structure of O-COF and C-COF, an extensive crystallographic analysis was accomplished by Pawley refinements (BIOVIA, Materials Studio 2017R2) using PXRD data of respective COFs. The PXRD data were indexed, and the X-cell program was used for fitting. Pawley refinement was used to determine the space group of both COFs. The figure represents the PXRD pattern (red line, experimental), Pawley refinement (blue line, simulated pattern), and reflection (green line) with minimum differences (black line) and the PXRD pattern (red line, experimental), Pawley refinement (black line, simulated pattern), and reflection (green line) with minimum differences (black line) for O-COF and C-COF, respectively. The fit was obtained with good Rp = 1.01% and Rwp = 1.52% for O-COF and Rp = 0.35% and Rwp = 0.60% for C-COF. The structure solution of O-COF and C-COF was done by Pawley refinement in the space group *P*6/m with unit cell parameters: a = b = 48.05 Å, c = 6.75 Å, $\alpha = \beta = 90°$, $\gamma = 120$ and a = b = 47.98 Å, c = 6.73 Å, $\alpha = \beta = 90°$, $\gamma = 120$, respectively.

Eclipsed structure (AA) and staggered structures (AB and ABC) were optimized using the DFT-D calculation (CASTEP method) using the hexagonal system, and simulated PXRD patterns were generated for AA, AB and ABC structures. A comparison of simulated and experimental PXRD patterns shows that both O-COF and C-COF have good agreement with the AA stacking structure. The peak (100) tells about the crystallinity and order network in the framework. The high-intensity peak of O-COF at (100) indicates that O-

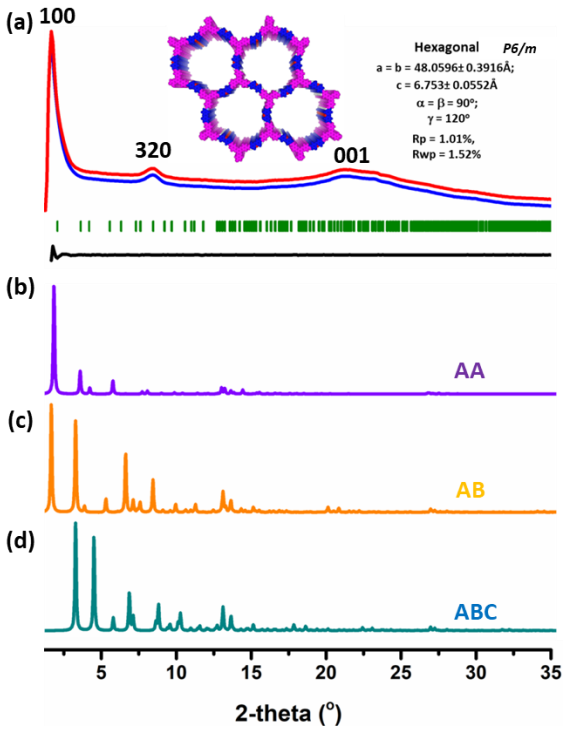

Figure 3.9. The structure analysis of **O-COF**: (a) Pawley refinement (simulated, blue line), the PXRD pattern (experimental, red line) of O-COF that is showing minimum difference (small black line) with Rwp and Rp of 1.01% and 1.52%, respectively. (b) Simulated PXRD pattern with space group *P6/m* for the AA structure (violet), (c) AB structure (orange), and (d) ABC structure (cyan).

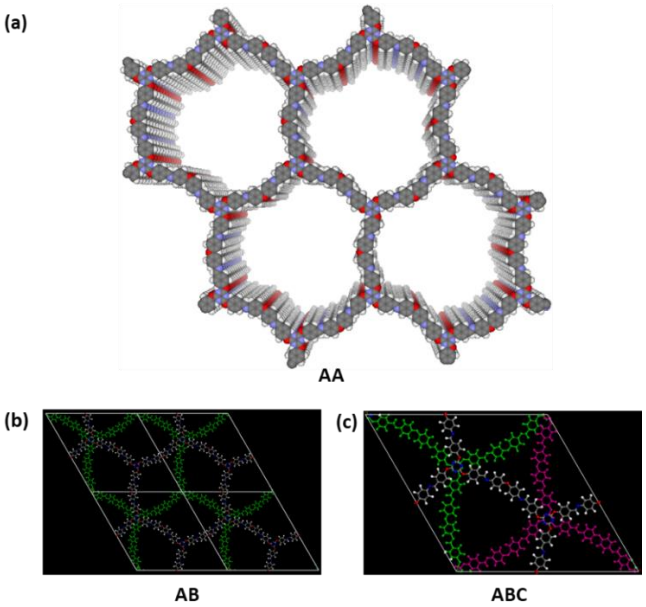

Figure 3.10. (a) AA structure of **O-COF**. (b) AB structure of O-COF. (c) ABC structure of O-COF. The structure colour code used here - carbon: gray, oxygen: red, nitrogen: violet, hydrogen: yellow.

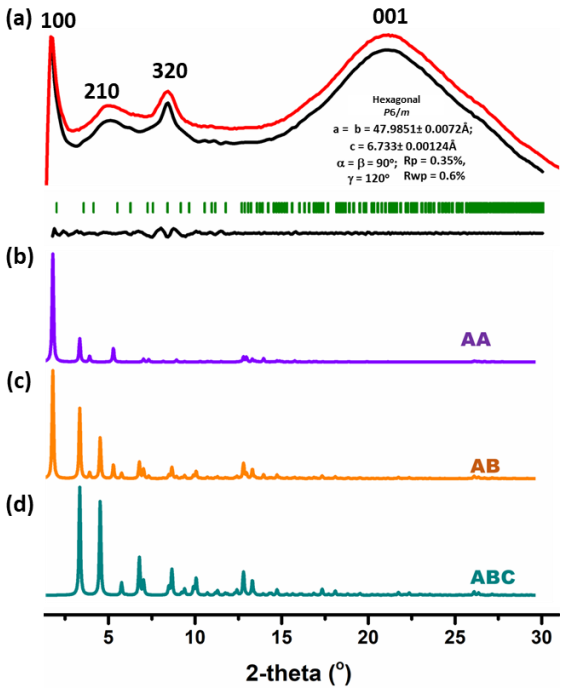

Figure 3.11. The structure analysis of **C-COF**: (a) Pawley refinement (simulated, black line), the PXRD pattern (experimental, red line) of C-COF that is showing minimum difference (small black line) with Rwp and Rp of 0.35% and 0.6%, respectively. (b) Simulated PXRD pattern with space group *P6/m* for the AA structure (violet), (c) AB structure (orange), and (d) ABC structure (cyan).

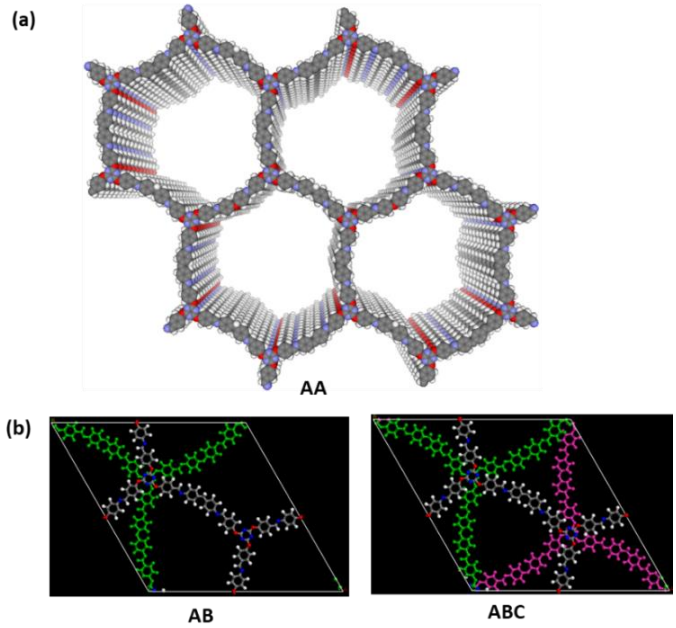

Figure 3.12. (a) AA structure of **C-COF**. (b) AB structure of C-COF. (c) ABC structure of C-COF. The structure colour code used here - carbon: gray, oxygen: red, nitrogen: violet, hydrogen: yellow.

COF is more crystalline than C-COF. This result indicates that the high electronegativity Oxygen atom plays a crucial role to provide better crystallinity than C-COF and CF_3-COF.

3.2.2.3 Thermogravimetric Analysis

TGA profiles of O-COF, C-COF and CF_3-COF are shown in Figures 3.13, 3.14 and 3.15. The results suggest that O-COF are stable upto 270ºC, C-COF stable up to 300 ºC, and CF_3-COF upto 250 ºC. At these temperatures a significant weight loss attributes to decomposition of imine and ether linkages. It shows good thermal stability up to 300 ºC which is very useful in high temperature applications.

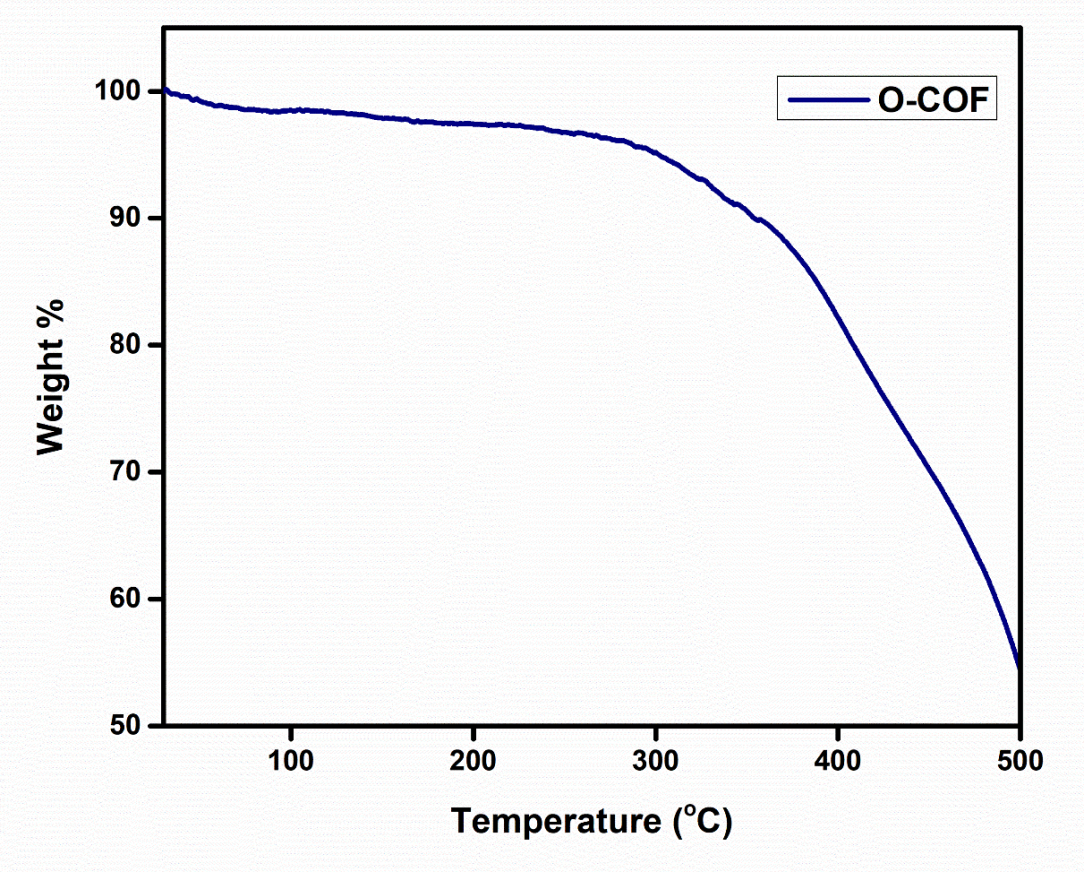

Figure 3.13. TGA profile of **O-COF**.

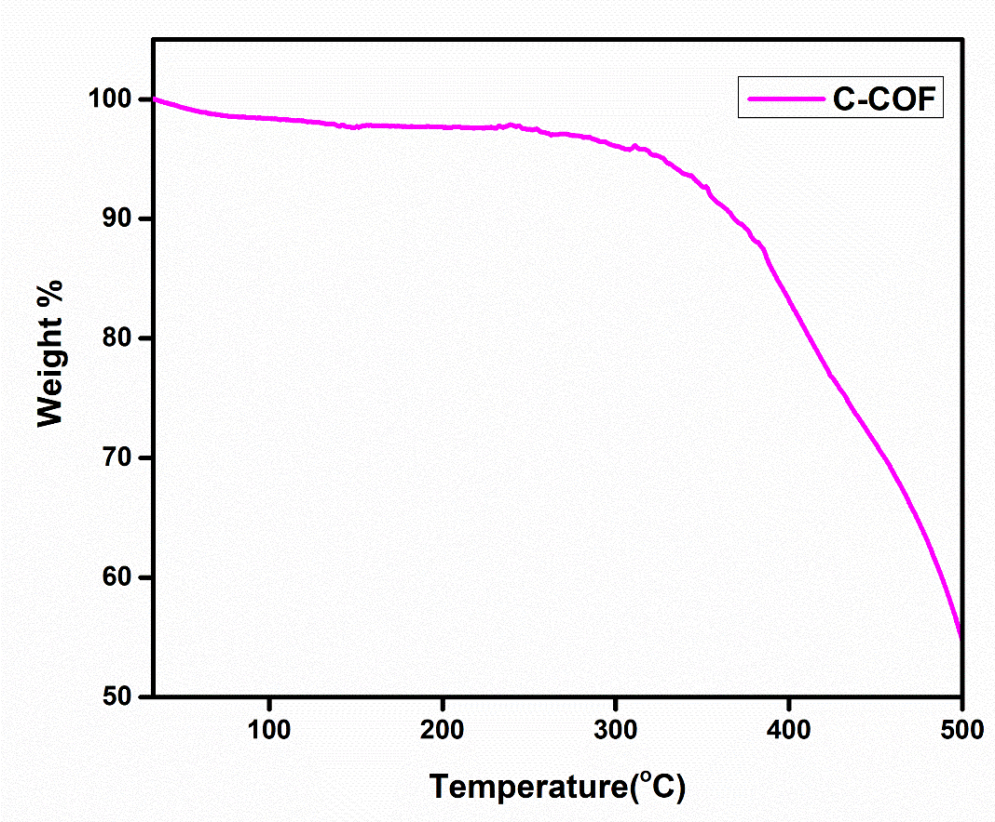

Figure 3.14. TGA profile of **C-COF**.

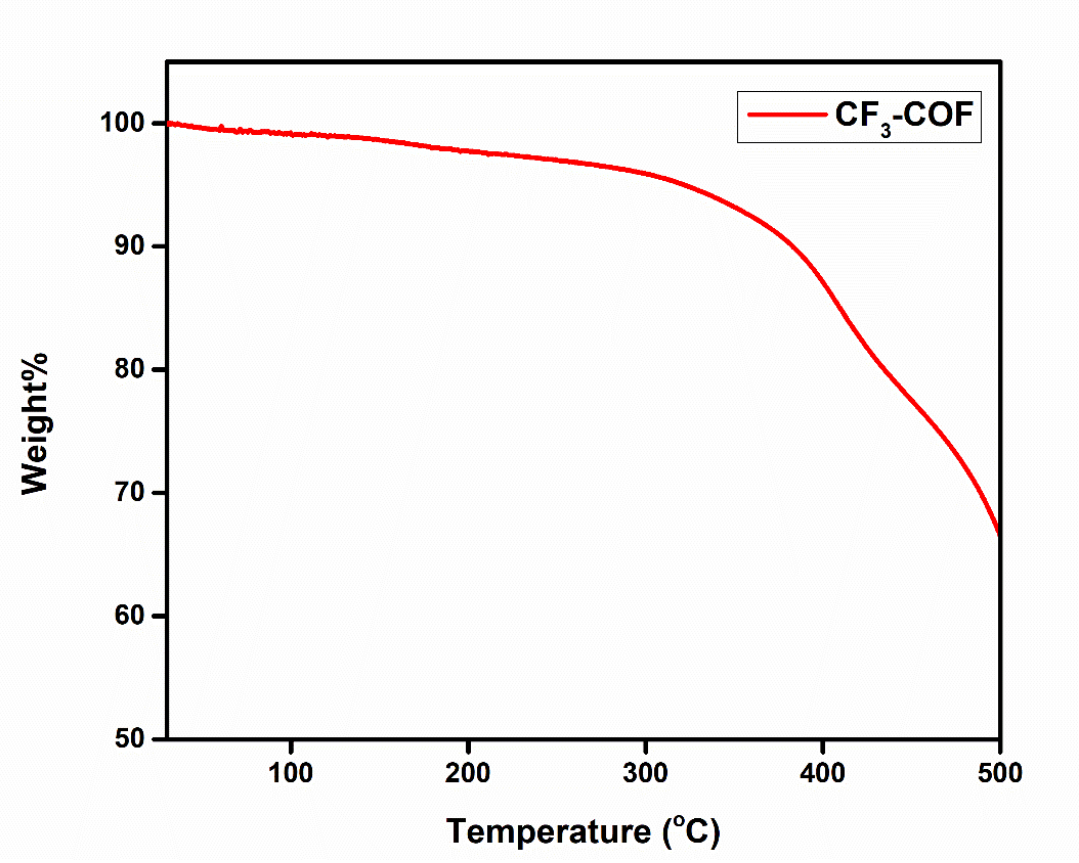

Figure 3.15. TGA profile of **CF_3-COF**.

3.2.2.4 Solid State Reflectance Spectrum

The electronic and optical properties of the synthesized COFs have been investigated by using Diffuse Reflectance Spectroscopy. The optical bandgap of O-COF, C-COF and CF_3-COF was calculated from the optical diffuse reflectance spectra (Figures 3.16, 3.17 and 3.18). Tauc plot derived from the diffuse reflectance spectrum was plotted using the equation is shown below:

$$(\boldsymbol{\alpha h\nu})^2 = \boldsymbol{A}\,(\boldsymbol{h\nu} - \boldsymbol{E_g})$$

where, h = Planck's constant,

ν = the photon's frequency,

A = proportionality constant,

E_g = Band gap,

α = absorbance value

After plotting the graph between ($h\nu$) and $(\alpha h\nu)^2$, the bandgap was determined by linear extrapolation of an indirect Tauc plot. The calculated band gap from the plot is 2.73, 2.80, and 2.93 for O-COF, CF_3-COF, and C-COF respectively.

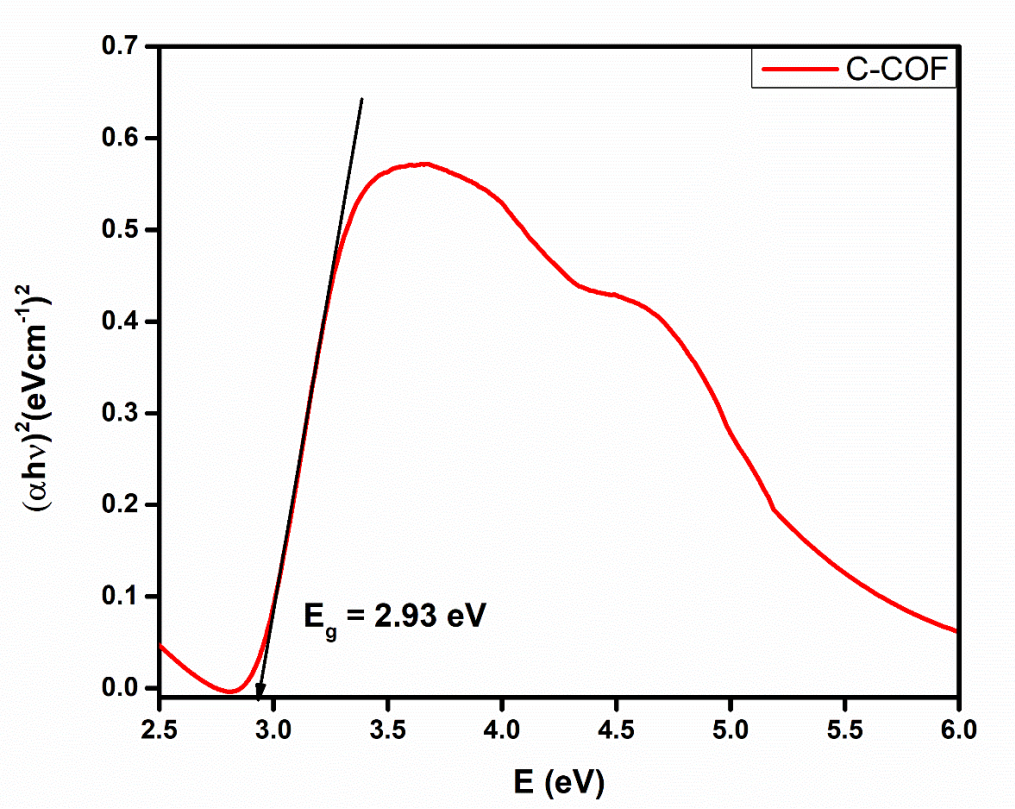

Figure 3.16. Solid state reflectance spectrum of **C-COF**.

The E_g value indicates synthesized COFs exhibit semiconducting properties. The less value of bandgap of O-COF attributed to the presence of oxygen atom in comparison with CF_3-COF and C-COF. Oxygen is an electronegative atom and increases the conjugation that reduces the HOMO and LUMO gap.

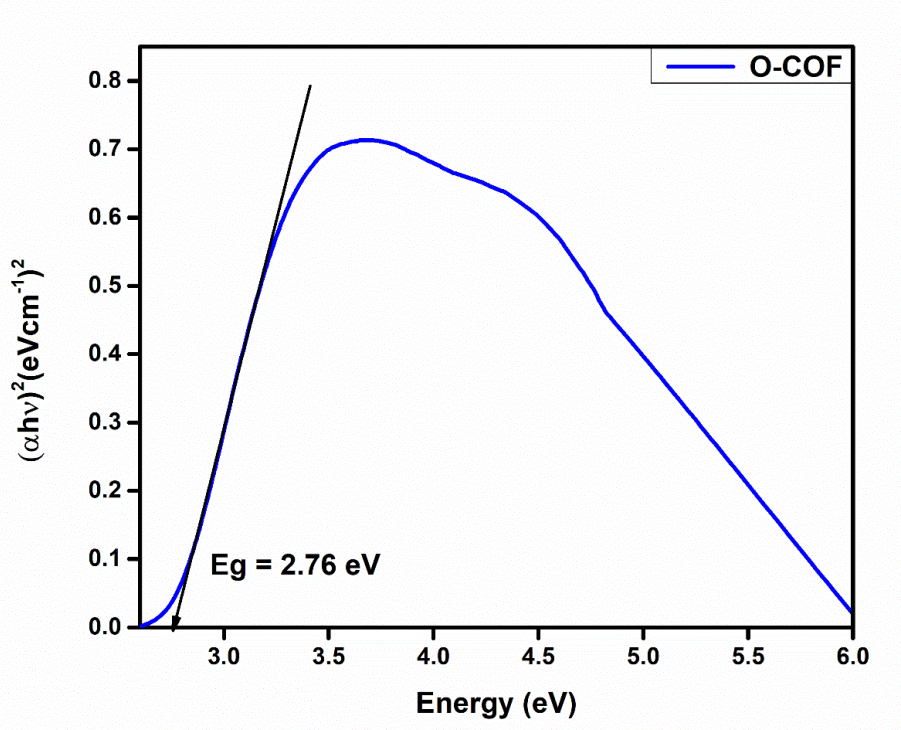

Figure 3.17. Solid state reflectance spectrum of **O-COF**.

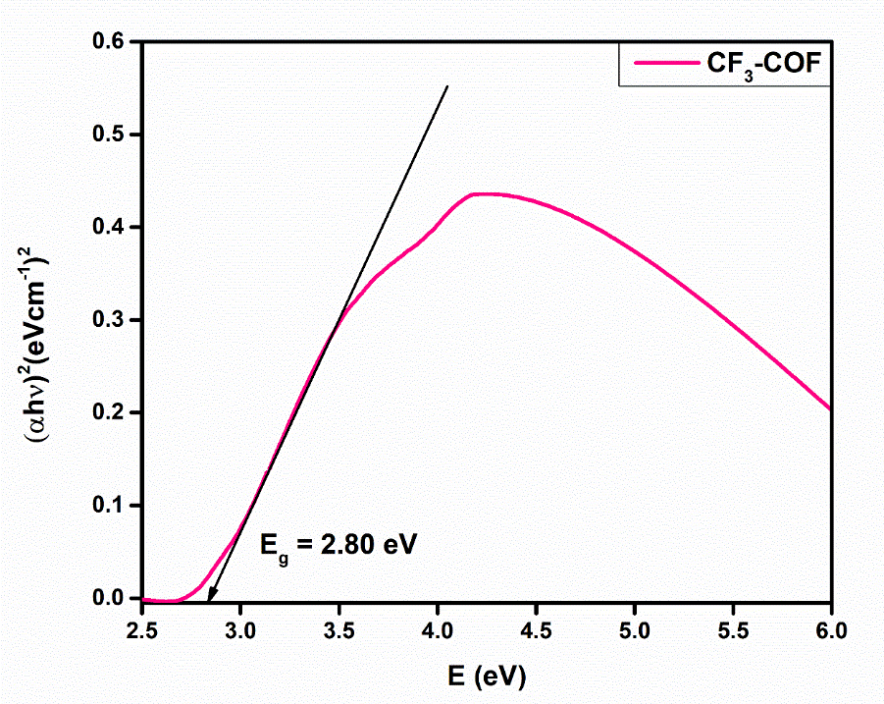

Figure 3.18. Solid state reflectance spectrum of **CF_3-COF**.

3.2.2.5 Solid-state NMR spectroscopy

The solid-state cross-polarization magic angle spinning NMR spectrum of O-COF, C-COF and CF_3-COF was recorded and efficient construction of all COFs was confirmed by showing characteristic signal at 153.8, 154.2 and 154.3 ppm which corresponds to imine bond in C-COF, O-COF and CF_3-COF, respectively. The peak at 173 ppm is due to carbon present in the triazine ring in all the Solid-State NMR spectrum. The spectrum of O-COF, C-COF and CF_3-COF exhibit total 10, 11 and 12 signals from 80-180, 20-180 and 40-220 ppm range, respectively. All the peaks are assigned to the corresponding carbon and shown in Figures 3.19, 3.20 and 3.21 for O-COF, C-COF and CF_3-COF, respectively.

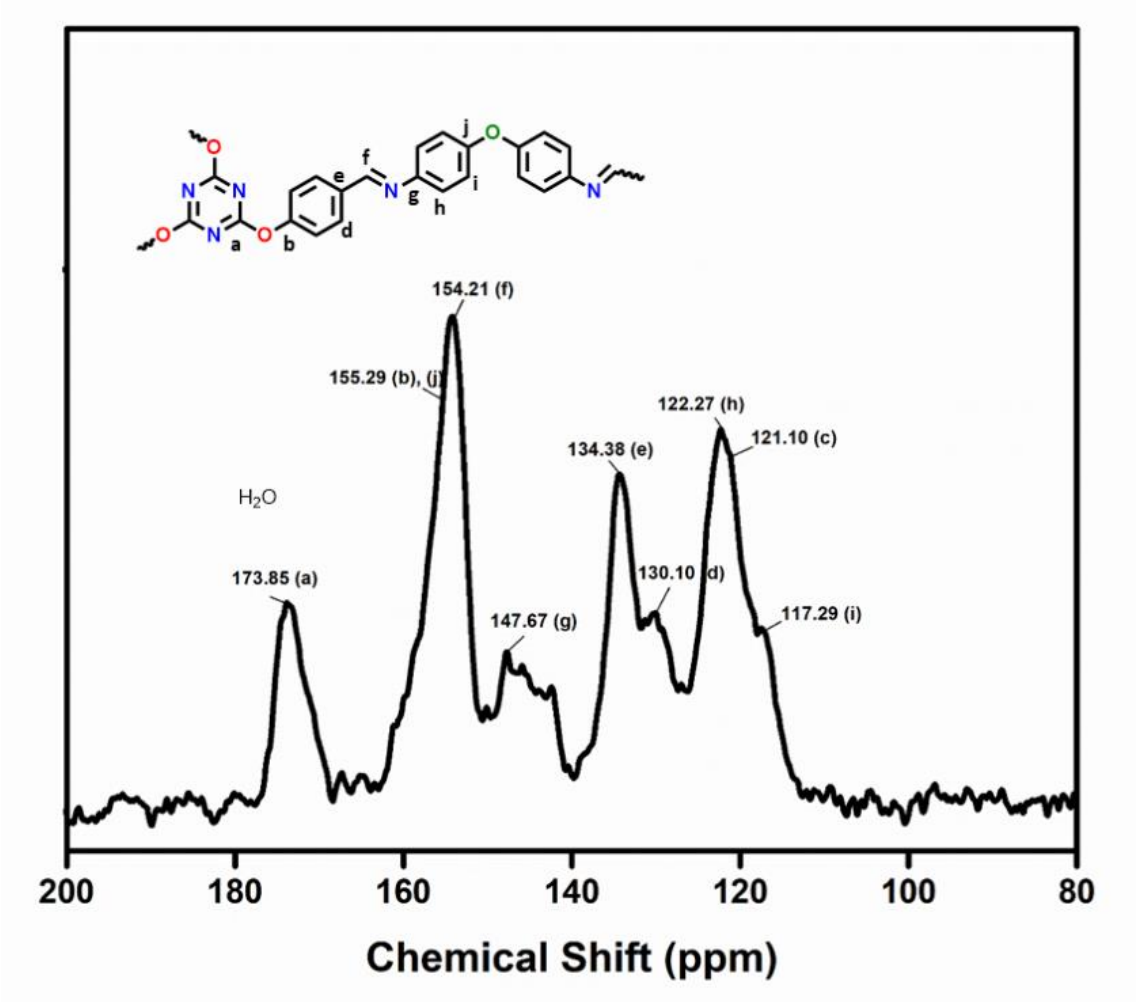

Figure 3.19. ^{13}C CP/MAS NMR spectrum of **O-COF**.

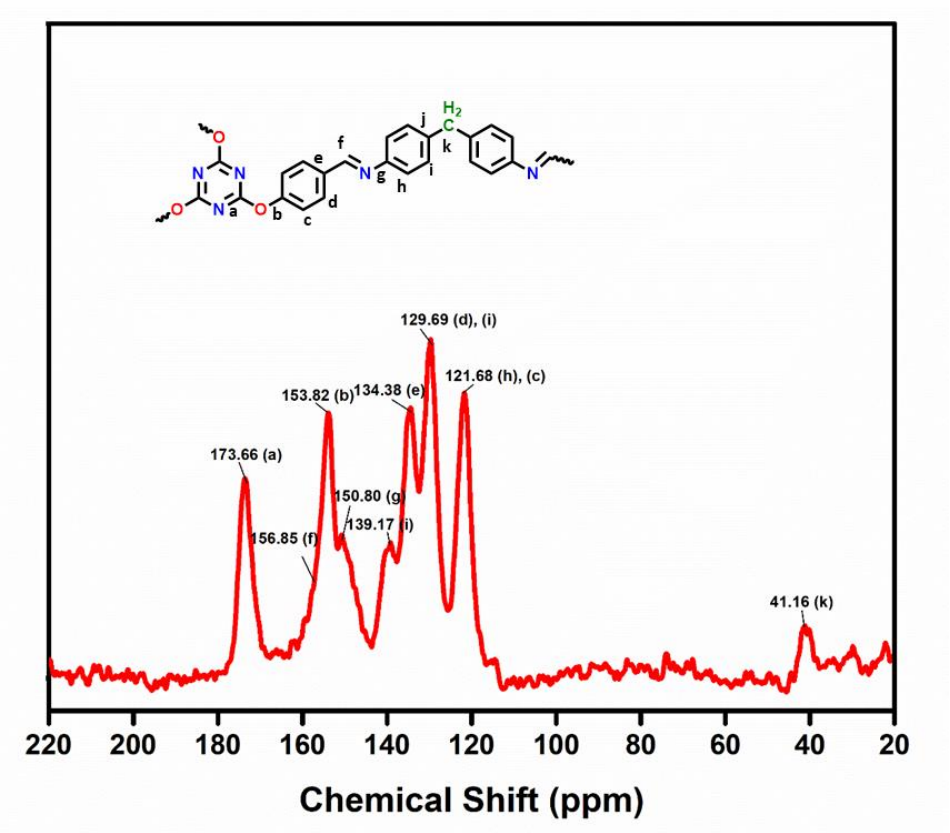

Figure 3.20. ^{13}C CP/MAS NMR spectrum of **C-COF**.

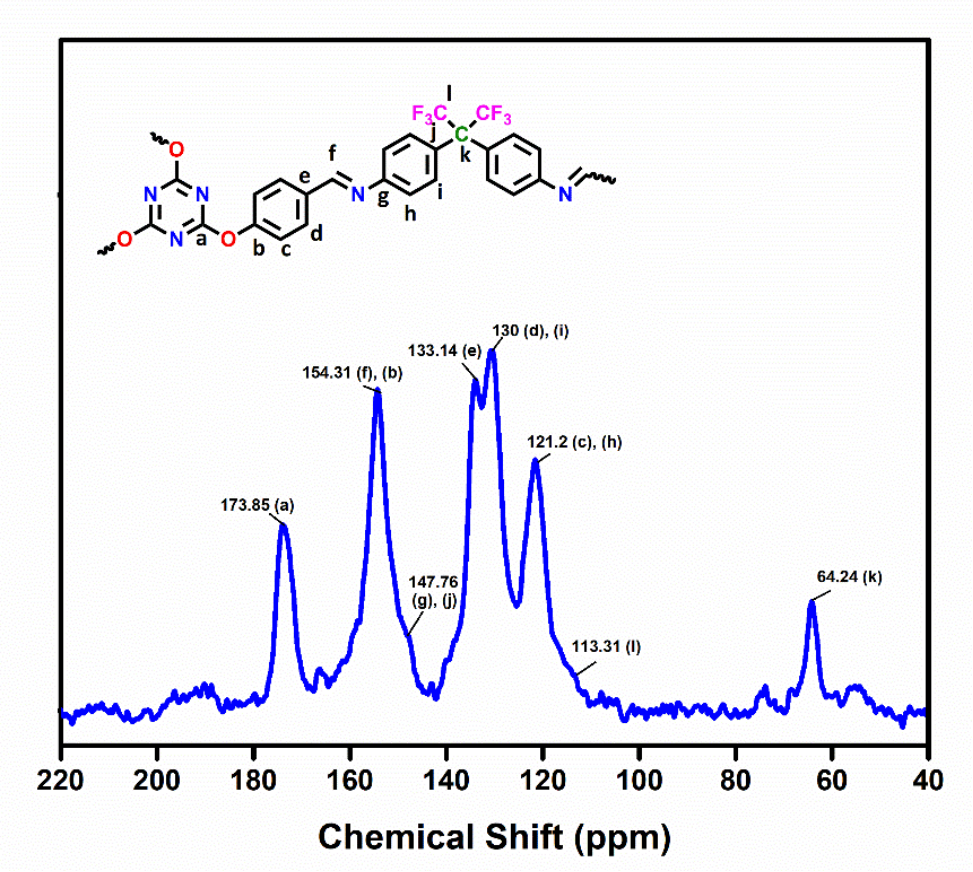

Figure 3.21. ^{13}C CP/MAS NMR spectrum of **CF_3-COF**.

3.2.2.6 Field Emission Scanning Electron Microscopy (FESEM) Study

FESEM was used to investigate the surface morphology of the synthesized COFs. FESEM images are shown in the Figure 3.22. The FESEM image of O-COF with 1 μm scale shows that it exhibits very beautiful microtubular morphology with 0.18 μm hollow tubes. C-COF shows spherical morphology which are uniformly distributed. The size of the spheres around 2-5 nm. CF_3-COF exhibits gauzy shaped morphology which was formed from spherical-partials CF_3-COF. The wires of the gauze are around 690-700 nm. The images are shown in 1μm scale.

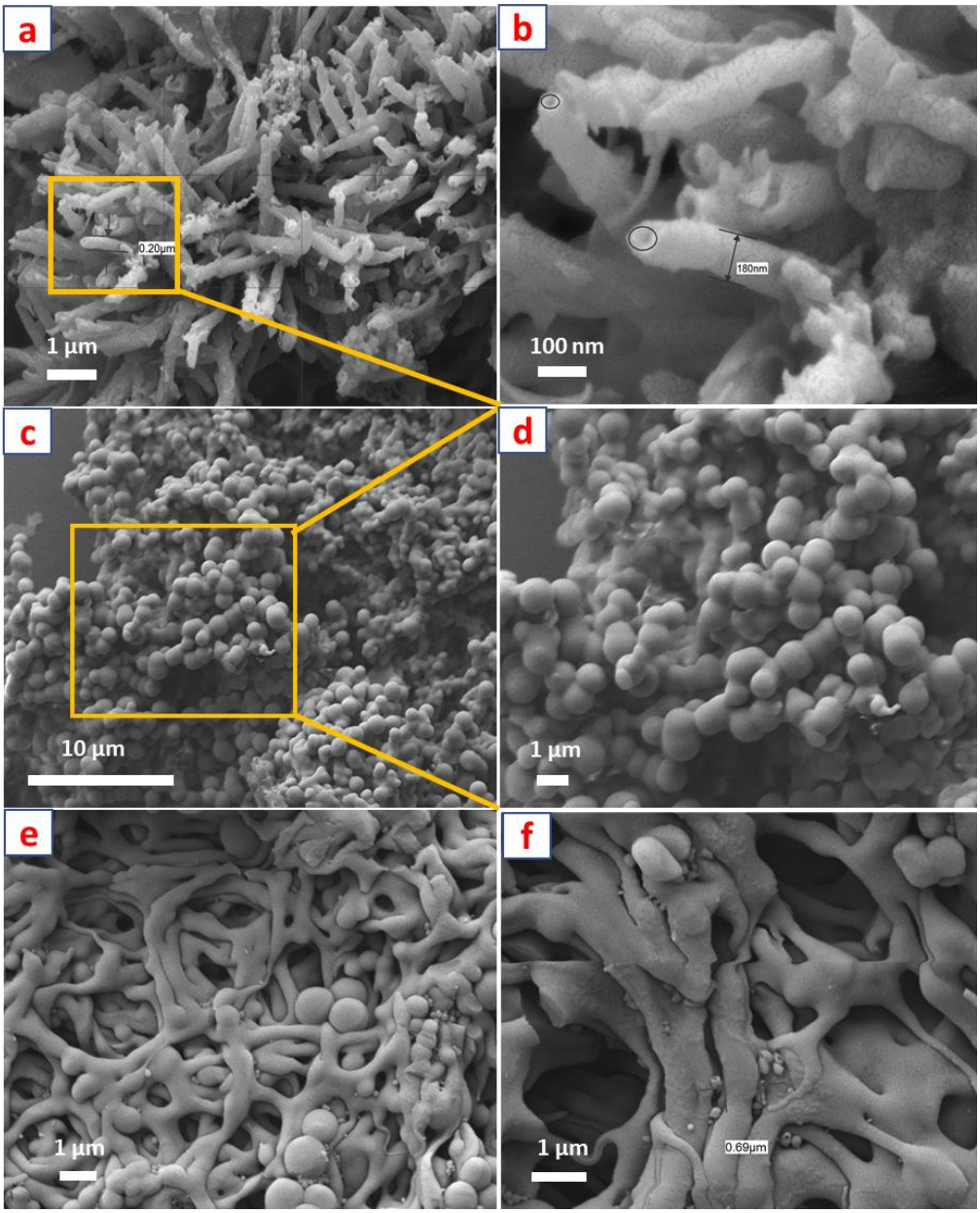

Figure 3.22. Morphology analysis: (a) and (b) FESEM images of **O-COF**. (c) and (d) FESEM images of **C-COF**. (e) and (f) FESEM images of **CF_3-COF**.

3.2.2.7 Gas sorption study

The sorption study of O-COF and C-COF was performed at different temperature such as N_2 sorption at 77 K (Figures 3.23 and 3.24) and CO_2 at 298, 273, 263 K (Figures 3.25 and 3.26).

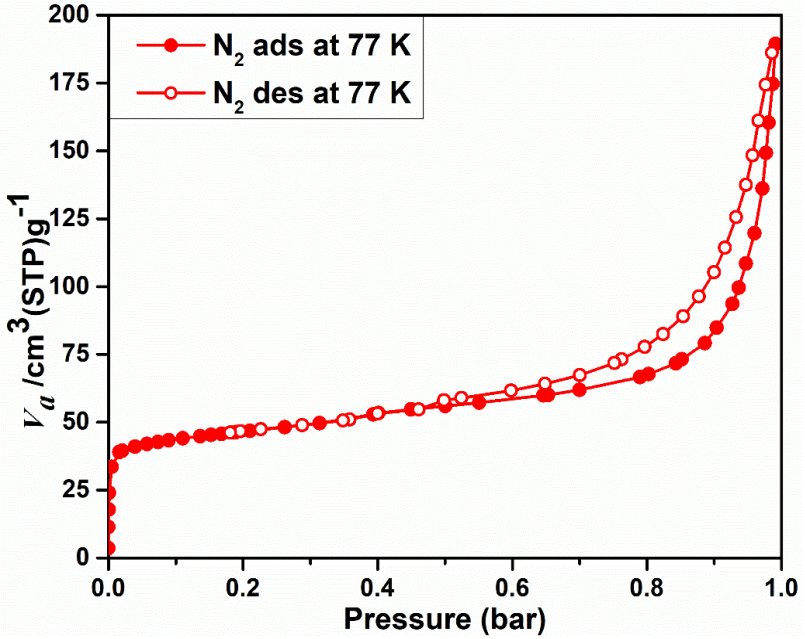

Figure 3.23. N_2 sorption isotherm of **O-COF** at 77 K**.** (Filled and open symbols represent adsorption and desorption, respectively).

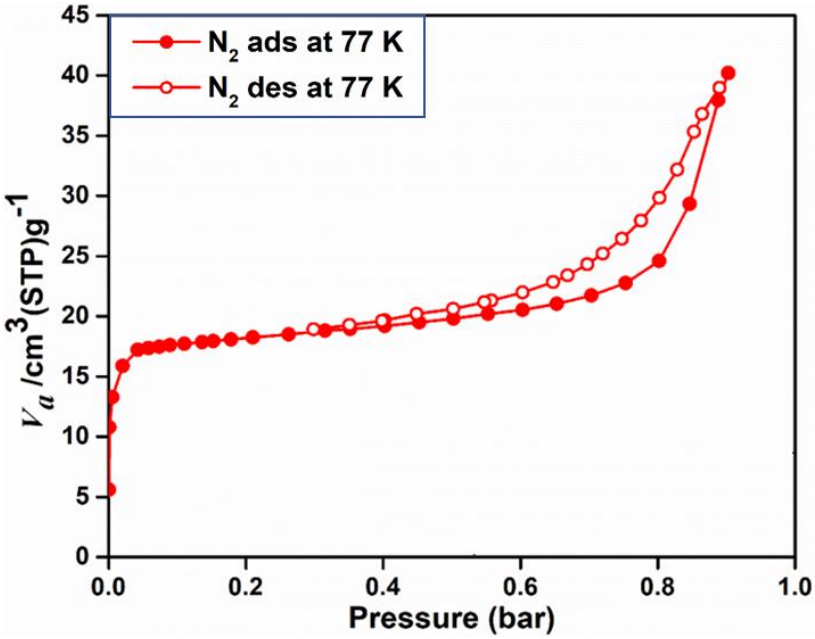

Figure 3.24. N_2 sorption isotherm of **C-COF** at 77 K. (Filled and open symbols represent adsorption and desorption, respectively)

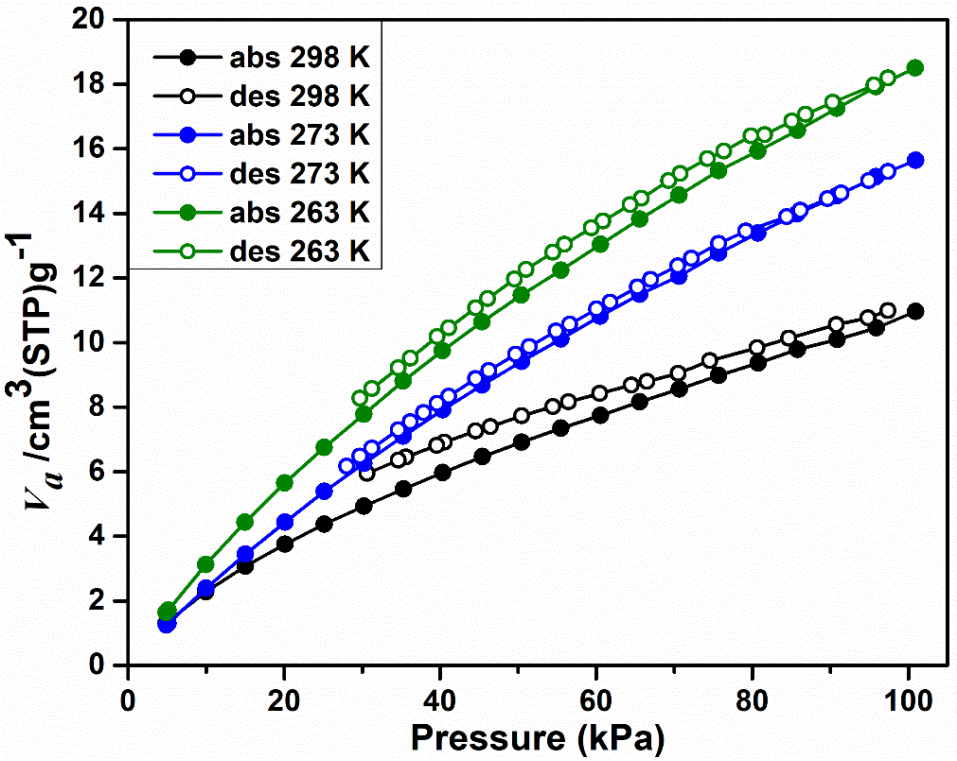

Figure 3.25. CO_2 sorption isotherms of **O-COF** at 298, 273 K and 163 K. (Filled and open symbols represent adsorption and desorption, respectively)

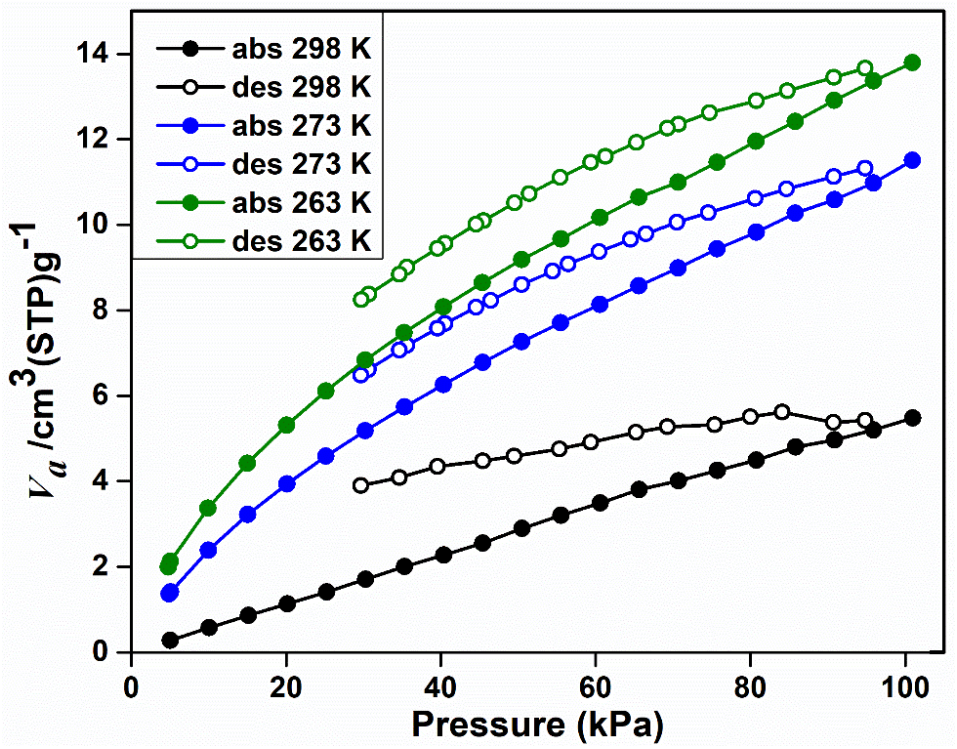

Figure 3.26. CO_2 sorption isotherms of **C-COF** at 298, 273 K and 163 K. (Filled and open symbols represent adsorption and desorption, respectively)

Both the COFs shows a mixture of type I and type IV reversible isotherm for N_2 at 77 K. After comparing N_2 isotherm, it was observed that O-COF has good porosity as compared to C-COF.

3.2.3 Growth Study of COFs

Surface analysis of all three COFs were investigated using FESEM and TEM ((Figures 3.27, 3.28 and 3.29). O-COF shows very beautiful hollow microtubular morphology. Although this is a flexible COF, it was really a challenge for us to make attractive COF. Thus, we were very much interested to study its formation. For this purpose, reactions at different time scale to understand the nucleation and the growth of COFs. During this time, the morphology was investigated using FESEM and TEM.

For the study, four different reactions are being done at same conditions but different time scales: 12 h, 24 h, 48 h, and 72 h. After each reaction the product was washed and dried completely. After drying, FESEM and TEM images were taken for individual product. In the case of O-COF, images after 12 h, indicated the formation of spherical agglomerated morphology. For the time being, the shape of the spheres is increased which was shown in Figure 3.29 (c) and (d) that was taken after 24 h. The spheres start opening up like flowers and converting into hollow tubular shaped as shown in the figure 3.29 (e) and (f). TEM image of O-COF after a reaction of revels that spheres are converting into hollow tubes. After a complete reaction, this shows full formation of microtubes which is confirmed by FESEM and TEM images (Figure 3.29). Morphology was also investigated for 5 days reaction which shows no further change in the morphology of O-COF. The same experiments were done with C-COF and CF_3-COF, but in the case of C-COF, morphology does not change much (Figure 3.27).

CF_3-COF shows small spherical particles after 12 h of reaction. FESEM image after 24 h shows that small particles are coming closer and start joining (Figure 3.28). Further, image after, 48 h indicates that CF_3-COF form a gauzy structure with joining small spheres. Finally, SEM image after 72 h shows no change in the morphology. After comparing SEM image of all three COFs, morphology wise O-COF is much more predominant and it was fully studied in terms of morphology using FESEM and TEM. The proposed mechanism of the formation of hollow tubular O-COF are shown in the Figure 3.30.

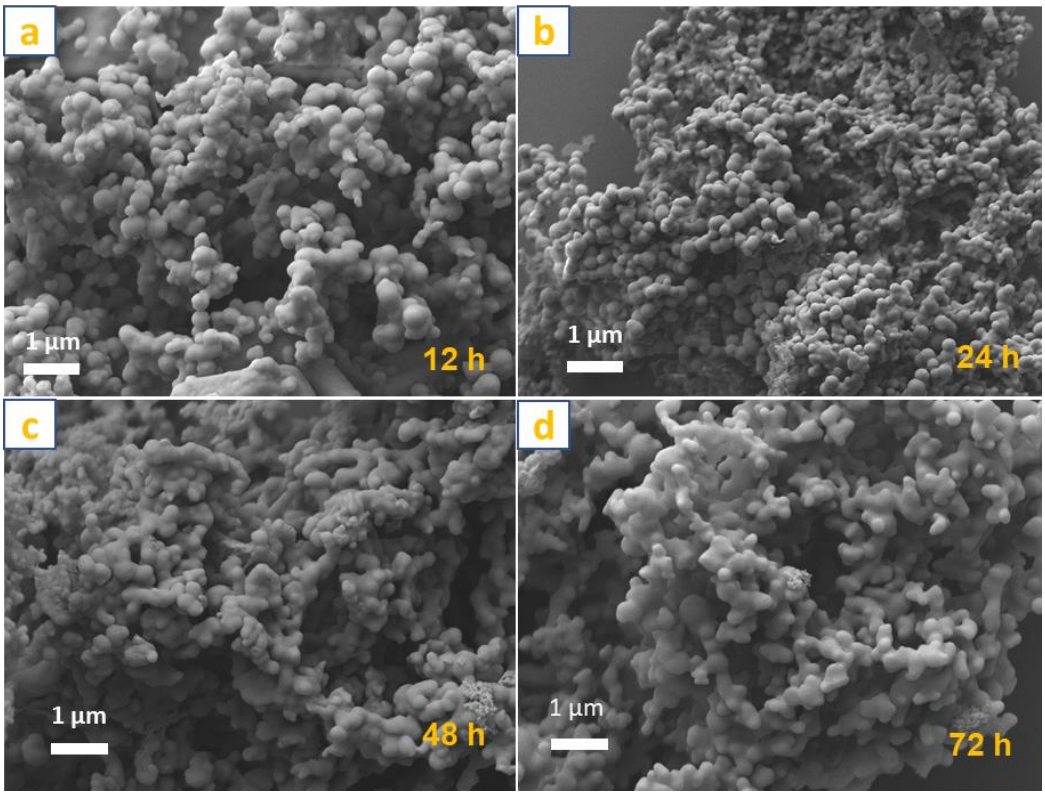

Figure 3.27. FESEM images of **C-COF** recorded at different time intervals: FESEM image taken after (a) 12 h, (b) 24 h, (c) 48 h, (d) 72 h.

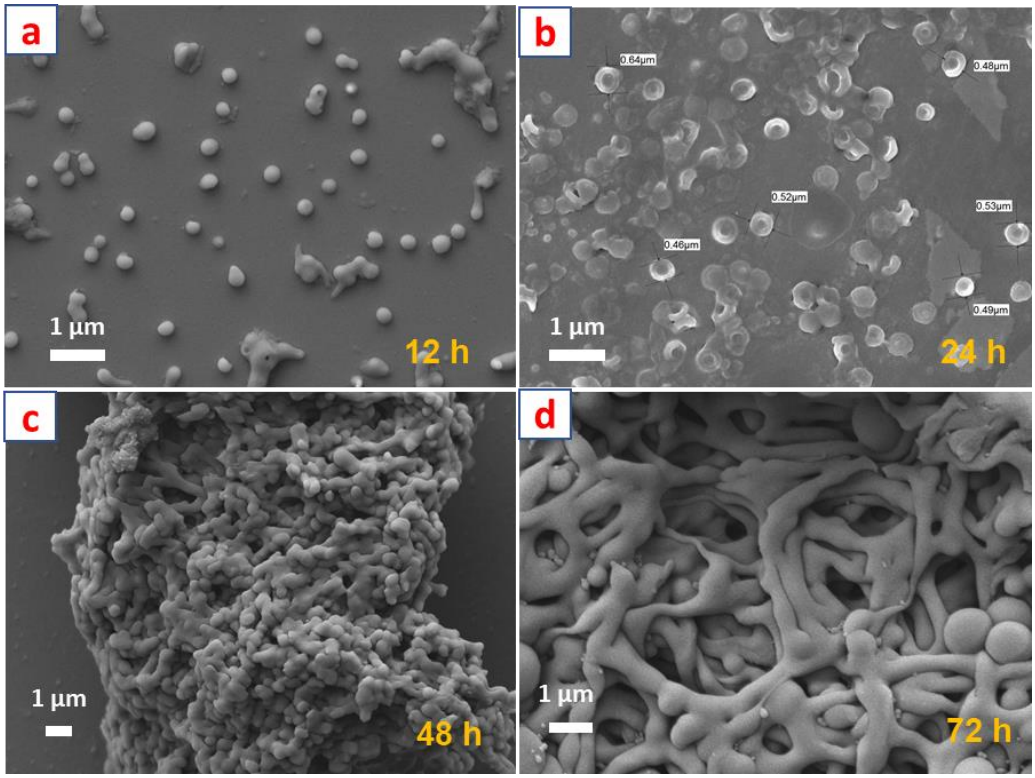

Figure 3.28. FESEM images of **CF_3-COF** recorded at different time intervals: FESEM image taken after (a) 12 h, (b) 24 h, (c) 48 h, (d) 72 h.

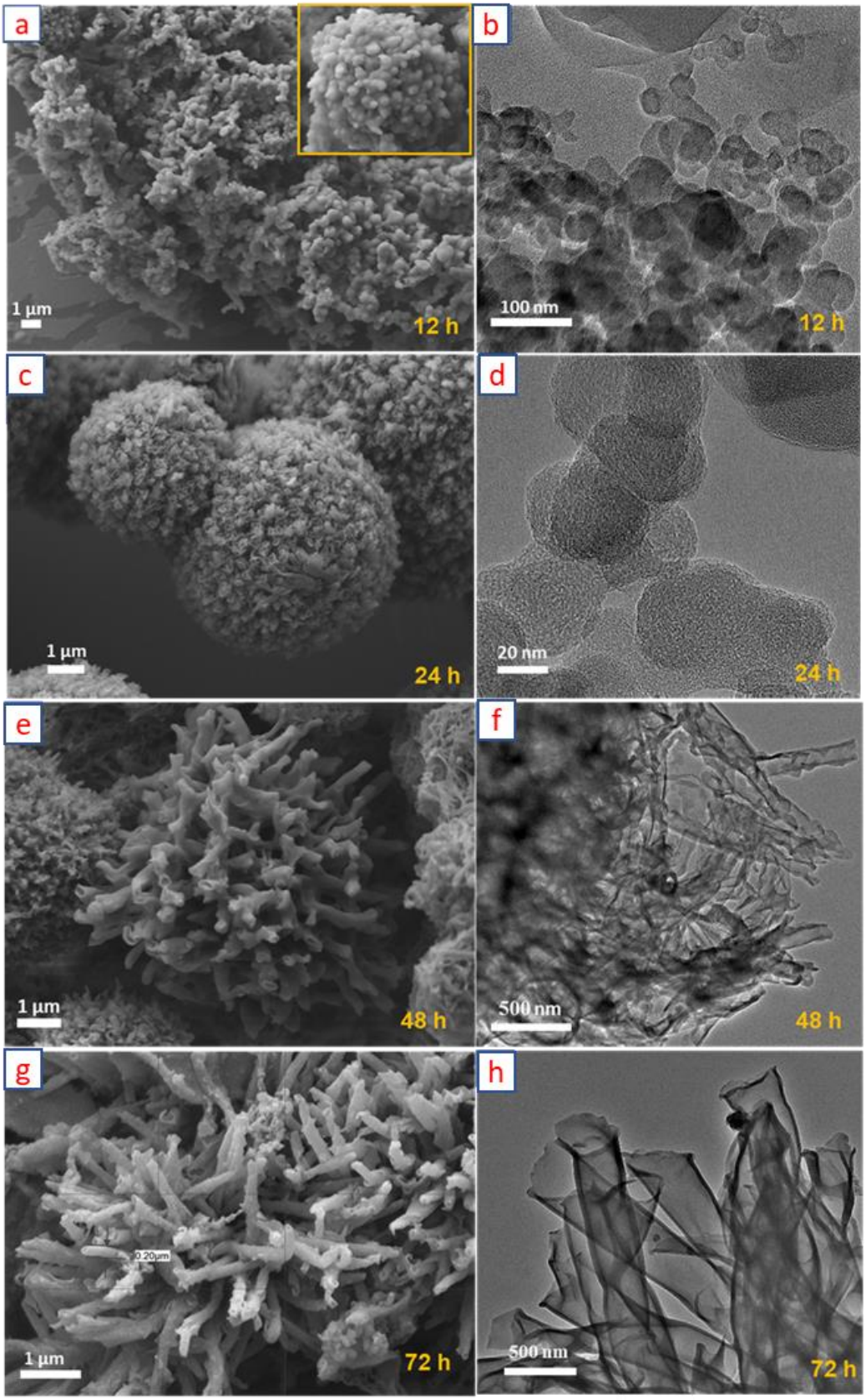

Figure 3.29. Growth study of **O-COF**: FESEM and TEM images of **O-COF** recorded at different time intervals. FESEM image taken after (a) 12 h, (c) 24 h, (e) 48 h, (g) 72 h. TEM image taken after (b) 12 h, (d) 24 h, (f) 48 h, (h) 72 h.

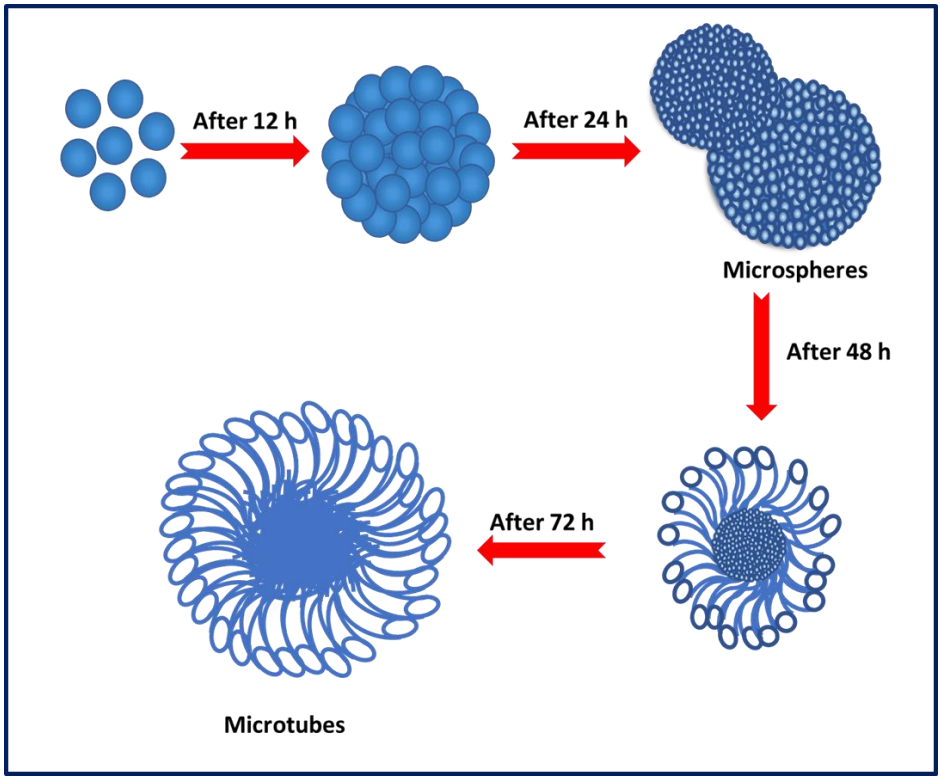

Figure 3.30. Proposed mechanism of the formation of hollow tubular **O-COF.**

3.2.4 Application: Water Purification

Since O-COF has hollow tumbler morphology, it is a potential candidate which can be used to adsorb any analyte inside the tube based on the interaction with the groups or atoms present in the COF. In upcoming decades, it is key challenge to access clean water that contains a complex range of organic pollutants which includes organic dyes, oils and other chemicals. So, it is necessary to find some solution to clean this. Based on the morphology and present requirement of the society synthesized O-COF was used in dye removal and separation from water. First of all, we have tested the stability of O-COF in water. The solid sample was put in water for 10 days, then, it was filtered, dried and PXRD pattern was recorded. The peak corresponds to plane (100) retained in the spectra which suggests that O-COF is stable in water (Figure 3.31). Having good stability in water, the dye adsorption experiments were performed using extensively, and commercially used dye solutions: Rhodamine B (RhB), Methyl orange (MO), sodium fluorescein (FL), Methylene blue (MB) and Methylene green (MG) (Figure 3.32). The freshly prepared dye solution and O-COF was used in the experiment which was immersed in the water solution of the respective dyes at room temperature. The quantitative analysis of the concentration of the dyes was

measured using UV-Vis spectrophotometer in every 10 minutes of interval during the uptake process (Figures 3.33- 3.37).

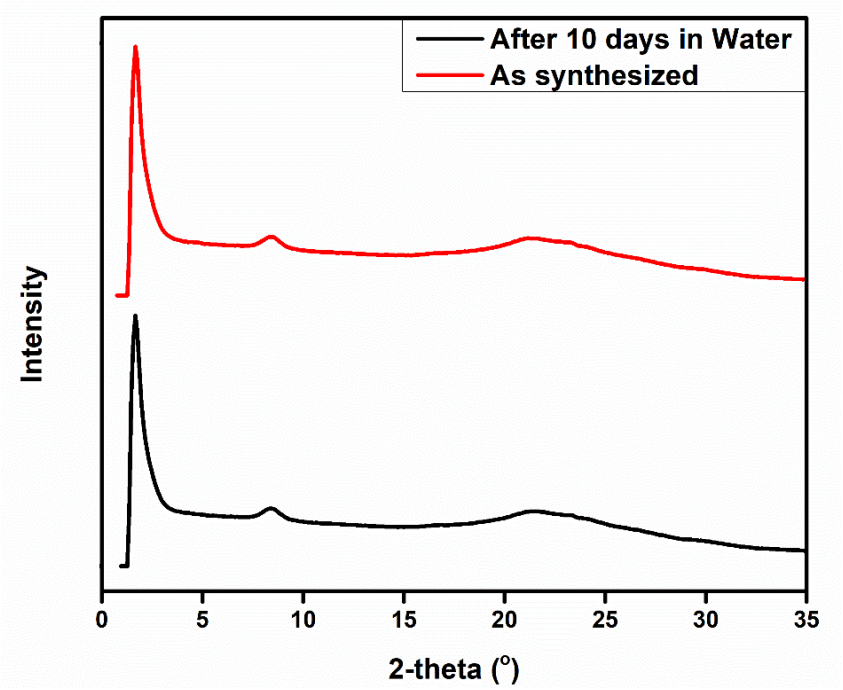

Figure 3.31. PXRD pattern of **O-COF** before and after putting 10 days in water.

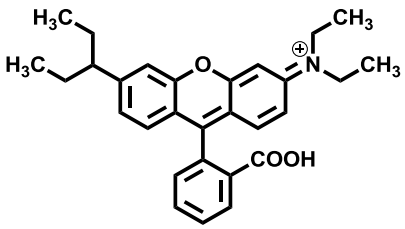

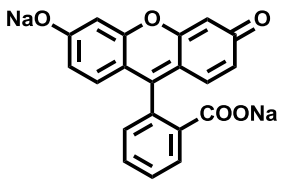

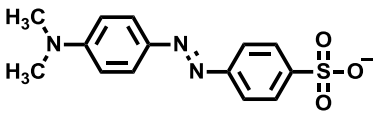

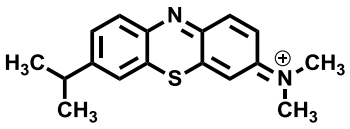

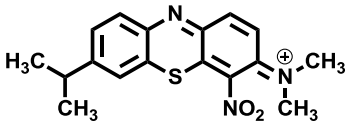

Figure 3.32. Molecular structure of organic pollutants used in the application.

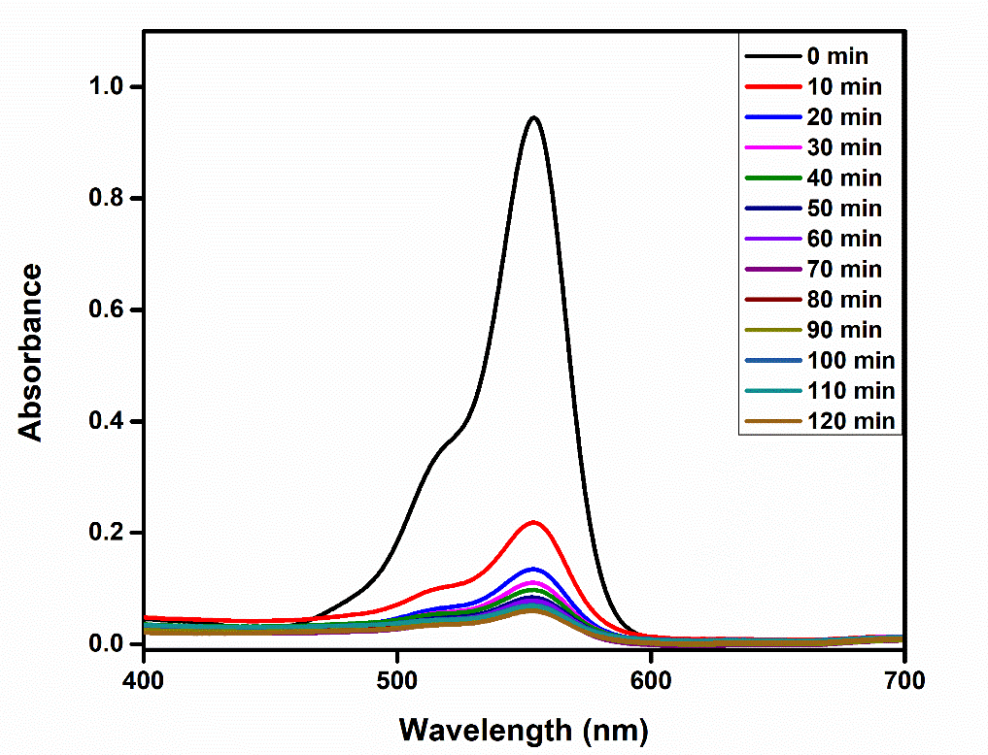

Figure 3.33. UV-Vis spectra of aqueous solution of cationic RhB dye in the presence of **O-COF** after different time intervals.

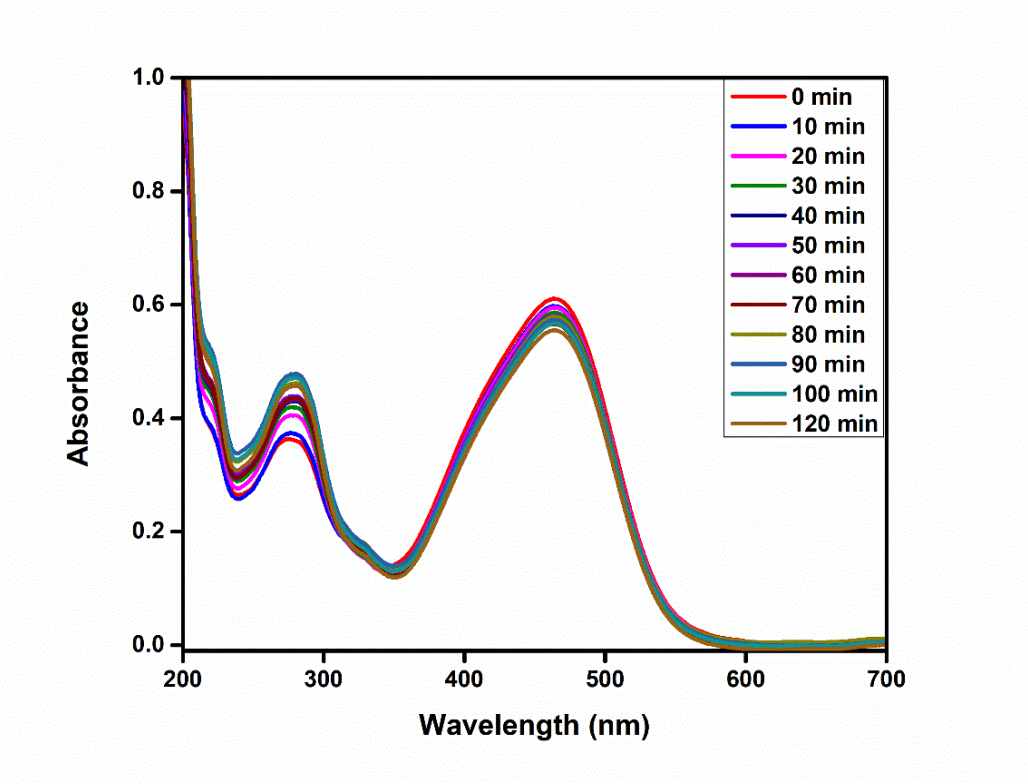

Figure 3.34. UV-Vis spectra of aqueous solution of anionic MO dye in the presence of **O-COF** after different time intervals**.**

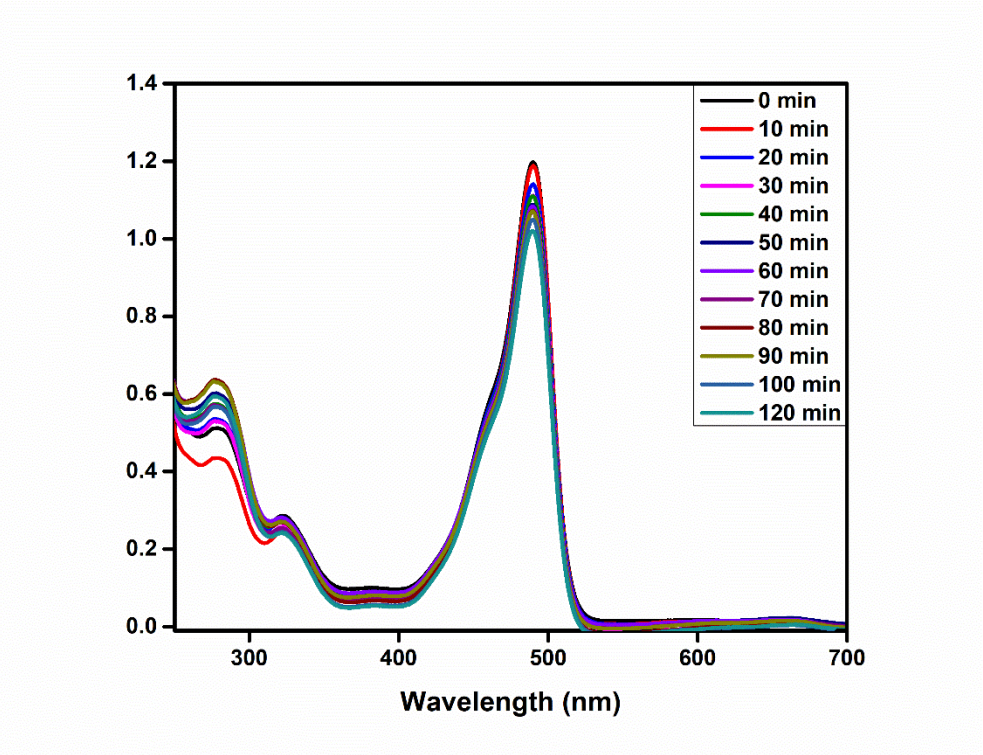

Figure 3.35. UV-Vis spectra of aqueous solution of anionic FL dye in the presence of **O-COF** after different time intervals**.**

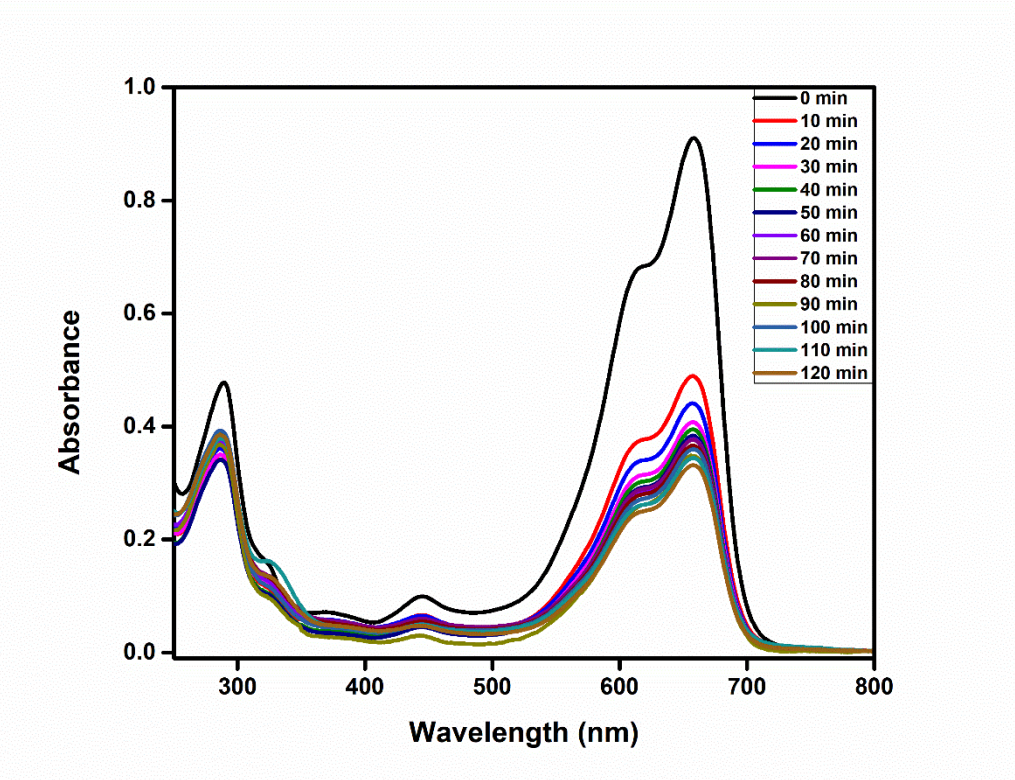

Figure 3.36. UV-Vis spectra of aqueous solution of cationic MG dye in the presence of **O-COF** after different time intervals**.**

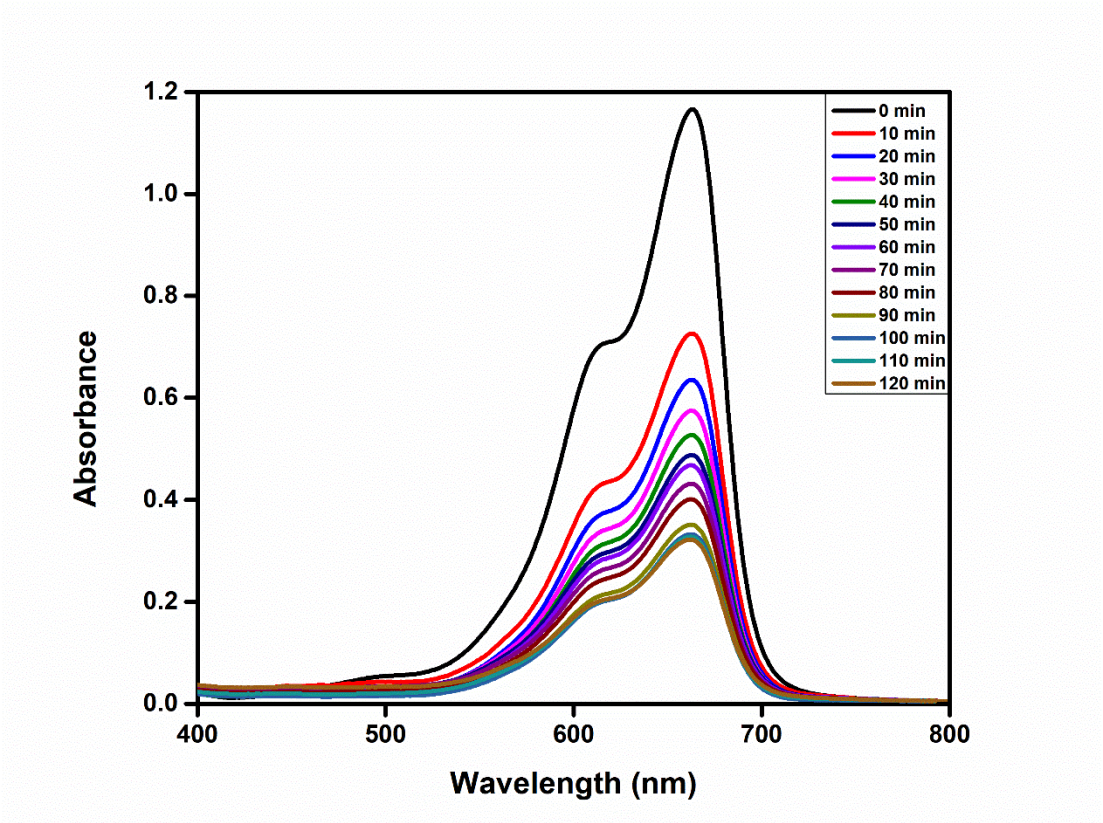

Figure 3.37. UV-Vis spectra of aqueous solution of cationic MB dye in the presence of **O-COF** after different time intervals**.**

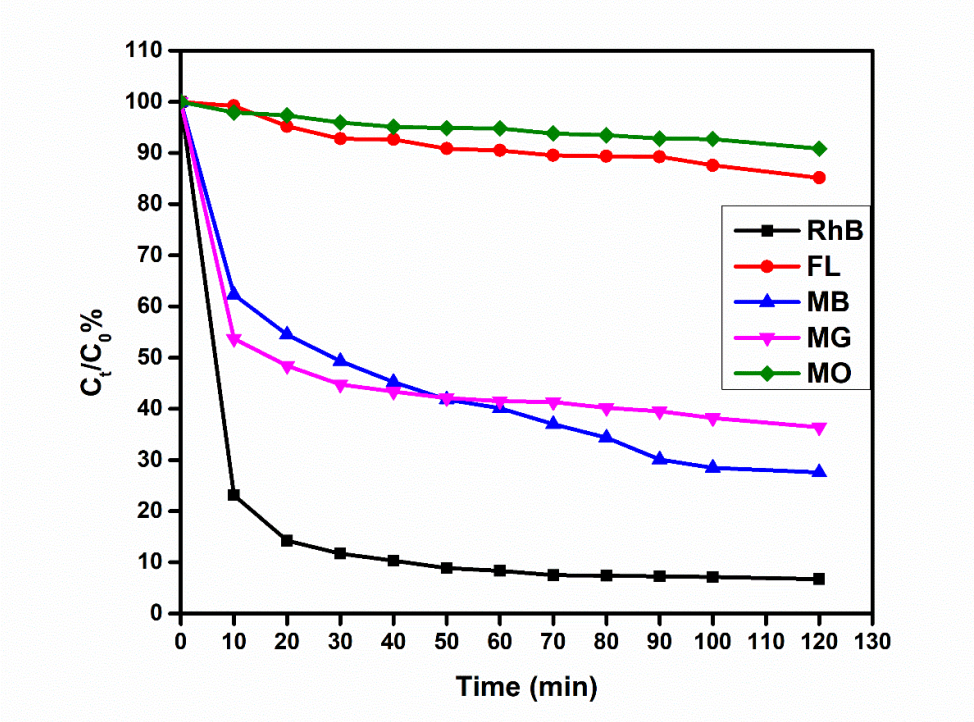

Figure 3.38. % dyes removal using **O-COF.**

After analysing uptake of various dyes from water, it was observed that mainly cationic dyes are getting adsorbed by the O-COF. Figure 3.38 shows that 93.3% of RhB, 14.85% of

FL, 72.43% of MB, 63.59% of MG and 9.16% of MO dyes were taken up within 120 minutes. The highest and the least uptake of RhB and FL was further elaborately experimented by performing competitive experiment of adsorption of the mixture of RhB and FL dye solution on O-COF (8 mg/L each) as shown in Figures 3.39. The concentration was measured by the same method as that for the single dye solution.

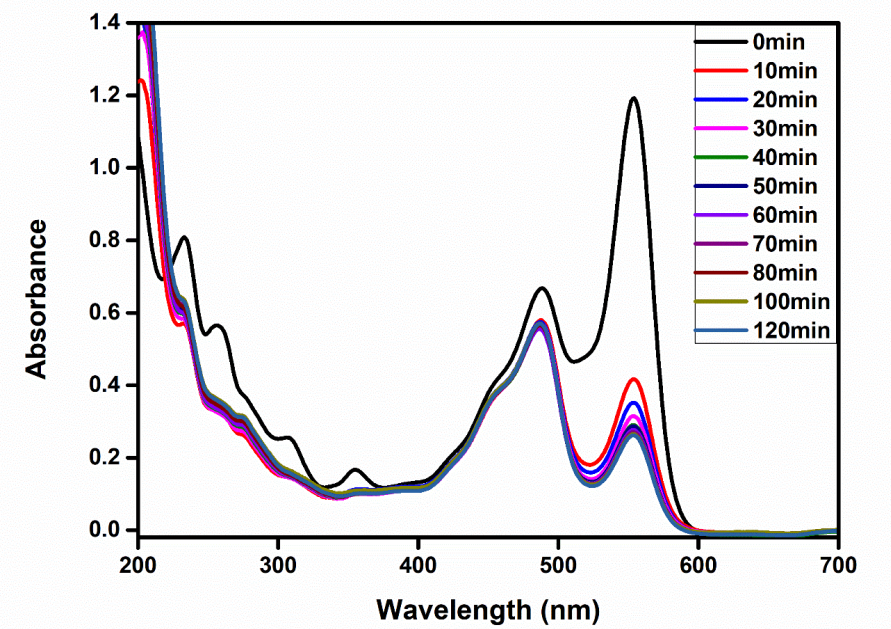

Figure 3.39. Selective adsorption of RhB from its aqueous mixture of FL (anionic dye) and RhB (cationic dye) using **O-COF.**

After seeing the results, we envisioned that O-COF can be used as stationary phase for liquid chromatography to separate cationic and anionic dyes. This chromatography can also be used to remove dyes from waste water. A prototype was made by using a column where O-COF powder was used as stationary phase and an equimolar mixture of FL and RhB dye solution (8 mg/L each) was used as an eluent (Figure 3.40). The prototype shows efficient separation of RhB (cationic) and FL (anionic) dye. To our best knowledge this is the first report when COF was used as stationary phase material to separate dyes.

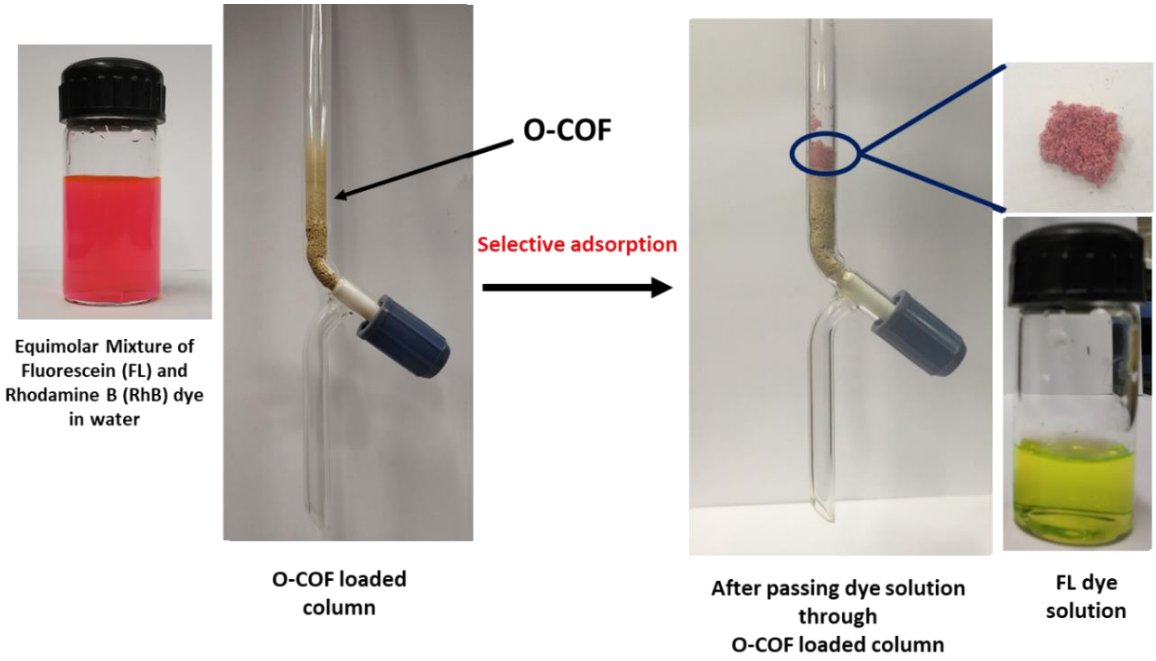

Figure 3.40. Use of **O-COF** as stationary phase material for liquid chromatography to selective separation of RhB dye.

When the solution was passed through the column, O-COF only allows the FL dye solution to pass through from the column. RhB dye was adsorbed by the COF. To understand more visual, photographs were taken in interval of 10 seconds during the separation process (Figure 3.41). The initial red colour solution lastly transforms into apple green after the selective adsorption and the initial yellow brown O-COF powder colour was transformed into red colour.

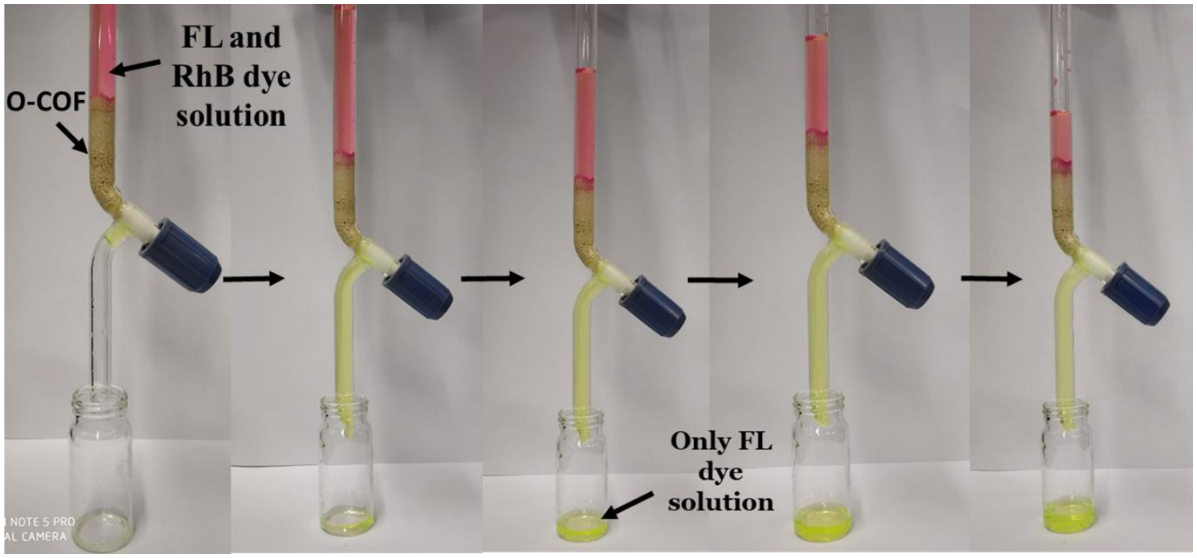

Figure 3.41. Selective RhB dye adsorption with time during separation process.

For the confirmation of efficient separation, UV-Vis spectrum of mixture of dyes solution was recorded before and after the separation from column (Figure 3.42). From the spectra, it was observed that there is no content of RhB in the solution after the separation that confirms the effective separation of FL dye from RhB dye.

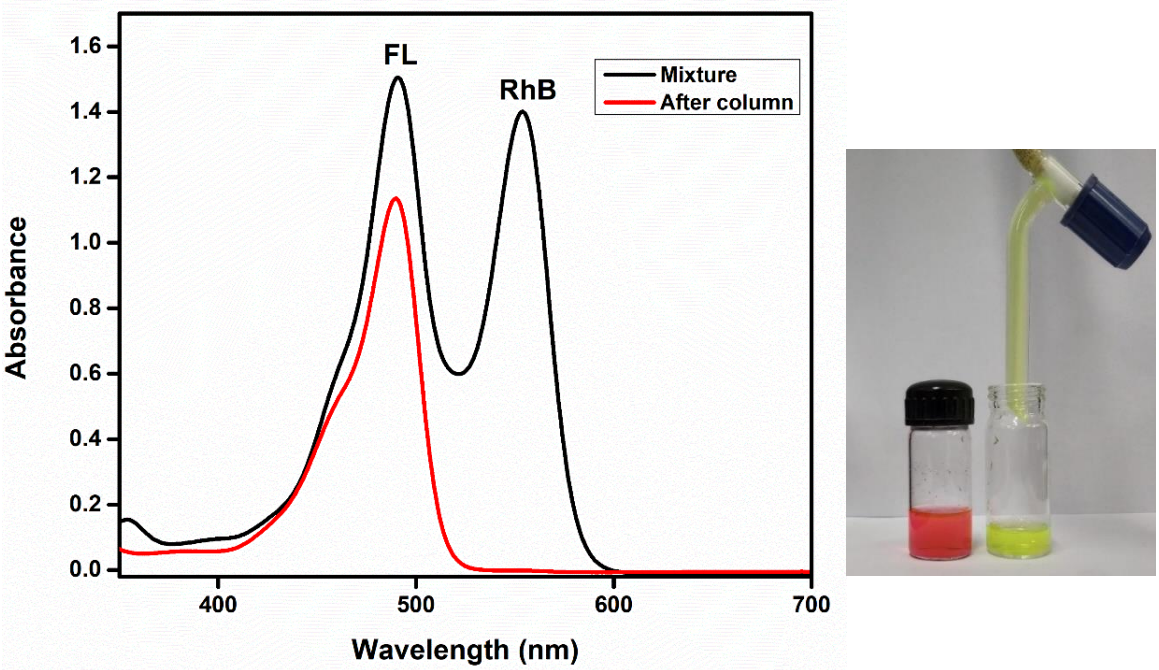

Figure 3.42. UV-Vis spectra of Equimolar Mixture of Fluorescein (FL) and Rhodamine B (RhB) dye before and after passing through the **O-COF** loaded packed column

After dye adsorption experiment, it was observed that cationic dyes RhB, MB and MG are adsorbed by O-COF over a period of time while anionic dyes FL and MO was not adsorbed. These results suggest that O-COF selectively adsorb cationic dyes. Since O-COF contains six oxygen atoms in one pore which is highly electronegative atom, and hence it will be having partial negative charge. The cationic dyes contain positive charge. Due to electrostatic interaction between the O-COF and cationic dyes, O-COF are taking only cationic dyes and rejecting the anionic dyes. This is the possible reason behind selective adsorption of dyes. There is the difference in the adsorption of cationic dyes too. RhB is adsorbing faster and efficiently by O-COF. This may be due to addition driving force that is H-bonding with -COOH proton of RhB dye with the O-COF which is not the case with MB and MG dye.

Same dye adsorption experiment was done by using C-COF and CF_3-COF with cationic and anionic dyes. C-COF does not adsorb much of dyes from the solution. It was shown in

Figures 3.43 - 3.47). This is because C-COF contains carbon atom in place of oxygen atom. and the dyes will feel minimum interaction with carbon atom as compared to oxygen atom and resulted to very less uptake of dyes.

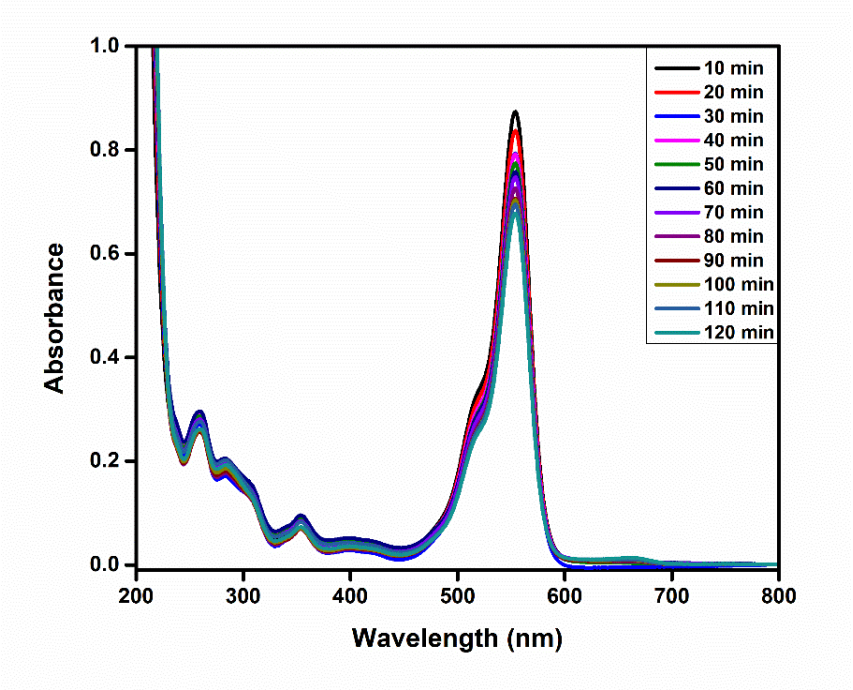

Figure 3.43. UV-Vis spectra of aqueous solution of cationic RhB dye in the presence of **C-COF** after different time intervals**.**

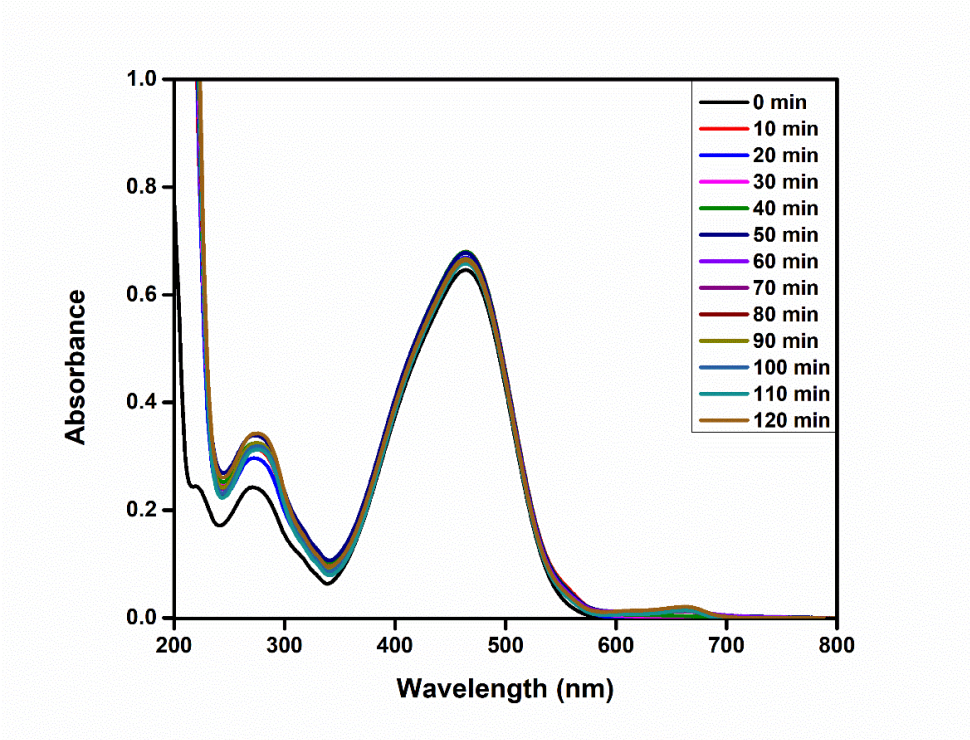

Figure 3.44. UV-Vis spectra of aqueous solution of anionic MO dye in the presence of **C-COF** after different time intervals.

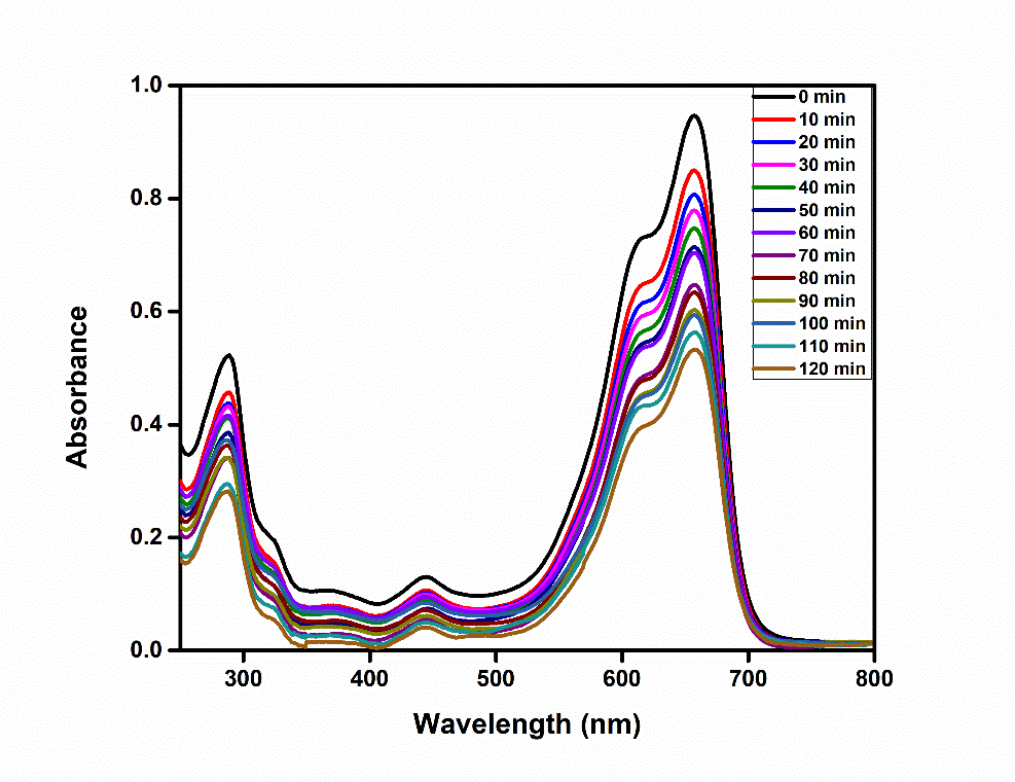

Figure 3.45. UV-Vis spectra of aqueous solution of cationic MG dye in the presence of **C-COF** after different time intervals**.**

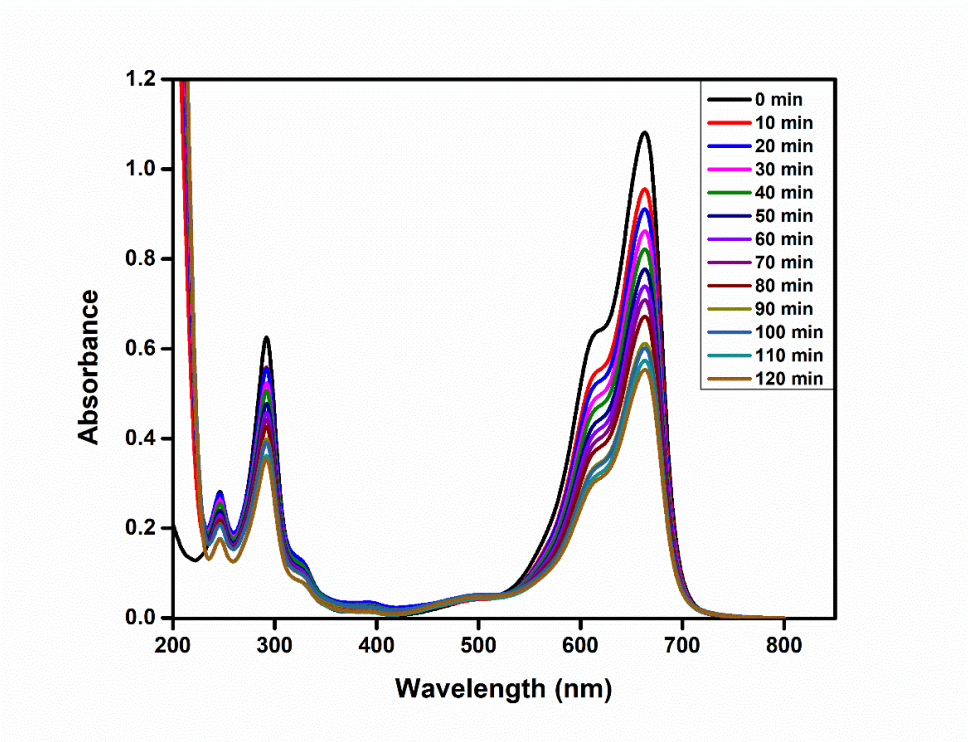

Figure 3.46. UV-Vis spectra of aqueous solution of cationic MB dye in the presence of **C-COF** after different time intervals**.**

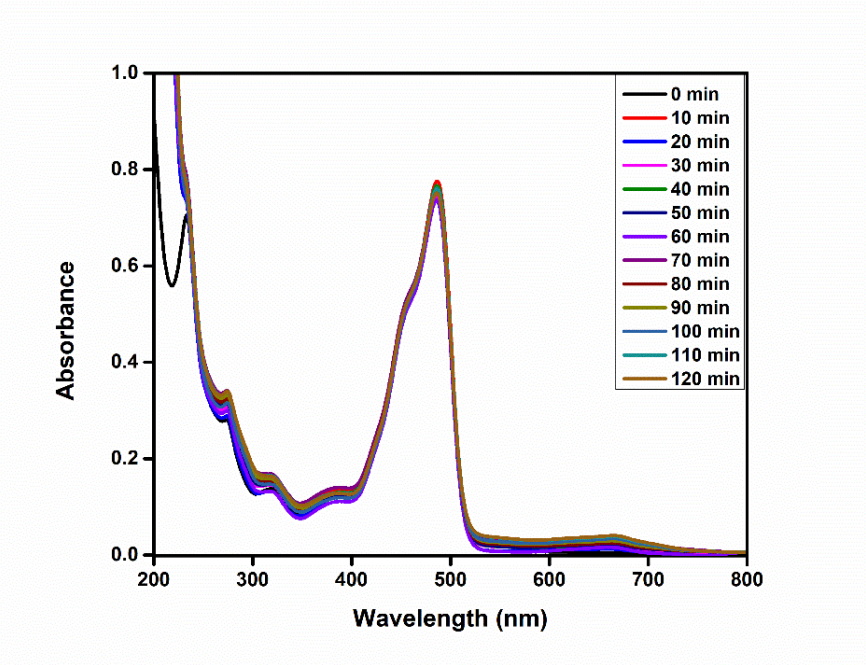

Figure 3.47. UV-Vis spectra of aqueous solution of anionic FL dye in the presence of **C-COF** after different time intervals**.**

Further, CF_3-COF was also used for dye adsorption experiments. Having less crystallinity and less porosity. CF_3-COF merely adsorb any content of dye. Figures 3.48-3.52 show the adsorption of dyes by CF_3-COF.

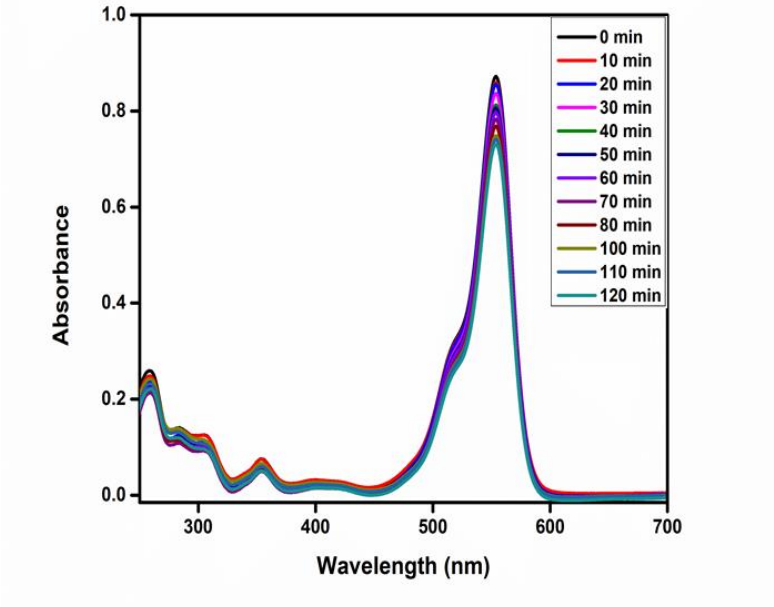

Figure 3.48. UV-Vis spectra of aqueous solution of cationic RhB dye in the presence of **CF_3-COF** after different time intervals**.**

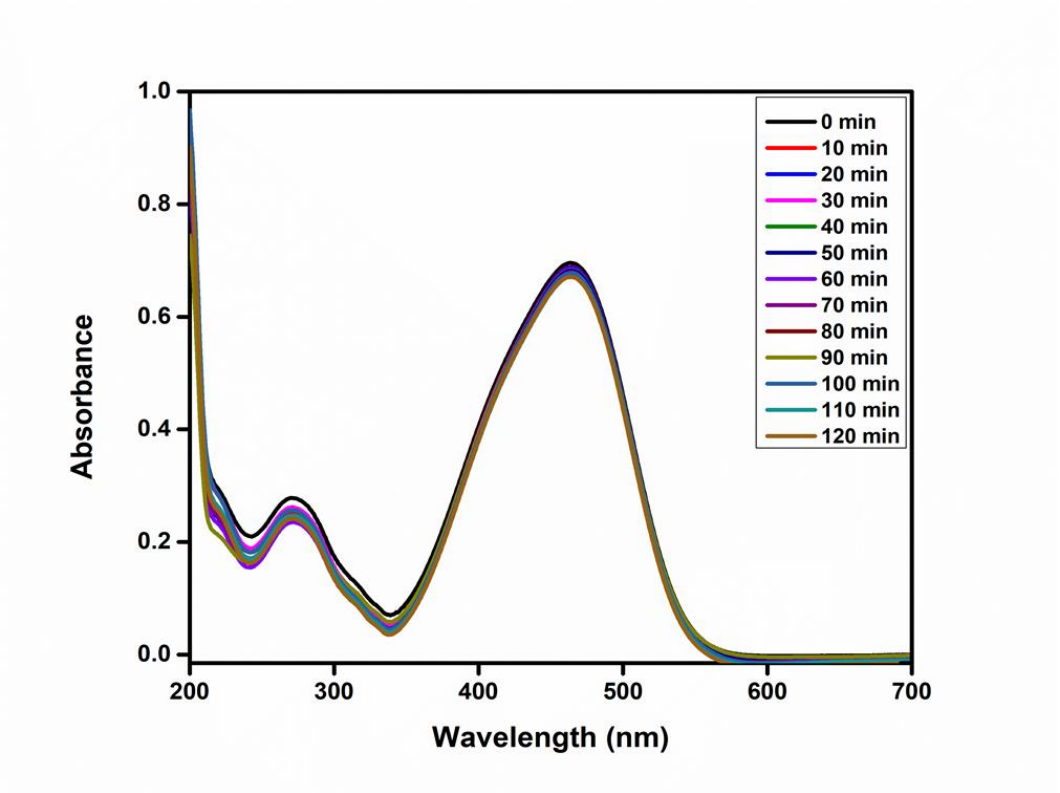

Figure 3.49. UV-Vis spectra of aqueous solution of anionic MO dye in the presence of **CF_3-COF** after different time intervals**.**

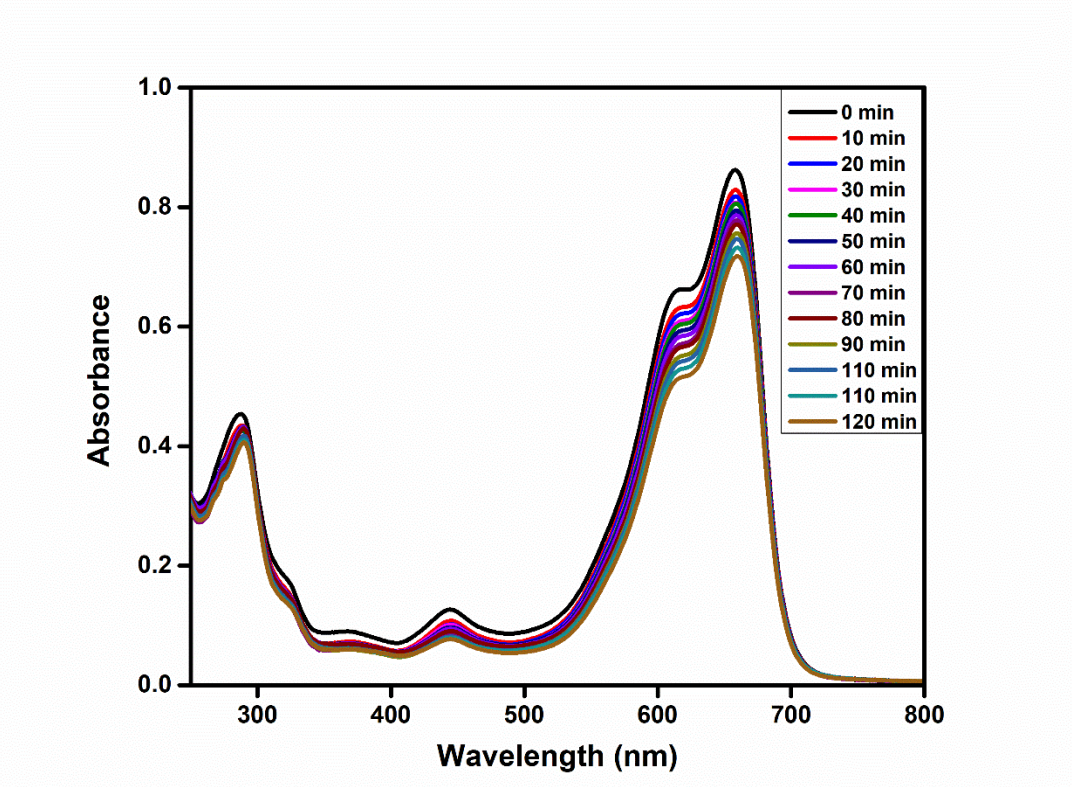

Figure 3.50. UV-Vis spectra of aqueous solution of cationic MG dye in the presence of **CF_3-COF** after different time intervals**.**

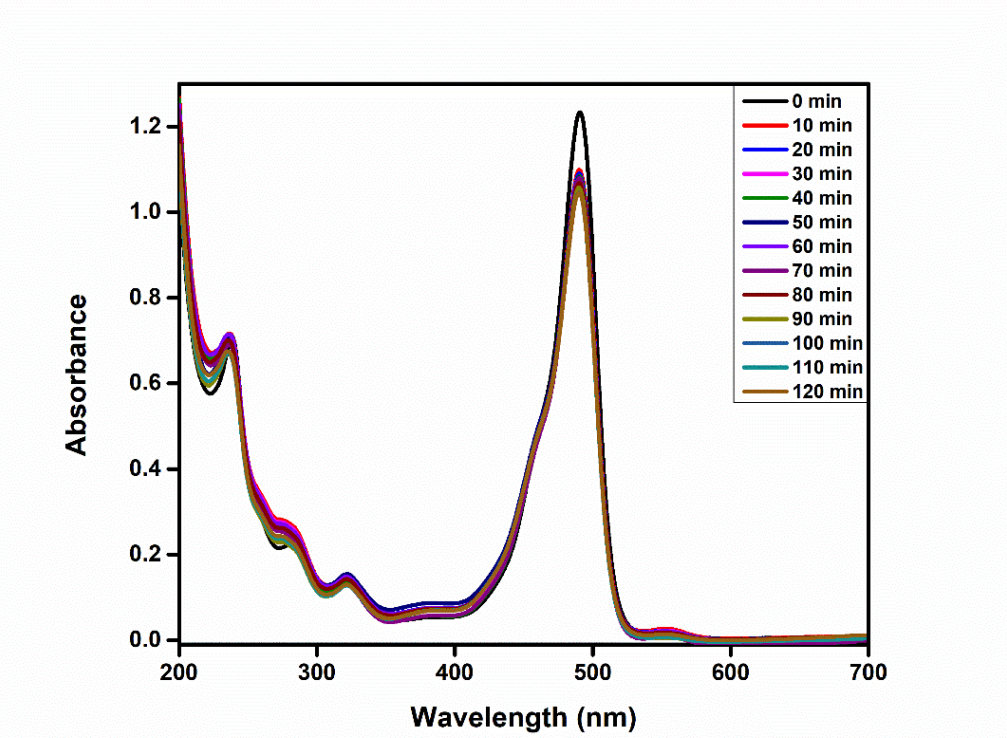

Figure 3.51. UV-Vis spectra of aqueous solution of anionic FL dye in the presence of **CF_3-COF** after different time intervals

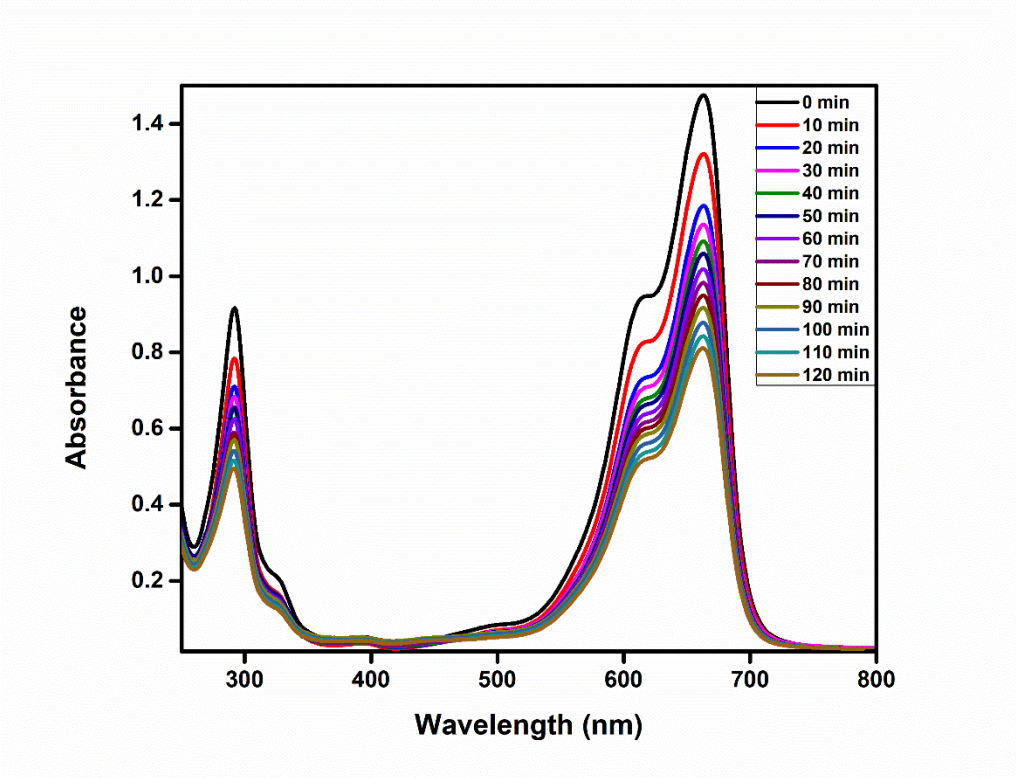

Figure 3.52. UV-Vis spectra of aqueous solution of cationic MB dye in the presence of **CF_3-COF** after different time intervals**.**

3.2.4.1 Adsorption Kinetics

RhB dye was giving good results in terms of adsorption. Adsorption kinetics was also studied using RhB dye solution with O-COF. A calibration curve was shown in Figure 3.53 which was used to calculate the absorbance value for high concentration solution.

To understand the kinetics of RhB adsorption several models were used such as intra-particle diffusion models, pseudo-first order, and pseudo-second order. The adsorption was studied over at the time range of 10-120 minutes and it was used to optimize the adsorption reaction time (Figure 3.54).

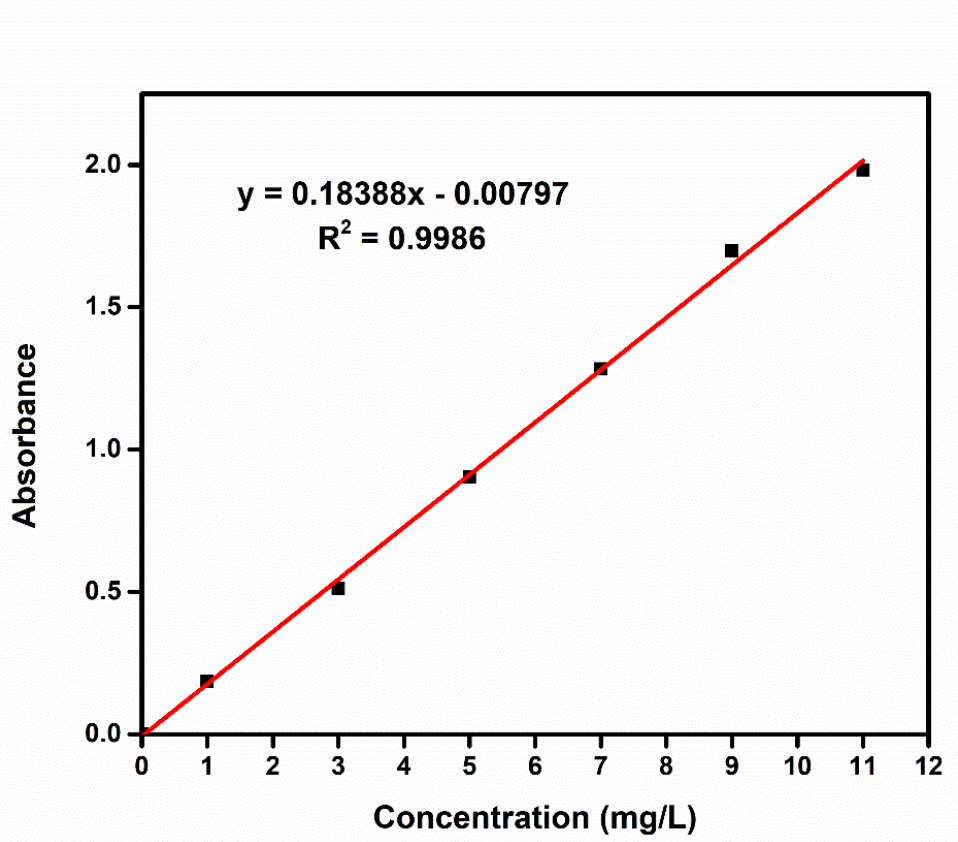

Figure 3.53. The calibration curve and fitting equation for RhB solutions.

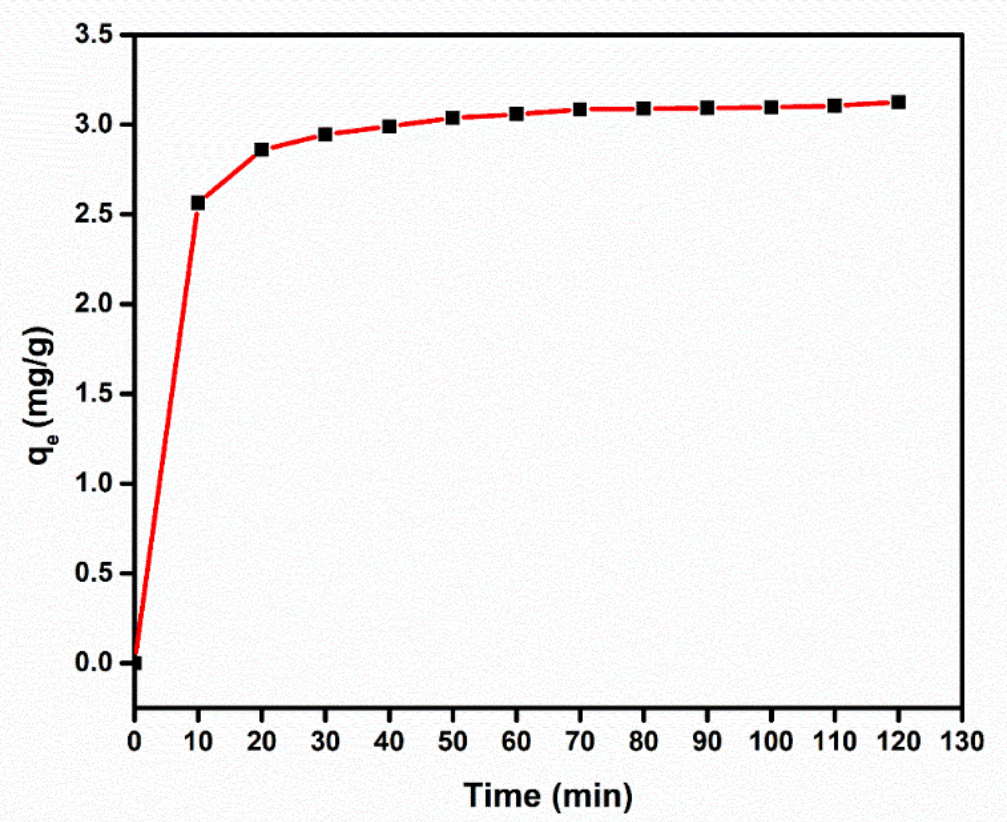

Figure 3.54. Effect of contact of RhB with **O-COF** as a function of adsorption time.

3.2.4.1.1 Pseudo-first order model:

Pseudo-first order model is the most widely used adsorption kinetic. The expression was given by Lagergren and the graph was plotted between ln(q_e – q_t) and t. The model equation which is used for linear plot:

$$\ln \frac{(q_e - q_t)}{q_e} = -K_1 t$$

where K_1 is the rate constant of pseudo-first order reaction (min^{-1}), q_e is the amount of adsorption at equilibrium (mg g^{-1}) and q_t (mg g^{-1}) is the amount of adsorbate retained at time (t).

3.2.4.1.2 Pseudo-second order model:

The pseudo-second order model which is another commonly used kinetic model developed by Ho and McKay. The graph was plotted between t/q_t and t, the equation was used:

$$\frac{t}{q_t} = \frac{1}{q_e^2 K_2} + \frac{t}{q_e}$$

where K_2 is the rate constant of pseudo-second-order adsorption (g mg^{-1} min^{-1}) and q_t (mg g^{-1}) is the amount of adsorbate retained at time (t).

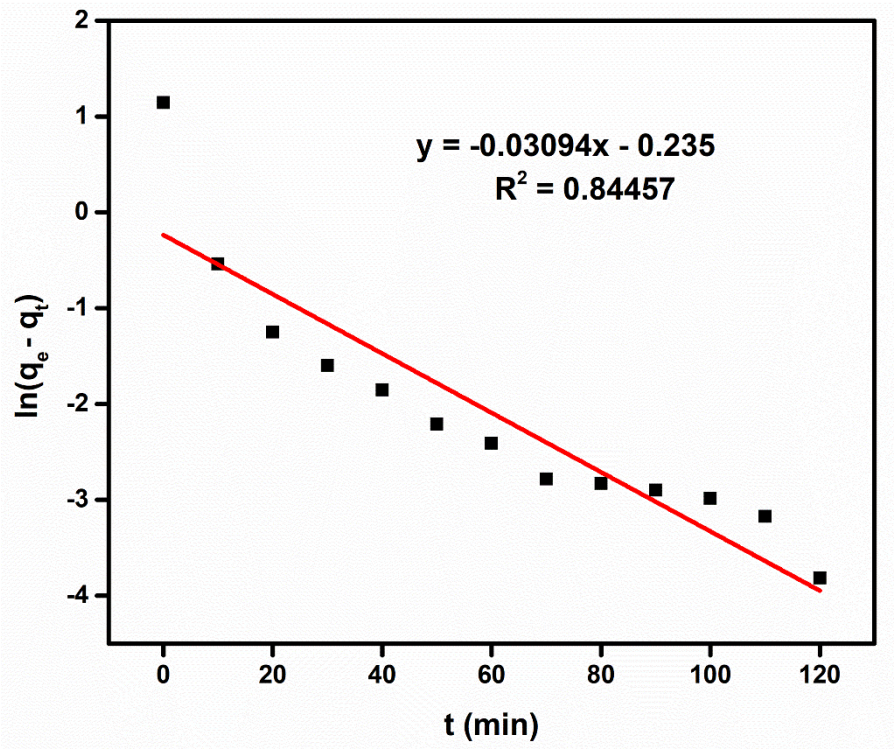

Figure 3.55. Pseudo-first order kinetics plot.

3.2.4.1.3 Intraparticle diffusion model:

The above two models do not describe about diffusion. This model defines that the rate of adsorption process is controlled by the speed of diffusion of adsorbate into the adsorbent. The equation of intra-particle diffusion which is given by Webber and Morris expressed as:

$$q_t = K_3 t^{1/2} + C$$

If the plot of q_t vs $t^{1/2}$ is linear and pass through the origin then the rate of adsorption is controlled by this model.

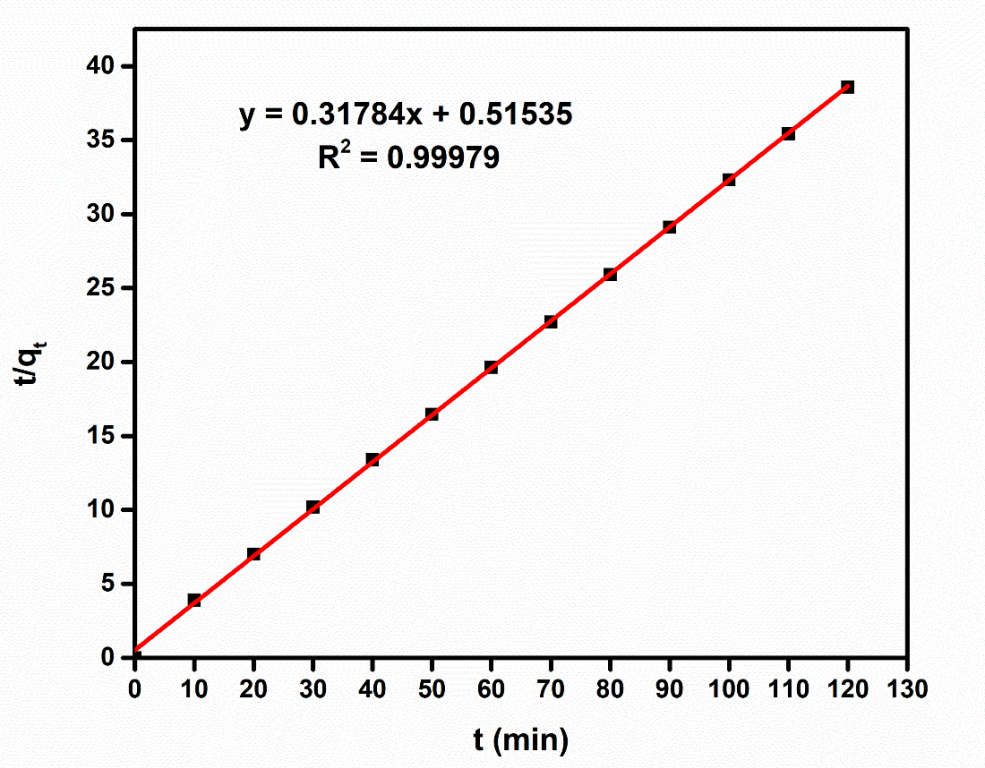

Figure 3.56. Pseudo-second order kinetics plot.

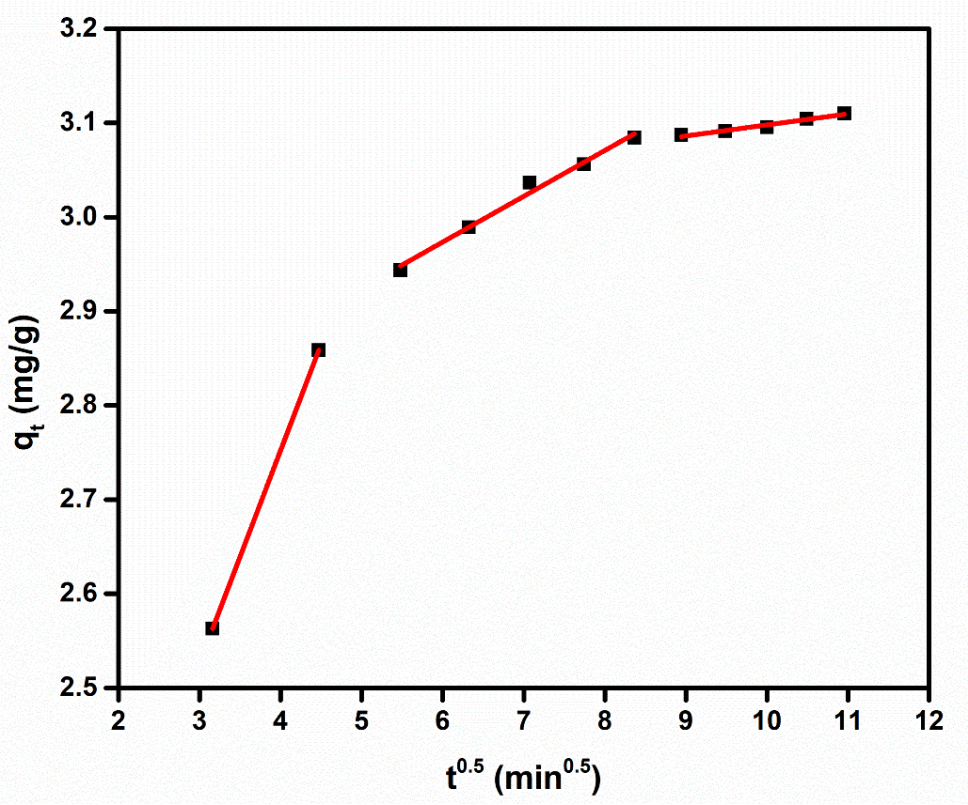

Figure 3.57. Intra-particle diffusion plots.

The values of each parameter, rate constant and correlation coefficient (R^2) for every model was described in Table 3.1.

Table 3.1. Kinetic parameters in the removal of RhB by O-COF absorbents

Models	Parameters	Values
Pseudo-first order	K_1 (min^{-1}) R^2	32.321 0.845
Pseudo-second order	K_2 (g mg^{-1} min^{-1}) q_{exp} ($mg \cdot g^{-1}$) q_{cal} ($mg \cdot g^{-1}$) R^2	5.101 3.102 3.146 0.999
Intra-particle diffusion	K_{11} (mg g^{-1} min^{-1}) K_{12} (mg g^{-1} min^{-1}) K_{13} (mg g^{-1} min^{-1}) C_1 ($mg \cdot g^{-1}$) C_2 ($mg \cdot g^{-1}$) C_3 ($mg \cdot g^{-1}$) R_1^2 R_2^2 R_3^2	0.226 0.047 0.0127 1.849 2.681 2.980 1 0.986 0.983

The graph shown in Figure 3.53 indicates the effect of contact time on the adsorption process. It expresses that most of the adsorption occurs within first 10 minutes, after that rate of adsorption decreases. From this we can conclude that initially surface is involved in the adsorption of RhB. Once surface got saturated, RhB start diffusing inside the pores and rate decreases. The pseudo-second order model works on the fact that adsorption process involves chemisorption. According to the results, among pseudo-first and second order, pseudo-second order have good correlation with the experimental data by showing high correlation coefficient (R^2 = 0.99). This suggests chemisorption is involved in the adsorption initially. Further, adsorption is process by diffusion-control mechanism.

For the investigating the diffusion mechanism inter-partial diffusion model was used. This model tells about the involvement of the diffusion in rate limiting step. The graph revels that there are three steps in the diffusion process which is clearly divided in the fitted curve. First is film diffusion, second is inter-particle diffusion and the third inter-particle repulsion

inside the pores. During the film diffusion, RhB dye molecules diffuse into the surface of O-COF. Initially, there are very less resistance among molecules so the rate of the adsorption is higher as shown in the first part of Figure 3.56 (K_1). After that, inter particle diffusion occurs where dye molecules start diffusing inside the pores and the molecules feels more resistance for the pores. The rate became lower than the first step. Further, when RhB dye molecules continuously goes inside the pores, molecules start feeling repulsion among the adsorbed dye molecules in the third step and rate of the adsorption is lower relatively until the equilibrium where adsorption and resistance force becomes equal. The graph is not passing through origin, that tells diffusion is not rate limiting process in this case.

3.2.4.2 Adsorption Isotherms

Adsorbates have different interaction with the adsorbents with respect to different concentrations. To understand more about the surface property, adsorption process and maximum adsorption capacity, two adsorption models are used: Langmuir and Freundlich. The adsorption isotherm was obtained by plotting the curve between equilibrium concentration (C_e) and equilibrium adsorption amount (q_e). Langmuir and Freundlich was used to calculate adsorption equilibrium point. These models also help to distinguish whether adsorption process is monolayer or multilayer.

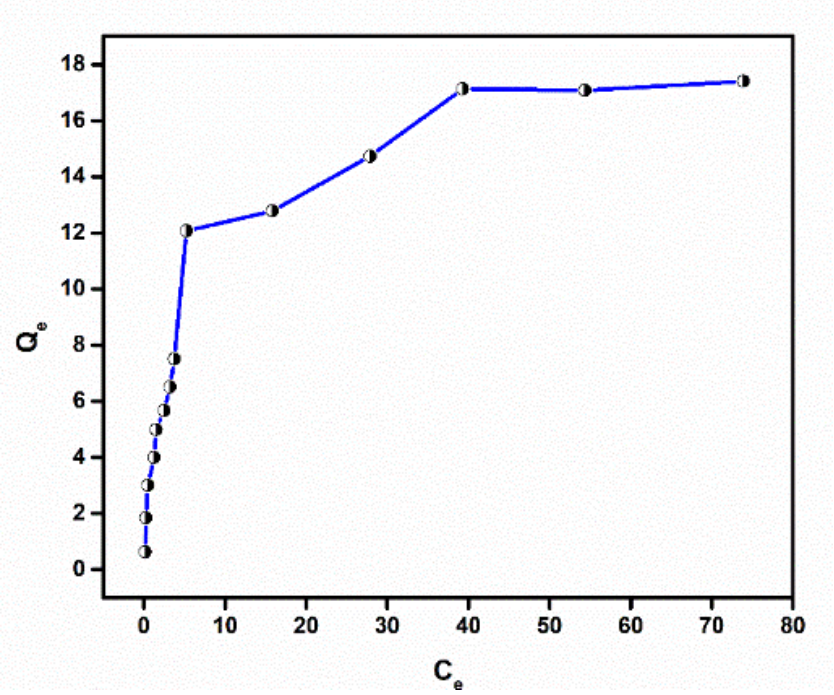

Figure 3.58. Adsorption isotherm for RhB dye at room temperature.

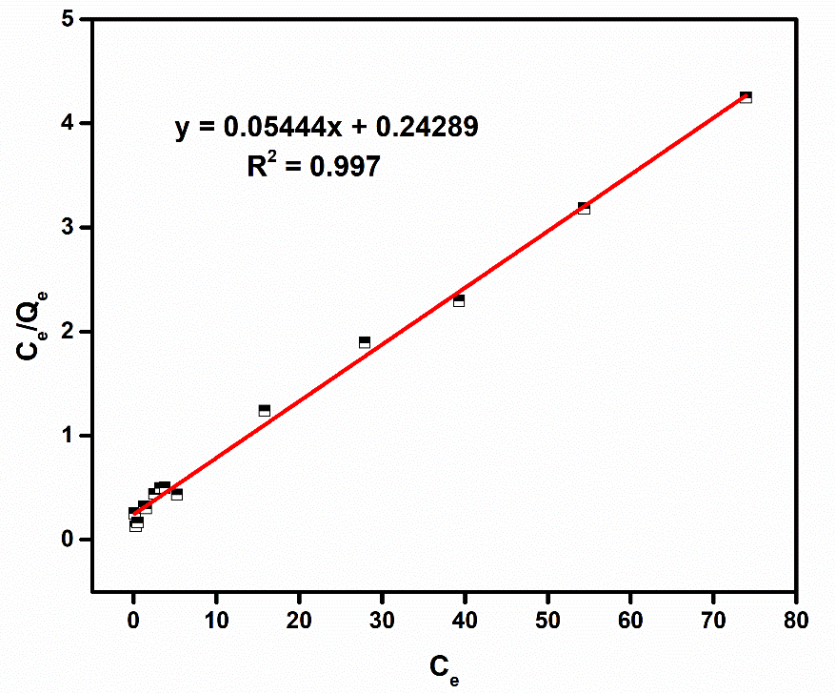

Figure 3.59. Langmuir isotherm for the adsorption of RhB using **O-COF**.

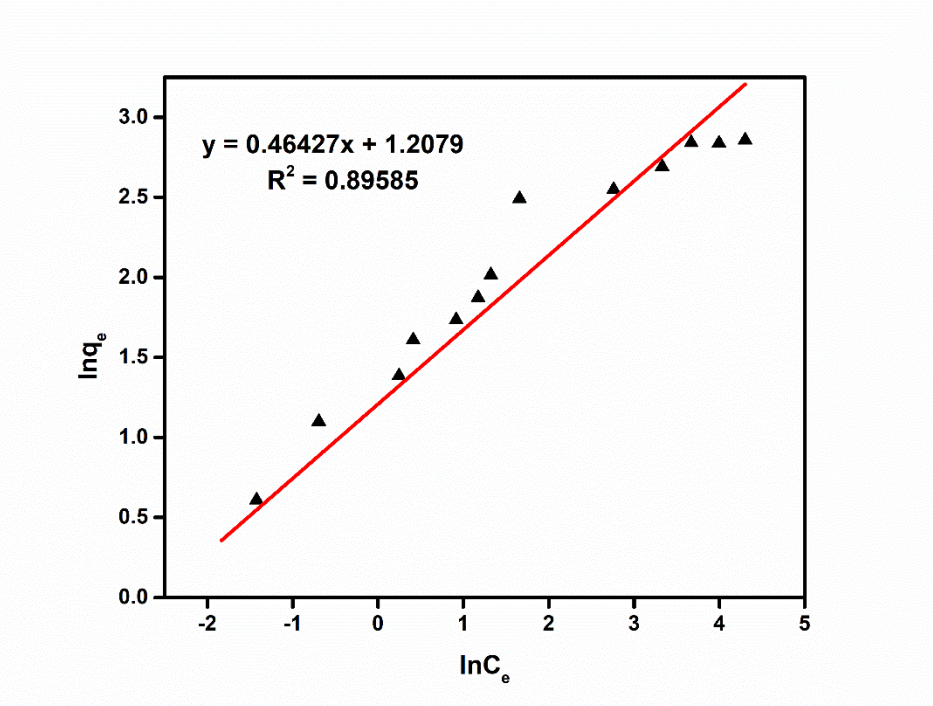

Figure 3.60. Freundlich isotherms for the adsorption of RhB using **O-COF**.

As the equilibrium concentration of RhB dye increases, the adsorption capacity increases very fast, and then it gets saturated (Figure 3.56). The maximum equilibrium adsorption of RhB dye by O-COF is 17.39 $mg.g^{-1}$. Results for the Langmuir and Freundlich model fitting

are listed in Table 3.2. Figure 3.57 shows the Langmuir model has a high correlation coefficient (R^2 = 0.997) as compared to the Freundlich model. These results suggest that RhB dye adsorption on the O-COF surface is a monolayer process where adsorption sites have a similar affinity for each dye molecule and dyes are homogeneously adsorbed on the O-COF surface. From the Langmuir model, monolayer adsorption capacity was calculated (18.37 $mg.g^{-1}$), which is almost close to the experimental value.

Table 3.2. Calculated parameters from the Langmuir isotherm and the Freundlich isotherm models.

Models	Parameters	Values
Langmuir	K_1 (L.min^{-1}) q_{max} (mg.g^{-1}) R^2	0.2241 18.37 0.997
Freundlich	K_F (g mg^{-1} min^{-1}) n R^2	3.346 2.153 0.895

3.2.5 Recyclability

Recyclability has great significance because it is a characteristic of the material which is going to use for practical application that preserves the structural and chemical properties of the material even after serving for the purpose. It is essential for industrial applications. In order to check the durability and stability of O-COF, it was isolated, washed with methanol, and dried. After that, the PXRD pattern of O-COF was recorded. We observed that the PXRD pattern is retained after the absorption process, which indicates that there is no structural deformation of O-COF.

Further, to evaluate the recyclability, we have repeated the adsorption and regeneration experiment with the same material up to five cycles. There is no change in the adsorption capacity observed (Figures 3.61 and 3.62). SEM images (Figure 3.63) and PXRD (Figure 3.64) after 5 cycles show no change in the structure and morphology. These results indicate, O-COF has the potential to use efficiently in water purification and selective removal of dyes.

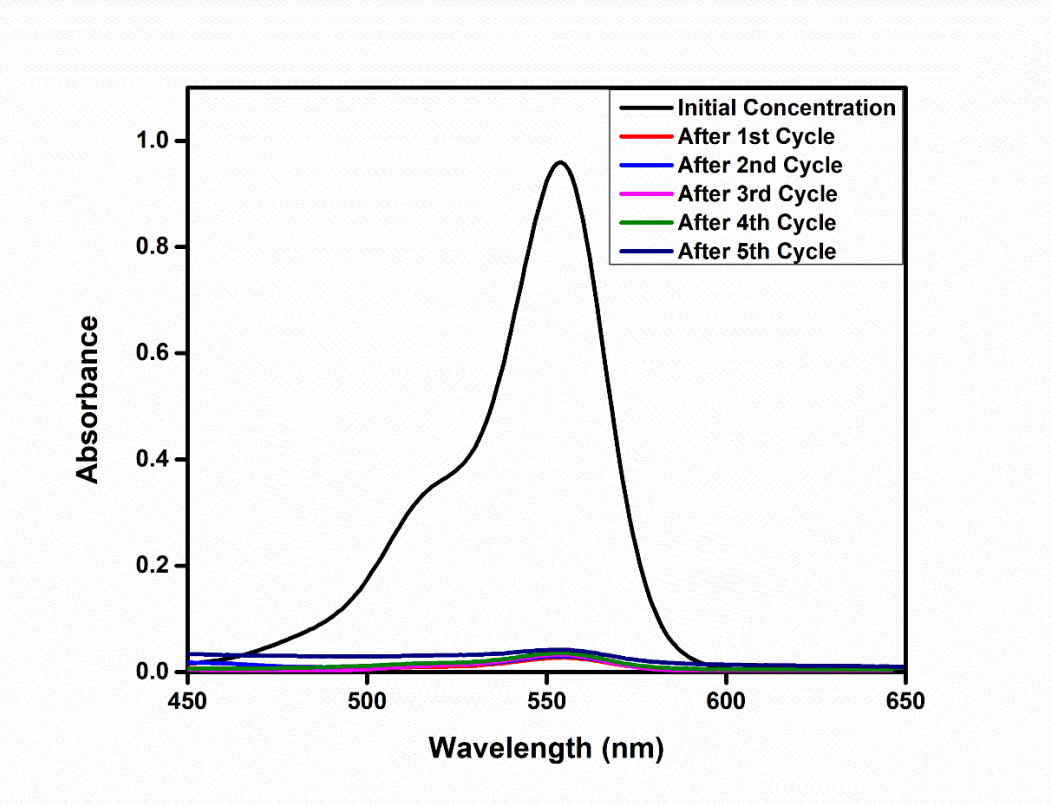

Figure 3.61. Reusability of **O-COF** shown by UV-Vis spectrum of RhB.

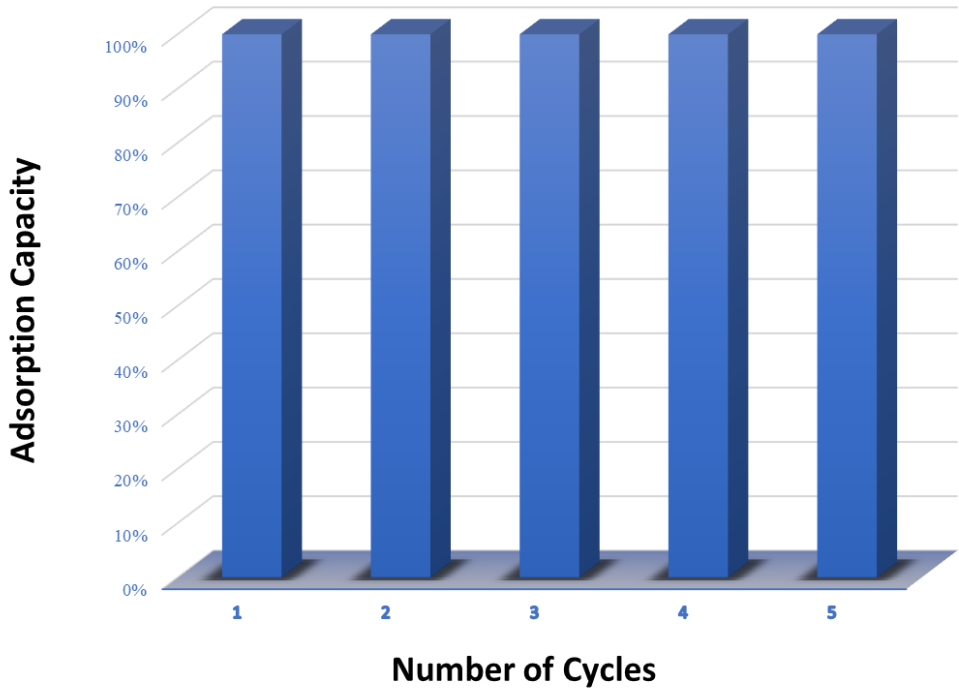

Figure 3.62. Bar graph up to 5 cycles for recyclability of **O-COF**.

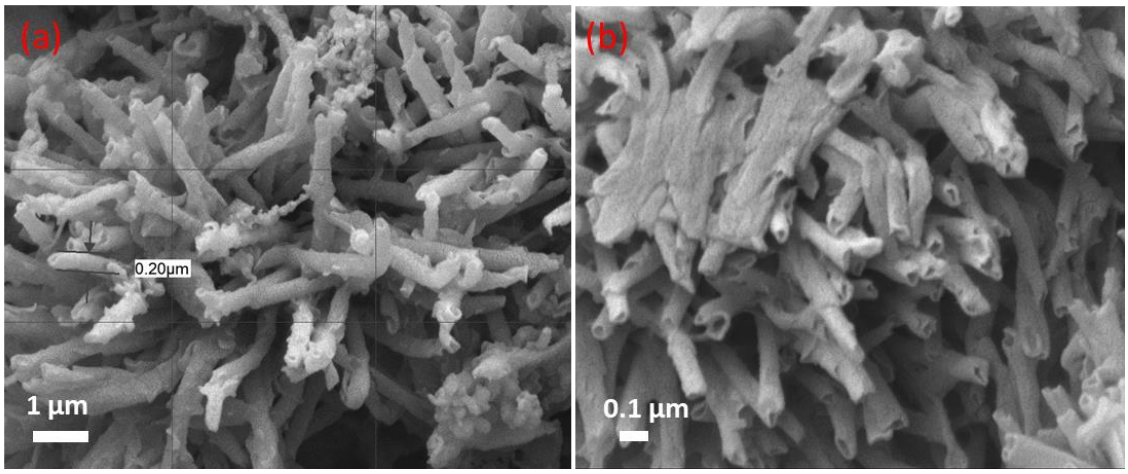

Figure 3.63. FESEM images **O-COF** (a) before and, (b)after, 5 cycles of adsorption-desorption of RhB dye.

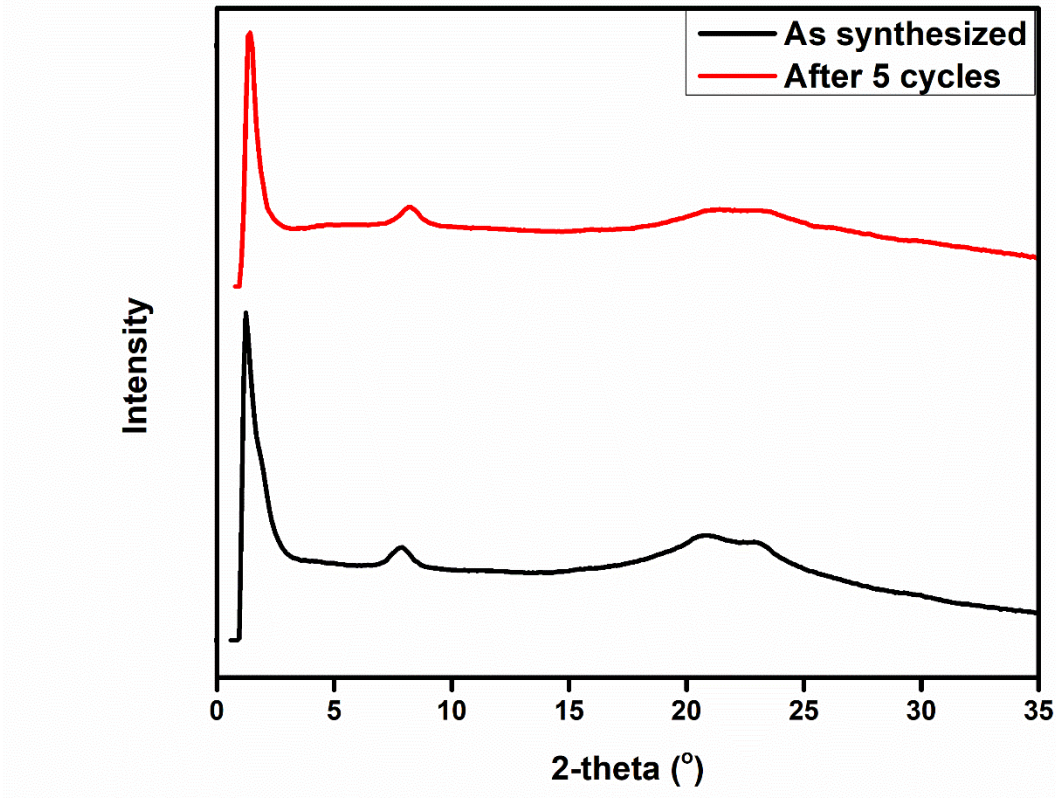

Figure 3.64. PXRD patterns of **O-COF** before and after 5 cycles of adsorption-desorption of RhB dye.

Chapter IV

Conclusions and Future Directions

In summary, three new highly flexible COFs were designed, synthesized and well characterized using FTIR, solid state NMR, solid-state UV-vis spectroscopy, TGA, X-ray diffraction, FESEM and HRTEM. The PXRD pattern of the COFs are consistent with simulated PXRD pattern that confirms AA stacked hexagonal structure. TGA shows that the synthesized COFs have good thermal stability and Tauc plot analysis reveals the semiconducting nature of the COFs by showing the band gap between 2-3 eV.

In this work, the growth mechanism of all three COFs was also studied. Remarkably, O-COF crystallites self-assemble into hollow tubular aggregates with size around 200 nm confirmed by FESEM and HRTEM images. Time-dependent studies helps to understand growth of the COFs extensively. We devoted our efforts to compare of morphologies of three different highly flexible COFs with small change in chemical units to showcase their role in dye purification and separation. In this work, it has been demonstrated that O-COF is selectively adsorbed cationic dyes compared with their very close structural difference COFs. Thus, a prototype was shown where O-COF was successfully employed as stationary phase in liquid chromatography for the dye separation. The UV-Vis spectrophotometer confirms the efficient separation dyes. The selective and effective separation of RhB over FL dye directed by electrostatic interaction between oxygen and cationic dye. Along with this, various kinetic models were also used to investigate, adsorption process. It was found that pseudo second kinetic model has good agreement with experiment data. The O-COF was highly stable in the aqueous condition and found recyclable without no change in the structure, morphology and adsorption capacity upto five cycles. To our best knowledge, this is the first report where COF was used as stationary phase material in liquid chromatography.

This complete study shows the difficulties of synthesizing highly flexible COF and its potential application in water purification which is very important for upcoming generation and environmental monitoring. We are preparing manuscript for this work and it will be published very soon, after a few remaining elaborations.

Bibliography

(1) Cundy, C. S.; Cox, P. A. The Hydrothermal Synthesis of Zeolites: History and Development from the Earliest Days to the Present Time. *Chem. Rev.* **2003**, *103*, 663-702.

(2) Sun, Q.; Wang, N.; Bing, Q,; Si, R.; Liu, J.; Bai, R.; Zhang, P.; Jia, M.; Sun, J. Y. Subnanometric Hybrid Pd-$M(OH)_2$, M = Ni, Co, Clusters in Zeolites as Highly Efficient Nanocatalysts for Hydrogen Generation. *Chem.* **2017,** *3*, 477–493.

(3) Kitagawa, S.; Kitaura, R.; Noro, S. I. Functional porous coordination polymers. *Angew. Chem., Int. Ed.* **2004,** *43*, 2334-2375.

(4) Chen, X.; Addicoat, M.; Jin, E.; Xu, H.; Hayashi, T.; Xu, F.; Huang, N.; Irle, S.; Jiang, D. Designed synthesis of double-stage two-dimensional covalent organic frameworks. *Sci. Rep.* **2015**, 5, 14650.

(5) Diercks, C. S.; Yaghi, O. M. The atom, the molecule, and the covalent organic framework. *Science* **2017,** *355*, 1585-593.

(6) Slater, A. G; Andrew I. Cooper Function-led design of new porous materials. *Science* **2015**, *348*, 8075-8085.

(7) Sing, K.S.W.; Everett, D.H.; Haul, R.A.W.; Moscou, L.; Pierotti, R.A.; Rouquerol, J.; Siemieniewska, T. Reporting Physisorption Data for Gas/Solid Systems. *Handbook of Heterogeneous Catalysis* **2008**, *603*, 1217–1230.

(8) Das, S.; Heasman, P.; Ben, T.; Qiu, S. Porous Organic Materials: Strategic Design and Structure–Function Correlation *Chem. Rev.* **2017,** *117*, 1515–1563.

(9) Bisbey, R. P.; Dichtel, W. R. Covalent Organic Frameworks as a Platform for Multidimensional Polymerization *ACS Cent. Sci.* **2017,** *3*, 533-443.

(10) DeCoste, J. B.; Peterson, G. W. Metal–Organic Frameworks for Air Purification of Toxic Chemicals. *Chem. Rev.* **2014,** *114*, 5695-5727.

(11) Yoon, M.; Srirambalaji, R.; Kim K. Homochiral Metal-Organic Frameworks for Asymmetric Heterogeneous Catalysis. *Chem. Rev.* **2012,** *112*,1196-1231.

(12) Lin, C.- Y.; Zhang, D.; Zhao, Z.; Xia, Z. Covalent Organic Framework Electrocatalysts for Clean Energy Conversion. *Adv. Mater.* **2018**, *30*, 1703646.

(13) Beuerle, F.; Gole, B. Covalent Organic Frameworks and Cage Compounds: Design and Applications of Polymeric and Discrete Organic Scaffolds *Angew. Chem., Int. Ed.* **2018,** *57*, 4850-4878.

(14) Yuan, S.; Feng, L.; Wang, K.; Pang, J.; Bosch, M,; Lollar, C.; Sun, Y.; Qin, J.; Yang, X.; Zhang, P.; Wang, Q.; Zou, L.; Zhang, Y.; Zhang, L.; Fang, Y.; Li, J.; Zhou, H.-C. Stable Metal–Organic Frameworks: Design, Synthesis, and Applications. *Adv. Mater.* **2018,** *30*, 1704303.

(15) Lohse, M. S.; Bein, T. Covalent Organic Frameworks: Structures, Synthesis, and Applications. *Adv. Funct. Mater.*, **2018,** *28,* 1705553.

(16) Côté, A. P.; Benin, A. I.; Ockwig, N. W.; Keeffe, M.; Metzger, A. J.; Yaghi, O. M. Porous, Crystalline, Covalent Organic Frameworks. *Science*, **2005,** *310,* 1166-1170.

(17) Côté, A. P.; El-Kaderi, H. M.; Furukawa, H.; Hunt J. R.; Yaghi, O. M. Reticular Synthesis of Microporous and Mesoporous 2D Covalent Organic Frameworks. *J. Am. Chem. Soc.*, **2007,** *129,* 12914-12915.

(18) Segura, J. L.; Mancheño, M. J.; Zamora F. Covalent organic frameworks based on Schiff-base chemistry: synthesis, properties and potential applications. *Chem. Soc. Rev.*, **2016,** *45,* 5635-5671.

(19) Dalapati, S.; Jin, S.; Gao, J.; Xu, Y.; Nagai, A.; Jiang, D. An Azine-Linked Covalent Organic Framework. *J. Am. Chem. Soc.*, **2013**, *135*, 17310 —17313.

(20) Wan, S.; Guo, J.; Kim, J.; Ihee, H.; Jiang, D. A Photoconductive Covalent Organic Framework: Self- Condensed Arene Cubes Composed of Eclipsed 2D Polypyrene Sheets for Photocurrent Generation. *Angew. Chem., Int. Ed.*, **2009**, *48,* 5439 —5442.

(21) Guo, J.; Xu, Y.; Jin, S.; Chen, L.; Kaji, T.; Honsho, Y.; Addicoat, M.; Kim, J.; Saeki, A.; Ihee, H.; Seki, S.; Irle, S.; Hiramoto, M.; Gao, J.; Jiang, D. Conjugated organic framework with three-dimensionally ordered stable structure and delocalized π clouds. *Nat. Commun.* **2013,** 4**,** 2736.

(22) Rao, M. R.; Fang, Y.; Feyter S. D.; Perepichka, D. F. Conjugated Covalent Organic Frameworks via Michael Addition–Elimination. *J. Am. Chem. Soc.* **2017,** *139***,** 2421-2427.

(23) Fang, Q.; Zhuang, Z.; Gu, S.; Kaspar, R. B.; Zheng, J.; Wang, J.; Qiu S.; Yan, Y. Designed synthesis of large-pore crystalline polyimide covalent organic frameworks. *Nat. Commun.* **2014**, *5*, 4553.

(24) Baldwin, L. A.; Crowe, J. W.; Pyles, D. A.; McGrier, P. L.; Metalation of a Mesoporous Three-Dimensional Covalent Organic Framework *J. Am. Chem. Soc*. **2016,** *138*, 15134-15137.

(25) Wilson, A.; Gasparini, G.; Matile, S. Functional Systems with Orthogonal Dynamic Covalent Bonds. *Chem. Soc. Rev*. **2014**, *43*, 1948– 1962.

(26) Geng, K.; He, T.; Liu, R.; Dalapati, S.; Tian, Tan, K. T.; Li, Z.; Tao, S.; Gong, Y.; Jiang, Q.; Jiang, D. Covalent Organic Frameworks: Design, Synthesis, and Functions. *Chem. Rev*. **2020.**

(27) Xu, L.; Ding, S.-Y.; Liu, J.; Sun, J.; Wang, W.; Zheng, Q.-Y. Highly crystalline covalent organic frameworks from flexible building blocks *Chem. Commun.* **2016,** *52***,** 4706-4709.

(28) Sharma, R. K.; Yadav, P.; Yadav, M.; Gupta, R.; Rana, P.; Srivastava, A.; Zbořil, R.; Varma, R. S.; Antonietti , M.; Gawande, M. B. Recent development of covalent organic frameworks (COFs): synthesis and catalytic (organic-electro-photo) applications. *Mater. Horiz.* **2020,** *7***,** 411-454.

(29) Campbell, N. L.; Clowes, R.; Ritchie, L. K.; Cooper A. I. Rapid Microwave Synthesis and Purification of Porous Covalent Organic Frameworks *Chem. Mater*. **2009,** *21*, 204-206.

(30) Wei, H.; Chai, S. Z.; Hu, N. T.; Yang, Z.; Wei, L. M.; Wang, L. The Microwave-Assisted Solvothermal Synthesis of a Crystalline Two-Dimensional Covalent Organic Framework with High CO_2 Capacity. *Chem. Commun.* **2015**, *51*, 12178-12181.

(31) Ritchie, L. K.; Trewin, A.; Reguera-Galan, A.; Hasell, T.; Cooper, A. I. Synthesis of COF-5 Using Microwave Irradiation and Conventional Solvothermal Routes. *Microporous Mesoporous Mater.* **2010**, *132*, 132-136.

(32) Biswal, B. P.; Chandra, S.; Kandambeth, S.; Lukose, B.; Heine, T.; Banerjee, R. Mechanochemical Synthesis of Chemically Stable Isoreticular Covalent Organic Frameworks. *J. Am. Chem. Soc.* **2013,** *135*, 5328-5331.

(33) Chandra, S.; Kandambeth, S.; Biswal, B. P.; Lukose, B.; Kunjir, S. M.; Chaudhary, M.; Babarao, R.; Heine, T.; Banerjee, R. Chemically Stable Multi-layered Covalent Organic Nanosheets from Covalent Organic Frameworks via Mechanical Delamination. *J. Am. Chem. Soc.* **2013**, *135*, 17853–17861.

(34) Furukawa, H.; and Yaghi, O. M. Storage of Hydrogen, Methane, and Carbon Dioxide in Highly Porous Covalent Organic Frameworks for Clean Energy Applications *J. Am. Chem. Soc.* **2009,** *131*, 8875–8883.

(35) Doonan, C. J.; Tranchemontagne, D. J.; Glover, T. G.; Hunt, J. R.; Yaghi, O. M. Exceptional ammonia uptake by a covalent organic framework. *Nat. Chem.* **2010,** *2*, 235-238.

(36) Nagai, A.; Guo, Z.; Feng, X.; Jin, S.; Chen, X.; Ding, X.; Jiang, D. Pore surface engineering in covalent organic frameworks *Nat. Commun.* **2011,** *2*, 536.

(37) Stegbauer, L.; Hahn, M. W.; Jentys, A.; Savasci, G.; Ochsenfeld, C.; Lercher, J. A.; Lotsch, B. V. Tunable Water and CO_2 Sorption Properties in Isostructural Azine-Based Covalent Organic Frameworks through Polarity. *Chem. Mater.* **2015,** *27*, 7874-7881.

(38) Huang, N.; Krishna, R.; Jiang, D. Tailor-Made Pore Surface Engineering in Covalent Organic Frameworks: Systematic Functionalization for Performance Screening *J. Am. Chem. Soc.* **2015**, *137*, 7079-7082.

(39) Ma, H.-C.; Kan, J.-L.; Chen, G.-J.; Chen C.-X.; Dong, Y.-B. Pd NPs-Loaded Homochiral Covalent Organic Framework for Heterogeneous Asymmetric Catalysis *Chem. Mater.* **2017**, *29*, 6518–6524.

(40) Lu, S.; Hu, Y.; Wan, S.; McCaffrey, R.; Jin, Y.; Gu, H.; Zhang, W.; Synthesis of Ultrafine and Highly Dispersed Metal Nanoparticles Confined in a Thioether-Containing Covalent Organic Framework and Their Catalytic Applications. *J. Am. Chem. Soc.*, **2017,** *139*, 17082–17088.

(41) Ding, S.-Y; Gao, J.; Wang, Q.; Zhang, Y.; Song, W.-G.; Su, C.-Y.; and Wang, W.; Construction of Covalent Organic Framework for Catalysis: Pd/COF-LZU1 in Suzuki–Miyaura Coupling Reaction *J. Am. Chem. Soc.*, **2011,** *133*, 19816–19822.

(42) Wu, Y.; Xu, H.; Chen, X.; Gao, J.; Jiang, D. A π-electronic covalent organic framework catalyst: π-walls as catalytic beds for Diels–Alder reactions under ambient conditions *Chem. Commun.*, **2015,** *51*, 10096–10098.

(43) Chan-Thaw, C. E.; Villa, A.; Katekomol, P.; Su, D.; Thomas A.; Prati, L. Covalent Triazine Framework as Catalytic Support for Liquid Phase Reaction *Nano Lett.*, **2010,** *10*, 537–541.

(44) Mu, M.; Wang, Y.; Qin, Y.; Yan, X.; Li, Y.; Chen, L.; Two-Dimensional Imine-Linked Covalent Organic Frameworks as a Platform for Selective Oxidation of Olefins. *ACS Appl. Mater. Interfaces* **2017,** *9*, 22856–22863.

(45) Ma, H.-C.; Kan, J.-L.; Chen, G.-J.; Chen, C.-X.; Dong, Y.-B. Pd NPs-Loaded Homochiral Covalent Organic Framework for Heterogeneous Asymmetric Catalysis *Chem. Mater.* **2017,** *29*, 6518–6524.

(46) Fang, Q.; Gu, S.; Zheng, J.; Zhuang, Z.; Qiu S.; Yan, Y. 3D Microporous Base-Functionalized Covalent Organic Frameworks for Size- Selective Catalysis *Angew. Chem.*, **2014,** *126*, 2922–2926

(47) Wang, Y.; Chen, J.; Wang, G.; Li, Y.; Wen, Z Perfluorinated Covalent Triazine Framework Derived Hybrids for the Highly Selective Electroconversion of Carbon Dioxide into Methane *Angew. Chem.*, **2018,** *130*, 13304–13308.

(48) Das, P.; Mandal, S. K. In-Depth Experimental and Computational Investigations for Remarkable Gas/Vapor Sorption, Selectivity, and Affinity by a Porous Nitrogen-Rich Covalent Organic Framework. *Chem. Mater.* **2019**, *31*, 1584-1596.

(49) Wang, X.; Chen, L.; Chong, S. Y.; Little, M. A.; Wu, Y.; Zhu, W.-H.; Clowes, R.; Yan, Y.; Zwijnenburg, M. A.; Sprick, R. S.; Cooper, A. I. *Nat. Chem.*, **2018,** *10,* 1180-1189.

(50) Diercks, C. S.; Lin, S.; Kornienko, N.; Kapustin, E. A.; Nichols, E. M.; Zhu, C.; Zhao, Y.; Chang, C. J.; Yaghi, O. M. Reticular Electronic Tuning of Porphyrin Active Sites in Covalent Organic Frameworks for Electrocatalytic Carbon Dioxide Reduction. *J. Am. Chem. Soc.*, **2018,** *140,* 1116–1122.

(51) Schwinghammer, K.; Hug, S.; Mesch, M. B.; Senker J.; Lotsch, B. V.; Phenyl-triazine oligomers for light-driven hydrogen evolution. *Energy Environ. Sci.*, **2015**, *8,* 3345–3353.

(52) Dalapati, S.; Jin, S.; Gao, J.; Xu, Y.; Nagai, A.; Jiang, D. An Azine-Linked Covalent Organic Framework. *J. Am. Chem. Soc.*, **2013,** *135***,** 17310-17313.

(53) Ding, S.- Y.; Dong, M.; Wang, Y.- W.; Chen, Y.- T.; Wang, H.- Z.; Su, C.- Y.; Wang, W. Thioether-Based Fluorescent Covalent Organic Framework for Selective Detection and Facile Removal of Mercury(II) *J. Am. Chem. Soc.* **2016**, *138,* 3031-3037.

(54) Li, Z.; Zhang, Y.; Xia, H.; Mu, Y.; Liu, X. Covalent organic frameworks as pH responsive signaling scaffolds. *Chem. Commun.* **2016,** *52,* 11088-11091.

(55) Qian, H.-L.; Yang, C.-X.; Yan, X.-P.; Bottom-up synthesis of chiral covalent organic frameworks and their bound capillaries for chiral separation. *Nat. Commun.* **2016,** *7,* 12104.

(56) Ma, H.; Ren, H.; Meng, S.; Yan, Z.; Zhao, H.; Sun, F.; Zhu, G. A 3D microporous covalent organic framework with exceedingly high C_3H_8/CH_4 and C_2 hydrocarbon/CH_4 selectivity. *Chem. Commun.*, **2013**, ***49***, 9773–9775

(57) Li, Z.; Feng, X.; Zou, Y.; Zhang, Y.; Xia, H.; Liu, X.; Mu, Y. A 2D azine-linked covalent organic framework for gas storage applications *Chem. Commun.*, **2014**, *50,* 13825–13828.

(58) Dey, K.; Pal, M.; Rout, K. C.; Kunjattu H, S.; Das, A.; Mukherjee, R.; Kharul, U. K.; Banerjee, R. Selective Molecular Separation by Interfacially Crystallized Covalent Organic Framework Thin Films. *J. Am. Chem. Soc.* **2017**, *139*, 13083–13091.

(59) Huang, N.; Zhai, L.; Xu H.; Jiang, D. Stable Covalent Organic Frameworks for Exceptional Mercury Removal from Aqueous Solutions. *J. Am. Chem. Soc.* 2017, **139**, 2428–2434.

(60) Oh, H.; Kalidindi, S. B.; Um, Y.; Bureekaew, S.; Schmid, R.; Fischer R. A.; Hirscher, M. A Cryogenically Flexible Covalent Organic Framework for Efficient Hydrogen Isotope Separation by Quantum Sieving. *Angew. Chem., Int. Ed.* 2013, **52**, 13219–13222.

(61) Li, Z.; Feng, X.; Zou, Y.; Zhang, Y.; Xia, H.; Liu, X.; Mu, Y. A 2D azine-linked covalent organic framework for gas storage applications. *Chem. Commun.* **2014**, *50*, 13825–13828.

(62) Wang, Z.; Zhang, S.; Chen, Y.; Zhang, Z.; Ma, S. Covalent organic frameworks for separation applications. *Chem. Soc. Rev.* **2020**, *49*, 708-735.

(63) Elimelech, M.; Phillip, W. A. The Future of Seawater Desalination: Energy, Technology, and the Environment. *Science* **2011**, *333*, 712–717.

(64) Zhou, H.; Smith, D. W. Advanced technologies in water and wastewater treatment. *J. Environ. Eng. Sci.* **2002**, *1*, 247–264.

(65) Ning, G. H.; Chen, Z.; Gao, Q.; Tang, W.; Chen, Z.; Liu, C.; Tian, B.; Li, X.; Loh, K. P. *J. Am. Chem. Soc.* **2017**, *139*, 8897–8904.

(66) Zhang, W.; Zhang, L.; Zhao, H.; Li, B.; Ma, H. A two-dimensional cationic covalent organic framework membrane for selective molecular sieving. *J. Mater. Chem. A* **2018**, *6*, 13331–13339.

(67) Ding, S. Y.; Dong, M.; Wang, Y. W.; Chen, Y. T.; Wang, H. Z.; Su, C. Y.; Wang, W. Thioether-Based Fluorescent Covalent Organic Framework for Selective Detection and Facile Removal of Mercury(II) *J. Am. Chem. Soc.* **2016**, *138*, 3031–3037.

(68) Da, H. J.; Yang, C. X.; Yan, X. P. Cationic Covalent Organic Nanosheets for Rapid and Selective Capture of Perrhenate: An Analogue of Radioactive Pertechnetate from Aqueous Solution. *Environ. Sci. Technol.* **2019**, *53*, 5212–5220.

(69) Mattrey, F. T.; Makarov, A. A.; Regalado, E. L.; Bernardoni, F.; Figus, M.; Hicks, M. B.; Zheng, J.; Wang, L.; Schafer, W.; Antonucci, V.; Hamilton, S. E.; Zawatzky, K.; Welch, C. Current Challenges and Future Prospects in Chromatographic Method Development for Pharmaceutical Research *TrAC, Trends Anal. Chem.* **2017**, *95*, 36–46.

(70) Ismayil, K. M.; Manaf, O.; Sujith, A.; Antony, R. Polymer thin films for chromatographic separation of plant pigments. *Mater. Lett.* **2019**, *252*, 321–324.

(71) Wu, C.; Xu, P.; Wang, X.; Shou, D.; Wang, N.; Zhu, Y. In situ modification of silica with poly(vinyl alcohol) for normal-phase liquid chromatographic separation of bioactive compounds in traditional Chinese medicines. *Anal. Methods* **2019**, *11*, 3590–3596.

(72) Speltini, A.; Merli, D.; Profumo, A. Analytical application of carbon nanotubes, fullerenes and nanodiamonds in nanomaterials-based chromatographic stationary phases: A review. *Anal. Chim. Acta* **2013**, *783*, 1–16.

(73) Yang, C. X.; Liu, C.; Cao, Y. M.; Yan, X. P. Facile room-temperature solution-phase synthesis of a spherical covalent organic framework for high-resolution chromatographic separation. *Chem. Commun.* **2015**, *51*, 12254–12257.

(74) Morris, R. E.; Bu, X. Induction of chiral porous solids containing only achiral building blocks. *Nat. Chem.* **2010**, *2*, 353–361.

(75) Xuan, W.; Ye, C.; Zhang, M.; Chen, Z.; Cui, Y. A chiral porous metallosalan-organic framework containing titanium-oxo clusters for enantioselective catalytic sulfoxidation. *Chem. Sci.* **2013**, *4*, 3154–3159.

(76) Ahmad, A.; Mohd-Setapar, S. H.; Chuong, C. S.; Khatoon, A.; Wani, W. A.; Kumar, R.; Rafatullah, M. Recent advances in new generation dye removal technologies: novel search for approaches to reprocess wastewater. *RSC Adv.* **2015**, *5*, 30801-30818.

(77) Zou, L.; Yang, X.; Yuan, S.; Zhou, H. C. Flexible monomer-based covalent organic frameworks: design, structure and functions. *CrystEngComm*. **2017**, *19*, 4868-4871.

(78) Li, Y.; Chen, W.; Hao, W.; Li, Y.; Chen, L. Covalent Organic Frameworks Constructed from Flexible Building Blocks with High Adsorption Capacity for Pollutants. *ACS Appl. Nano Mater.* **2018**, *1*, 4756−4761.

(79) Guo, X.; Tian, Y.; Zhang, M.; Li, Y.; Wen, R.; Li, X.; Li, X.; Xue, Y.; Ma, L.; Xia, C.; Li, S. Mechanistic Insight into Hydrogen-Bond-Controlled Crystallinity and Adsorption Property of Covalent Organic Frameworks from Flexible Building Blocks. *Chem. Mater.* **2018**, *30*, 2299−2308.

(80) Konavarapu, S. K.; Kumar, B. Luminescent Triazene-Based Covalent Organic Frameworks Functionalized with Imine and Azine: N2 and H2 Sorption and Efficient Removal of Organic Dye Pollutants. *Cryst. Growth Des*. **2019**, *19*, 362−368.

(81) Li, Y.; Han, Y.; Chen, M.; Fengab, Y.; Zhang, B. Construction of a flexible covalent organic framework based on triazine units with interesting photoluminescent properties for sensitive and selective detection of picric acid. *RSC Adv.*, **2019**, *9*, 30937-30942.

(82) Modak, A.; Pramanik, M.; Inagakibc, S.; Bhaumik, A. A triazine functionalized porous organic polymer: excellent CO2 storage material and support for designing Pd nanocatalyst for C–C cross-coupling reactions. *J. Mater. Chem. A* **2014**, *2*, 11642–11650.

(83) Yu, J. T.; Chen, Z.; Sun, J.; Huang, Z. T.; Zheng, Q. Y. Cyclotricatechylene Based Porous Crystalline Material: Synthesis and Applications in Gas Storage. *J. Mater. Chem.*, **2012**, *22*, 5369-5373.

(84) Huo, J.; Luo, B.; Chen, Y. Crystalline Covalent Organic Frameworks from Triazine Nodes as Porous Adsorbents for Dye Pollutants. ACS *Omega* **2019**, *4*, 22504−22513.

(85) Xu, L.; Ding, S. Y.; Liu, J.; Sun, J.; Wang, W.; Zheng, Q. Y. Highly crystalline covalent organic frameworks from flexible building blocks. *Chem. Commun.* **2016**, *52*, 4706-47

(86) Wang, R. L.; Li, D. P.; Wang, L. J.; Zhang, X.; Zhou, Z. Y.; Mu, J. L.; Su, Z. M. The preparation of new covalent organic framework embedded with silver nanoparticles and its applications in degradation of organic pollutants from waste water**.** *Dalton Trans.* **2019**, *48*, 1051-1059.

(87) Das, P.; Mandal, S. K. A dual-functionalized, luminescent and highly crystalline covalent organic framework: molecular decoding strategies for VOCs and ultrafast TNP sensing. *J. Mater. Chem. A* **2018**, *6***,** 16246-16256.

(88) Das, P.; Chakraborty, G.; Mandal, S. K. Comprehensive Structural and Microscopic Characterization of an Azine–Triazine-Functionalized Highly Crystalline Covalent Organic Framework and Its Selective Detection of Dichloran and 4-Nitroaniline. *ACS Appl. Mater. Interfaces* **2020**, *12*, 10224−10232.

(89) Mullangi, D.; Nandi, S.; Shalini, S.; Sreedhala, S.; Vinod, C. P.; Vaidhyanathan, R. Pd loaded amphiphilic COF as catalyst for multi-fold Heck reactions, C-C couplings and CO oxidation. *Sci. Rep.* **2015**, *5*, 10876.